Università Politecnica delle Marche

Facoltà di Ingegneria

Dipartimento di Meccanica
Dottorato di Ricerca in Ingegneria Meccanica
VI CICLO

CARDIOVASCULAR PARAMETERS FOR HEALTHY STATE ASSESSMENT: AN OPTICAL-BASED, NON CONTACT APPROACH

Ing. Mirko De Melis

Coordinatore del dottorato : Prof. Enrico Evangelista

Promoter : Prof. Enrico Primo Tomasini

Tutors : PhD Umberto Morbiducci
PhD Lorenzo Scalise

2004 – 2007

Index

Abstract

This thesis will focus on the cardiovascular system monitoring , in particular on the frontiers of non invasive e non contact techniques .

A great interest has grown during the years on displacement cardiography as a methodology enabling the examination of the cardiovascular dynamics, with several alternative methods for the assessment of cardiac output proposed : phonocardiology, kinetocardiography, apex-cardiography, seismocardiography . All the previous techniques are specifically related to cardiac monitoring but it is also fundamental to characterize the vascular bed where is necessary applanation tonometry; a technique that allows continuous and non-invasive registration of the arterial pressure waveform.

In this field wide potentiality could be offered by the Laser Doppler Vibrometry (LDV) a laser- based vibration displacement and velocity measurement technique able to work without contact in a very accurate way. LDV technique has mainly been used in mechanical engineering, but in recent years some applications have been presented in biomedical areas.

In virtue of the above mentioned facilities, laser techniques could be an interesting alternative investigational methodology that was tested in the study of cardiac mechanics, in terms of displacement cardiology and blood pressure evaluation.. In fact, the monitoring of cardiovascular system is a typical task in clinical environment for a great variety of patient's condition. The possibility to obtain this information without any contact with the patient represents a future tool in many fields also outside of the clinics. In fact generally this task cannot be accomplished when patient's condition determine impairment of their health if contact with skin or any other surface has to be avoided, (e.g. severely burnt subject), or when the type of functional situation e.g. such as the case of people with (e.g. magnetic resonance imaging analysis) or people within confined environment (such as hyperbaric chamber) do not allow to put any sensor or electrodes within the examination environment. In all these situations an alternative method to the typical one must be provided to monitor cardiac functionality.

To my family … present … future …..

Introduction

The heart and the circulation, or the circulation and the heart, it is the story of the ball and chain: they are complementary in every way and to discuss one without mentioning the other is therefore pointless.

The investigation of heart and vessels goes back to ancient times. The Egyptians, Chinese and Greeks independently described the importance of palpation of the pulse in their medical literature. A characteristic of those times is the mystique that surrounds them and the peculiar way in which physiological phenomena were described. For example, in the Chinese manuscript 'Huang Ti Nei Ching Wen. The Yellow Emperor's Classic of Internal Medicine' by the emperor Huang Ti, one can read that: '*the pulse of a healthy heart should feel like continuous hammer blows…like the notes of a string instrument…like wood floating on water or like fish gliding through waves*'! Huang Ti is thought to have lived c. 2697-2597 BC, but some believe that he was only a legendary figure and the book was actually written by a large number of people, composed to one manuscript by the 2nd century BC.(Naqvi and Blaufox 1998)

It was the ancient civilization of Greece that established the relationship of the heart with the blood vessels, when the pulse was recognized as a function of the heart. Gradually through time, the knowledge about the cardiovascular system improved, but this journey was also full of misconceptions. The fact that arteries contract and relax was known since the time of Aristotle. Following this, the Alexandrian Erasistratus (310-250BC), also called 'the father of physiology', believed that the arteries were filled with air, or 'pneuma', which was released as soon as the artery was severed, and that the blood from the neighbouring veins quickly filled in to take its place. Claudius Galenus, or Galen (131-199) wrote more on the subject of the pulse than anyone before or since. Interesting is his experimental approach where he used a hollow reed to simulate an artery. However, though his teachings prevailed for at least five centuries, a lot of mistakes were also passed on in this way. He

wrongfully described the ebb and flow of blood in arteries and the passing of blood from the right side of the heart to the left side through pores, thinking of the circulation as an open-circuit. Only much later, Galileo Galilei (1564-1642) countered these findings and considered the circulation of blood to be in a closed system.(Allbutt 1921; Dobson 1927)

Despite the fact that the history of the investigation of heart and circulation dates back so far in time, the modern perception of the cardiovascular system is derived from the ideas stipulated only in 1616 by a contemporary of Galileo, named William Harvey (1578-1657). He described the circulation of the blood in the following way: '*the movement of the blood in a circle is caused by the beat of the heart.' and 'the pulsation of the arteries is nothing else than the impulse of the blood within them.*' Later, in 1628, Harvey wrote his famous book in Latin called: 'Exercitatio Anatomica de Motu Cordis et Sanguinis in Animalibus' about the anatomical treatise on the movement of the heart and blood in animals.(Bettman 1979)

Moving with this inspiration and history this thesis will focus on the cardiovascular system monitoring , in particular on the frontiers of non invasive e non contact techniques .

A great interest has grown during the years on displacement cardiography as a methodology enabling the examination of the cardiovascular dynamics, with several alternative methods for the assessment of cardiac output proposed.

Phonocardiology, as well as the simple use of stethoscope can be considered among this class of instruments, even if limited in sensitivity in the high frequency band due to audible range of such instruments.

Balistocardiography is a method by which body vibrations caused by heart activity are registered; it has been widely used in the past 40-50 years. It is based on the use of a special low-impedance instrumented bed, on which the patient is resting quietly: the bed is sensed by a low-frequency accelerometer which responds to the heart (and body) movements. Special signal processing is needed to allow separation of

displacement signals produced by heart from the other interfering inputs. To date the method has not gained the status of a valid clinical diagnostic tool probably because of the complexity of the method and the difficulty to carry out measurements.

Kinetocardiography is using a pressure sensor placed on top of a hollow cylinder, placed on the chest, to detect the pressure waves generated by heart wall displacement. Despite its capability to detect abnormalities in patients with coronary diseases, the technique has not been used widely.

In apex-cardiography, the movement of chest at the point of maximal cardiac impulse is detected and used to reveal the presence of coronary artery pathologies (it is a method of graphically recording the pulsations of the anterior chest wall over the apex of the heart).

In the 90's the seismo-cardiography has been presented as a novel non-invasive technique -although it is a contact procedure - for recording and analysing cardiac vibratory activity. This technique despite the reduced complexity and the relative simplicity in the use has not gained the status of standard and it is used only for research purpose.[8]

All the previous techniques are specifically related to cardiac monitoring but it is also fundamental to characterize the vascular bed where is necessary applanation tonometry; a technique that allows continuous and non-invasive registration of the arterial pressure waveform.

Applanation tonometry is a continuous registration procedure continuously measuring the pressure-time wave morphology that cannot be assessed by conventional cuff methods (Korotkoff/auscultation or oscillometry). Being non-invasive, it also means a fast and simple approach compared to an interventional pressure measurement.

A pressure transducer is placed upon the skin in correspondence of a superficial artery, which is supported by bone structure so that adequate applanation of the vessel can be achieved to obtain the pressure waveform (usually the carotid and

femoral arteries are used at this scope). As applanation tonometry can only provide for the waveform, this signal has to be calibrated by means of an external method, for example a cuff technique giving minimum and maximum blood pressure values, allowing the waveform to be rescaled to its correct offset and amplitude.

In this field wide potentiality could be offered by the Laser Doppler Vibrometry (LDV) a laser- based vibration displacement and velocity measurement technique able to work without contact in a very accurate way [1]. LDV technique has mainly been used in mechanical engineering, but in recent years some applications have been presented in biomedical areas. Among the first work demonstrating the possible use of LDV instrumentation for arterial pressure curve detection has been reported in 1998 by Tomasini et al [2]. In the following years others application have been reported for example for the study of dental problems [3,4] and tendons mechanics [5] is of great interest for their advantageous metrological characteristics. In particular, the high accuracy (about 1% of reading), high resolution (displacement resolution about 8 nm) and the non-contact nature of this measurement technique make these instruments suitable for diagnostic purposes, and also for in-vivo tests. For example, promising results have been obtained for the in vitro study of prosthetic heart valves kinematics [6] while in the in vivo study of tympanic membrane vibrations laser vibrometry has already been successfully applied . LDV has been used also for the measurement of human-vibration transmitted to the hand-arm system by vibrating tools.[7]

In virtue of the above mentioned facilities, laser techniques could be an interesting alternative investigational methodology to be tested in the study of cardiac mechanics, in terms of displacement cardiology and blood pressure evaluation.. In fact, the monitoring of cardiovascular system is a typical task in clinical environment for a great variety of patient's condition. The possibility to obtain this information without any contact with the patient represents a future tool in many fields also

outside of the clinics. In fact generally this task cannot be accomplished when patient's condition determine impairment of their health if contact with skin or any other surface has to be avoided, (e.g. severely burnt subject), or when the type of functional situation e.g. such as the case of people with (e.g. magnetic resonance imaging analysis) or people within confined environment (such as hyperbaric chamber) do not allow to put any sensor or electrodes within the examination environment. In all these situations an alternative method to the typical one must be provided to monitor cardiac .[8,10]

Chapter 1

1.1 The heart

The human heart acts like a pump, which provides for the blood circulation in the human body. The blood circulation in its turn takes care of the transportation of oxygen, nutrients and humoral agents necessary for a healthy functioning of muscles and organs. To fulfill this logistic task, the cardiovascular system has two circulatory blood flows at its disposal. On one hand, there is the small or pulmonary circulation, in which blood is pumped to the lungs, oxygenated and then taken back to the heart. On the other hand, there is the large or systemic circulation. The arterial part of the systemic circulation brings oxygenated blood to the muscles and organs where the exchange occurs after which the veins carry the oxygen deficient blood back to the heart. For this reason, oxygenated blood is commonly referred to as 'arterial blood', and oxygen deficient blood as 'venous blood'. Note that this is only correct when speaking of the systemic circulation, as in the pulmonary circulation oxygen deficient blood is transported by the lung arteries and oxygenated blood by the pulmonary veins.

1.2 General nomenclature

The heart is divided into four cavities or 'chambers'. The 'upper' chambers of the heart, the atria, are anatomically separated from the 'lower' chambers or ventricles by a fibrous ring. In order to maintain appropriate direction of flow in the chambers and to allow adequate pressure management during the heart cycle, four cardiac valves are situated within this ring.

One can say that the heart is divided into a right- and a left-sided pump, which propel oxygen deficient blood into the pulmonary circulation and oxygenated blood into the systemic circulation, respectively. Left and right side of the heart are separated by the septum.

A schematic overview is given in Figure 1.1. The upper and lower venae cavae (11,12) collect venous blood into the right atrium (1) from where it passes through a tricuspid valve (3) - the valve has three valve cusps or leaflets - into the right ventricle (2). Contraction of ventricle wall fibres pushes the blood through the pulmonal valve (4) via the pulmonal artery (5) towards the lungs where the oxygenation takes place. Via the pulmonal veins (6), the

blood reaches the left atrium (7), passes through the mitral valve (8) - a bicuspid valve with two cusps - during the relaxation or filling phase and fills the left ventricle. With the following contraction, the blood is pushed through the aortic valve (9) into the aorta (10) and the rest of the arterial circulation.

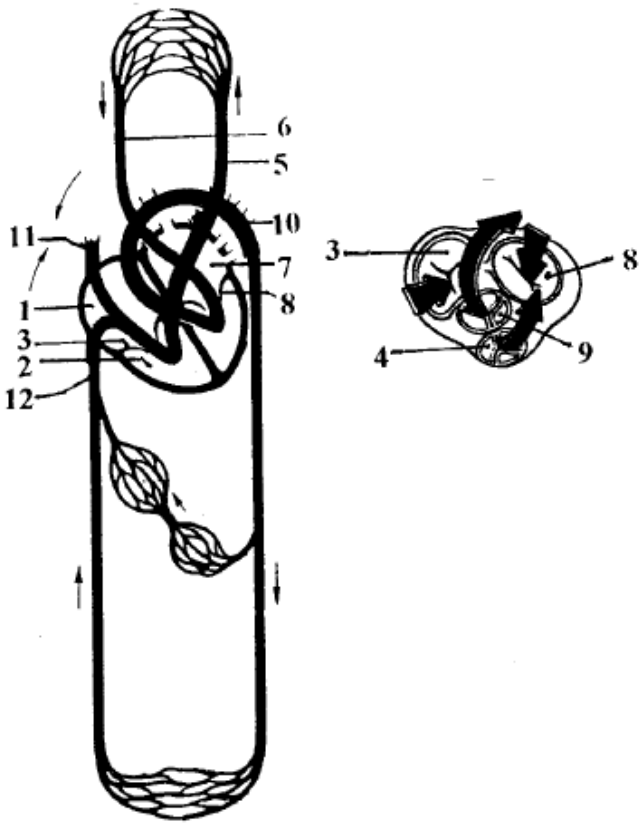

Figure 1.1 Schematically representation of the circulation, together with a cross-section of the heart at base showing the four valves.(Kahle, Leonhardt et al. 1992)

1.3 Heart wall structure

The heart is situated in the thoracic cavity in between the lungs. The pericardium, composed of two layers (visceral and parietal pericardium), encloses the heart. A small amount of lubricating fluid separates the two pericardial layers and reduces friction created by the pumping heart. The heart wall itself is composed of three layers (Figure 1–2). The myocardium is the middle, muscular layer. The outer epicardium and the inner endothelial layer (or endocardium) surround the muscular layer as thin, smooth protective tissues. Muscle development of the myocardium is dependent on location and function. The atrial walls are the thinnest since the atria are low-pressure chambers mainly serving as blood reservoirs. The

walls of the ventricles must endure higher pressures and are therefore more developed. The left ventricle wall is thicker than the right ventricle wall since the pressure build-up in the left ventricle is several times higher than the pressure build-up in the right ventricle.

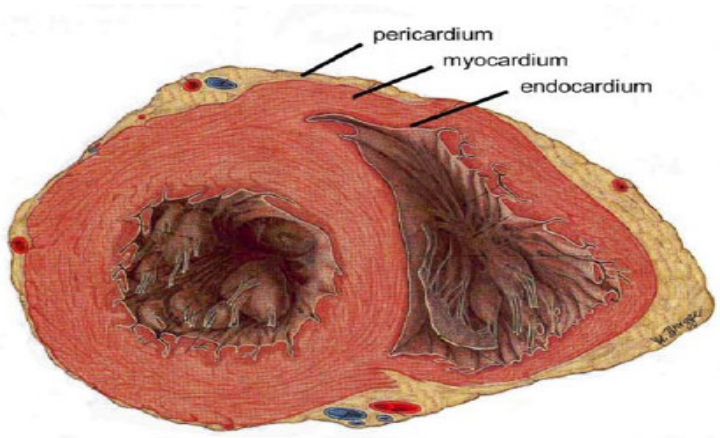

Figure 1.2 The different layers of the heart wall.(Putz and Pabst 1994b)

1.4 Physiological aspects

1.4.1 Electrical aspects

The myocardium of the heart consists of cardiac muscle cells or myocytes. When an electric excitation wave (a depolarization wave) stimulates the cardiac muscle, the subsequent calcium release in the cellular mechanisms induces a mechanical response of muscular contraction. It is followed by electrical recovery or repolarization, corresponding to muscular relaxation. A specialized conduction pathway exists in the myocardium to ensure rhythmic and synchronized excitation and contraction of the heart muscle (Figure 1.3, left). A cardiac impulse starting from the sinoatrial node (SA) spreads to the interatrial pathway and provokes contraction of the atria. The electric impulse then reaches the atrioventricular node (AV), which is positioned at the top of the intraventricular septum. Finally, the wave of electric excitation spreads from the AV node to the ventricles via the bundle of His, which branches into the Purkinje fibers.

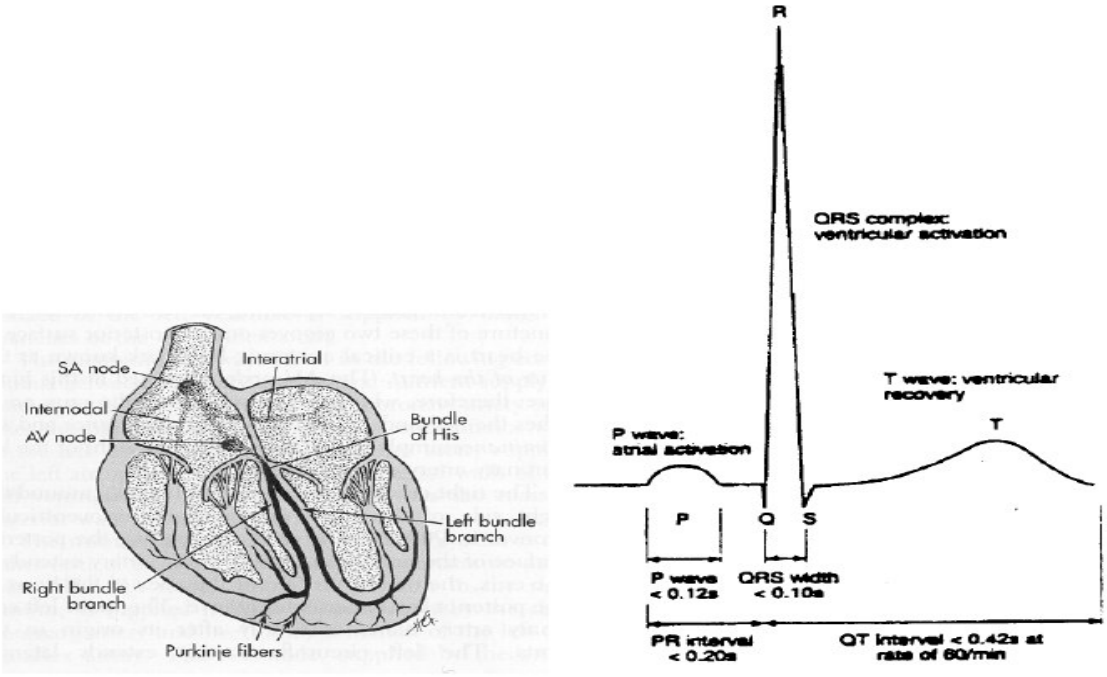

Figure 1.3 The cardiac conduction system and the electrocardiogram.(Price and Wilson 1992)

The electrocardiogram (ECG) reflects the summated electrical activity of all the myocardial cells recorded from the body surface (Figure 1.3, right). Characteristic wave complexes on the ECG are P, QRS, and T-waves. The P-wave corresponds to atrial depolarization, originating from an impulse from the SA node. The QRS complex represents ventricular depolarization. The amplitude of this wave is large as a result of the large muscle mass traversed by the electric impulse. The PR interval includes the transmission time through the atria and the delay of the impulse at the AV node. Ventricular repolarization generates the T wave.

1.4.2 Mechanical aspects

The heart can be looked upon as a mechanical pump generating the appropriate output that meets the needs of the metabolism. Pressure and flow signals during a cardiac cycle of an adult in rest are depicted in Figure 1.4. The ECG is shown to give an indication about the timing within the cardiac cycle.

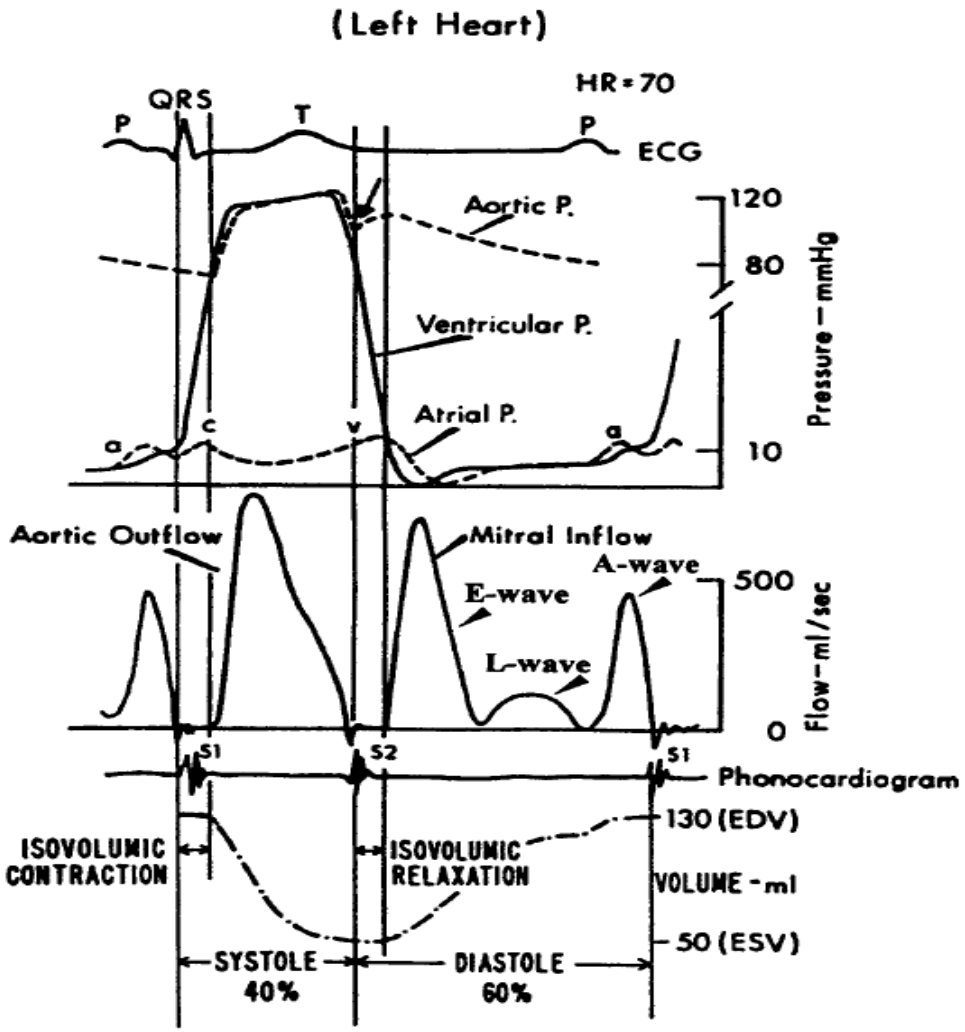

Figure 1.4 Pressure and flow during one cardiac cycle.(Yellin 1995)

During the systolic part of the heart cycle, left ventricular (LV) pressure rises from 0 to 120 mmHg. When LV pressure rises above aortic pressure, the aortic valve opens and blood is ejected from the LV into the arterial circulation. Approximately two thirds of the bloodvolume in the ventricle at the end of diastole (end-diastolic volume, EDV) is ejected

during systole. This portion of ejected blood is called the ejection fraction (EF). The residual ventricular volume at the end of systole is referred to as the end-systolic volume (ESV).

The diastolic portion of the heart cycle can be subdivided into four phases: (1) isovolumic relaxation, (2) rapid or early filling (E-wave), (3) diastasis (L-wave) and (4) atrial contraction (A-wave). In the first phase, between the time of aortic valve closure and mitral valve opening, LV pressure relaxes exponentially from the aortic pressure level to the pressure level existing in the left

atrium (LA). The next phase, i.e. early filling (E-wave), begins when pressure in the LV falls below that in the LA, causing the mitral valve to open and the LV to begin filling. The early filling phase coincides with and is dependent on continued LV relaxation. This phase ends when pressure in the two chambers is equalized. Although this rapid filling comprises only about 30% of diastole, it accounts for up to 80% of LV filling volume. The third phase is the diastasis. Little filling, if any, comes from pulmonary vein flow (L-wave). With increased heart rate this phase shortens more than the other three. The fourth phase, atrial contraction (A-wave), contributes for 15% to 25% of LV filling volume under normal conditions but can contribute as much as 40% if LV relaxation is diminished.(Guyton and Hall 2000)

Heart rate (HR) is defined as the amount of cardiac cycles or beats per minute (bpm). Stroke volume (SV) is the volume of blood ejected by the ventricles per heartbeat. The volume ejected by the ventricles per minute is called the cardiac output (CO). Cardiac output depends on the relationship between the two variables HR and SV and is defined as:

$$CO = HR \times SV \qquad \text{eq 1.1}$$

As an example, average CO in rest for a 'normal' adult person is about 5-6 l/min. For an average HR of 72 bpm, SV would then be around 70-80 ml. However, these values are strongly influenced by the definition of a 'normal adult'. CO also adapts to the demands of the peripheral tissues for oxygen and nutrients, and will go up for example during physical exercise.

	Before training	*After 6 month training*	*Top Runner*
HR at rest (bpm)	75	60	36
HR max (bpm)	195	192	174
SV rest (ml)	60	75	125
SV max (ml)	100	125	200
CO rest (l/min)	4.5	4.5	4.5
CO max (l/min)	19.5	24.0	34.8

Table 1–1 Values for HR, SV and CO for a 15 year old adolescent before and after a 6 months endurance training schedule, compared with the values for a top athlete.(Wilmore and Costill 1999)

Table 1–1 demonstrates how training can influence the HR, SV and CO values. Despite the fact that HRrest and SVrest for each subject are significantly different, the COrest (4.5 l/min, HRrest x

SVrest) is the same for the 3 subjects in rest. At exercise however, COmax values rise the more the person is trained (from 19.5 l/min to 34.8 l/min), and this while HR drops compared to a less-trained person under the same load conditions (from 195 to 174 bpm). A trained person has more economical energy consumption: he develops a larger CO with a lower HR, because of his trained heart that can deliver a bigger SV.

1.5 The coronary arteries

1.5.1 Anatomical aspects

In order to deliver a continuous amount of power, the heart muscle needs to have its own blood supply. An inadequate irrigation of the heart muscle is referred to as a state of 'ischaemia', which can lead to 'myocardial infarction' (tissue necrosis). The latter is one of the most common causes of mortality in all industrialized countries. The important task of providing the heart with oxygenated blood is taken care of by the coronary arterial network.

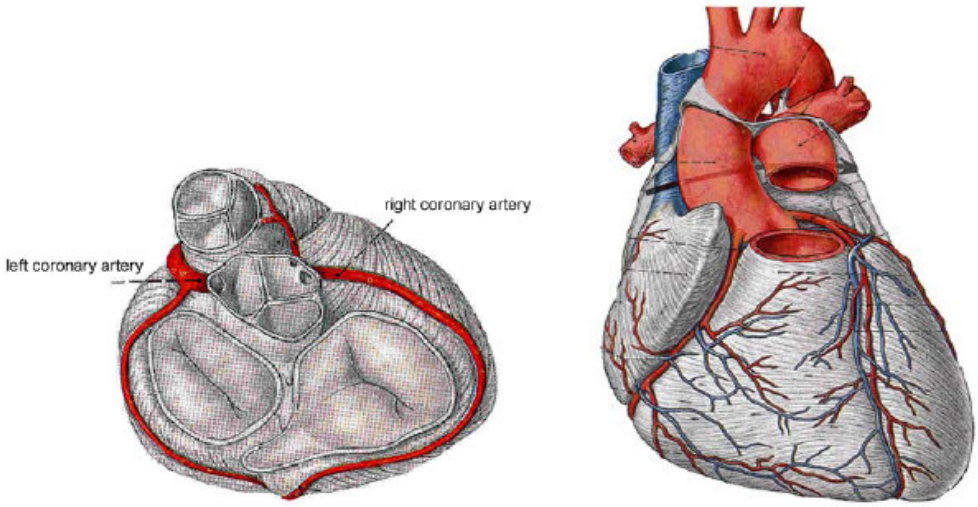

Figure 1.5 The coronary arterial network.(Putz and Pabst 1994b)

The branching of the coronary arterial network is different for every individual. Variations in anatomical structure are inherent to arteries and the coronaries make no exception to that rule. The most common situation is the one where 2 coronaries are branching from the aorta at the sinus aorta, slightly distal from the aortic valve (Figure 1.5, left). However, it happens (38%) that multiple (more than 2) coronaries branch from the aorta, and in seldom cases (less than 1%), the heart is fed by only one coronary artery.(Kahle, Leonhardt et al. 1992)

The area of irrigation can also vary. The following classification can be made using the blood supply to the posterior wall of the ventricles as a criterion: a 'balanced' type of supply is present when the posterior interventricular coronary branch originates from the right coronary artery (70%); a situation of 'left dominance' occurs when the posterior interventricular branch comes from the left coronary artery (20%), and a 'right dominance' occurs when the posterior ventricle walls are mainly supplied by several branches descending from the right coronary artery (10%).(Putz and Pabst 1994b)

Since the coronary network can have multiple individual variations, it is not easy to determine anatomical positioning and branching in a unique way. In general however, the nomenclature of epicardial and myocardial coronaries, capillaries and finally the collateral network is applied.(Brandenburg, Fuster et al. 1987; Kapoor 1989; Pijls and De Bruyne 1997)

1.5.2 Epicardial coronaries

Epicardial coronaries have a diameter ranging from a few millimeter down to 400 μm and are the beginning of the coronary network: arising from the aortic sinus above the aortic valve, they are positioned along the epicardial surface of the heart wall (Figure 1.6). The left main coronary artery (LCA) is split up into the left anterior descending coronary artery (LAD) and the left circumflex coronary artery (LCX). Occlusion of the LAD can reduce the pump capacity of the left ventricle by 2/3.(Van Nooten 1998) The right coronary artery (RCA) splits into a posterior descending (RPD) and marginal branch (RMB). The origin of the posterior descending artery determines the coronary dominance.(Brandenburg, Fuster et al. 1987)

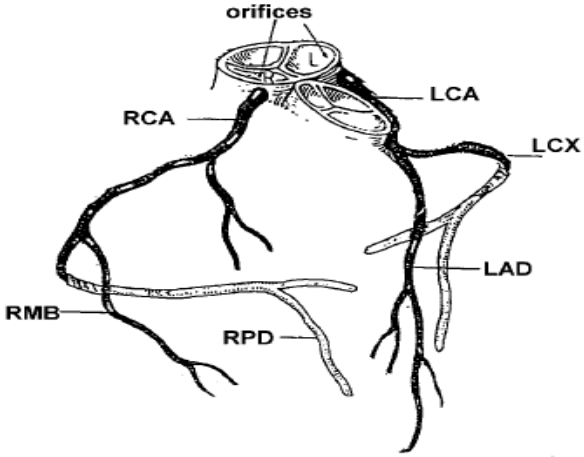

Figure 1.6 Nomenclature of the epicardial branches of the coronary arterial network.

Epicardial coronaries are clearly visible on a coronary angiogram (a diagnosis technique based on X-ray techniques which will be discussed further). Stenoses due to arteriosclerosis (degenerative changes in the artery wall) mainly occur in the epicardial part of the coronary tree. The occurrence of such a stenosis is the prevalent cause of myocardial ischaemia and can lead to thrombosis and myocardial infarction.

1.5.3 Myocardial coronaries

Myocardial coronaries are the prolongation of the epicardial coronaries, enter the myocardium and have diameters of 400 μm and less. The myocardial coronaries are no longer clearly visible on an angiogram and it is no longer possible to execute a mechanical revascularization in case lesions are present. Myocardial vessels are also called resistance vessels because of their significant resistance effect for the myocardial perfusion.

1.5.4 Capillaries

The capillaries compose a network of tiny blood vessels (diameters of 5 μm) with a density of 3500 vessels/mm². Small muscle cells are woven in between the capillaries, allowing the capillary bed to expand under the influence of internal pressure and the tone of these attached muscle cells.

1.5.6 Collateral network

The collateral bed or ‘anastomoses’ are the ‘bridging vessels’ between all other arteries in the coronary network. It is nowadays accepted that these rudimentary connection vessels are present in each heart from birth.(Pijls and De Bruyne 1997) They are not visible on arteriography because of their low flow range, but when a stenosis develops, this network expands and forms bridges or collateral pathways that deviate the blood alongside of the occlusion to irrigate the more distal locations together with the ischaemic area.

1.6 Physiological aspects

1.6.1 Myocardial resistance

Blood supply to peripheral tissues in the human body is done during the whole cardiac cycle but mainly in systole, the contracting phase of the heart. However, since this contraction of the heart muscles forces the myocardial coronary arteries to occlude, the heart itself is mainly irrigated during relaxation or diastole.(Khouri and Gregg 1963) Figure 1.7 shows the correlation between aortic blood pressure and blood flow in left and right coronary artery.

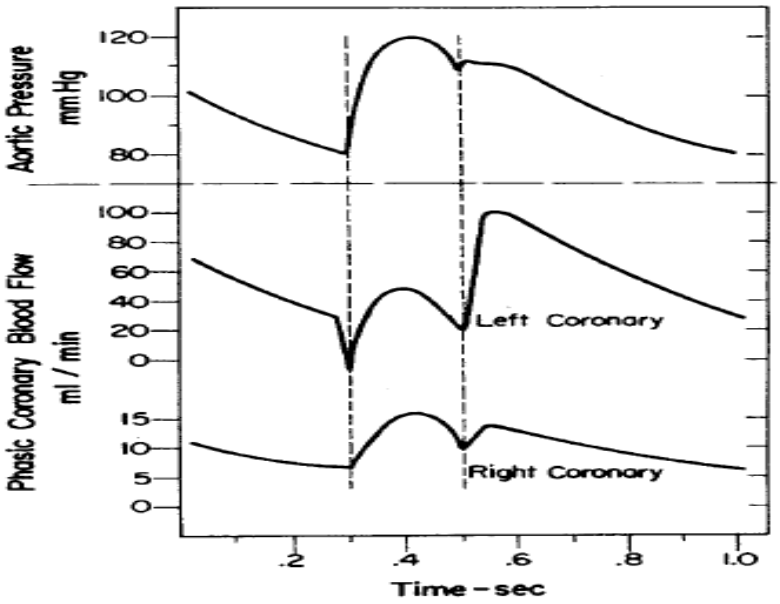

Figure 1.7 Effect of myocardial resistance: coronary perfusion occurs mainly during diastole.(Berne, Sperelakis et al. 1979)

1.6.3 Autoregulation

The coronary circulation has some regulatory properties that provide several blood flow responses to specific conditions. One is the 'autoregulation' mechanism. It is an intrinsic response that allows maintaining the coronary blood flow at a fairly constant level over a wide range of perfusion pressures. This phenomenon is illustrated in Figure 1.8 where the relationship is shown between autoregulation (A) and maximal vasodilatation (D). The difference between the two curves represents coronary reserve or flow reserve at a specific perfusion pressure, with constant aortic pressure and HR. Since the slope of curve (A) is much less steep than the slope of (D), one can understand that the autoregulation mechanism protects the coronary perfusion in this way from large fluctuations, which would already occur at moderate arterial pressure changes.

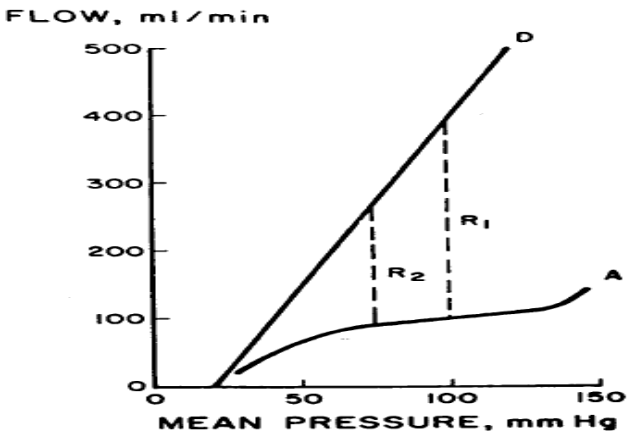

Figure 1.8 Relationship between coronary artery perfusion pressure and blood flow during autoregulation (A) and maximal vasodilatation (D). The difference between the two curves represents the flow reserve at a given pressure. (Hoffman 1984)

1.6.4 Metabolic regulation

Myocardial perfusion takes up 5 to 10% of the total SV. Oxygen demand in rest for the myocardium is up to 20 times higher than for the skeletal muscles.(Pijls and De Bruyne 1997) . As a consequence, the extraction of oxygen within the myocardium between coronaries and muscle cells is close to the maximum efficiency rate, meaning that a higher demand for oxygen leads to a higher demand in blood flow to be supplied by the coronaries. The myocardial oxygen consumption and the coronary flow thus have a strong linear relation. The regulation of the volume of coronary blood flow in proportion of the myocardial workload, or metabolic demands, is referred to as the 'metabolic regulation'.(Gregg and Shipley 1944)

As to the underlying mechanisms of this second intrinsic response, a lot of discussion is involved. Over the years, adenosine has been under attention as one of the most probable metabolic factors playing a principal role. The contribution of the endothelium cells of the inner vessel wall layer to blood flow regulation has also been acknowledged.(Ku 1982; Stewart, Pohl et al. 1988) However, most likely several factors instead of just a single one play their respective parts.(Olson and Bunger 1987) Given the fact that responses to stimuli or pharmaceutical agents can differ widely in larger or smaller arteries (Foreman and Kirk 1980), the net coronary flow response to an intervention is often not readily predictable.

1.6.5 Reactive hyperaemia

'Hyperaemia' is defined as a state of maximal flow. 'Reactive hyperaemia' is an intrinsic response of the coronary circulation occurring after release of an occlusion, when a coronary flow is suddenly delivered of typically 3 to 5 times the blood flow present before the occlusion. The peak level of this augmented flow during the reactive hyperaemic response is directly proportional to the duration of the occlusion, but attains the highest values with occlusions lasting about 20 s.(Olson and Gregg 1965; Pijls and De Bruyne 1997) This is a very useful condition during clinical measurements. Since longer occlusions do not produce a higher peak flow, one can assume a maximal vessel dilatation (and thus minimal resistance to flow) at that moment.

Pharmaceutical drugs such as adenosine, dipyridamole or papaverine also induce reactive hyperaemia.(Canty, Klocke et al. 1985) Figure 1.9 (lower signal) shows the effect of adenosine injections (ADO IC) and a temporary balloon occlusion (coronary interventions will be discussed further in detail) on a mean coronary flow velocity profile. The balloon occlusion makes coronary flow drop completely to zero. After removing the occlusion, flow velocity maximizes to more than 3 times the level it had before the balloon was put in place. This is the state of reactive hyperaemia, where blood flow becomes primarily function of the coronary cross-sectional area at any given perfusion pressure.

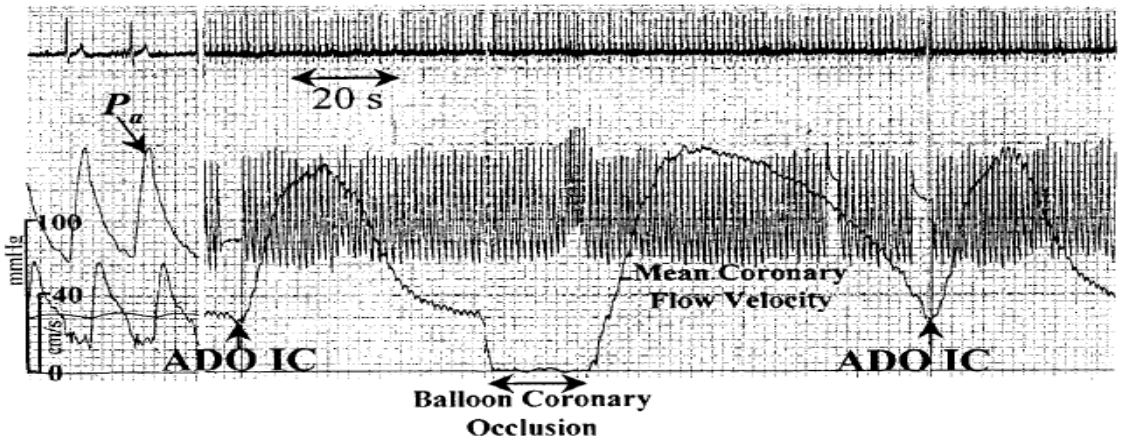

Figure 1.9 ECG, aortic pressure (mmHg) and mean coronary flow velocity (cm/s) during 3 events of induced reactive hyperaemia (ADO IC, balloon occlusion, ADO IC).(Pijls and De Bruyne 1997)

1.7 The large arteries

1.7.1 Anatomical aspects

The large arteries are the main branches of a well-designed and complex vessel network that has to provide for oxygen, nutrients and humoral agents to the whole human body. The anatomical highlights of the whole arterial tree are shown in Figure 1.11. The relevant arteries, for topics described in this thesis, are depicted in Figure 1.10 on the left. They involve the vessels of the 'aorta-radial' path: aortic arch (1), carotid artery (2), subclavian artery (3), axillary artery (4), brachial artery (5) and the radial artery (6).

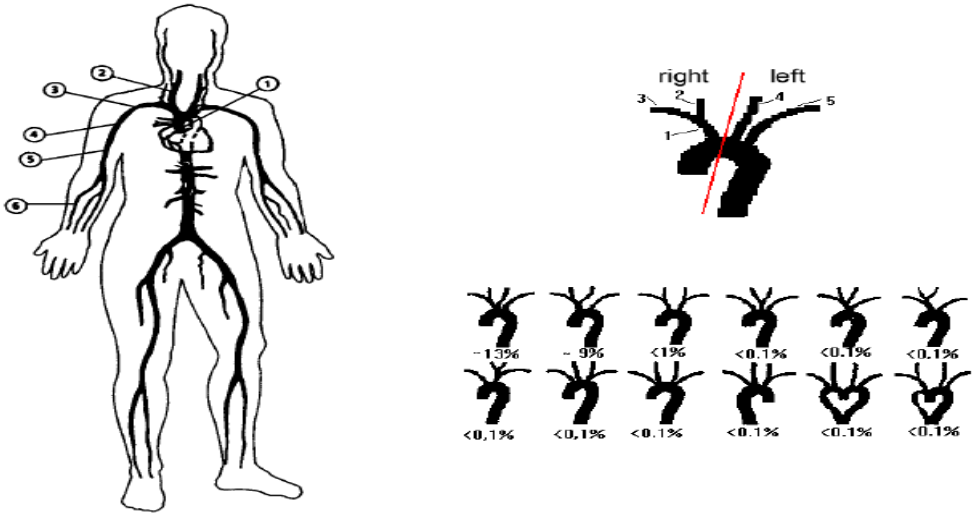

Figure 1.10 Left: The aorta-radial path.(Stergiopulos, Young et al. 1992) Right: Variations on the offspring of carotid and subclavian arteries from the aortic arch.

1.7.2 Central arteries

Central arteries include the aorta, the coronaries, the carotid arteries and the direct branches of the aorta descendens. All arterial vessels are - directly or indirectly - branches from the aorta. The aorta is the biggest artery in the body and is connected to the heart, communicating with the LV through the aortic valve. The aorta ascendens is the rising part of the aorta, from the heart towards the aortic arch. Further distal, the term aorta descendens is applied, which is the descending part of the aorta going down through the thorax.

Towards the upper limbs, direct branches of the aortic arch can have different configurations (Figure 1.10, upper right). Most common configuration (77%) is the one where the most right branch, the brachiocephalic artery (1), splits into the right carotid (2) and subclavian (3) artery, while on the left side the carotid (4) and subclavian (5) artery are directly branching from the aorta. Other configurations (23%) do occur sometimes (Figure 1.10). These anatomical variations develop during the embryonic phase and do not cause severe negative implications in terms of functionality.

Towards the lower limbs, direct branches of the aorta descendens supply internal organs such as liver and kidneys. Further down, the abdominal aorta (part of the aorta below the diaphragm) splits

into the right and left iliac artery, both having an internal branch towards the inner pelvis, and an external branch towards the legs.

1.7.3 Peripheral arteries

Peripheral arteries comprise the head and neck arteries, the brain arteries, and the arteries of upper and lower limbs. The carotid artery goes straight up the neck and splits into an external and internal branch. The latter enters the skull to supply blood to the eye cavities, hypophysis and the brains (vertebral arteries), while the external branch serves the region of the neck, face and skull (superficial temporal artery).

Shoulder and upper arm are being supplied with blood via the subclavian artery, evolving into axillary and brachial artery and splitting at the height of the elbow into the radial and ulnar artery, which irrigate the lower arm. The radial artery runs towards the thumb side and evolves into smaller, deeper lying hand arteries. The ulnar artery runs towards the pink side and evolves into smaller, superficial hand arteries. For the legs, the external iliac artery evolves into the femoral and tibial artery to finally reach the smaller foot arteries.

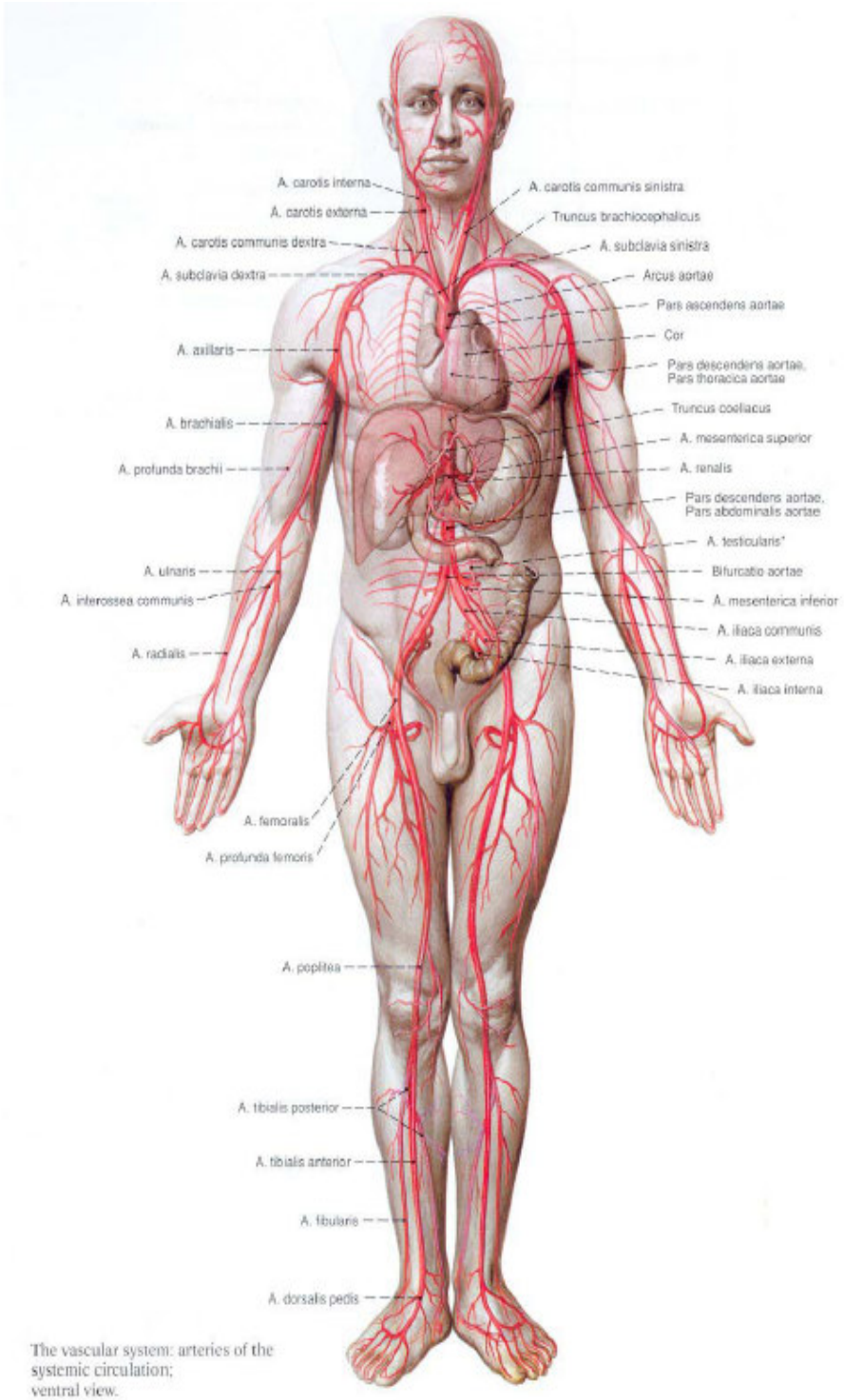

The vascular system: arteries of the systemic circulation; ventral view.

* in the female: A. ovarica

Figure 1.11 The systemic circulation.(Putz and Pabst 1994a)

1.7.4 Vessel wall structure and tapering

The vessels in the arterial tree do not have a constant diameter from beginning to end. The cross-sectional area of an artery becomes gradually smaller when moving further away from the heart. This is called 'geometric tapering'. Figure 1–12 (upper panel) shows the decrease of the mean external radius at various sites along the aorta, measured at physiological pressure in dogs.(Fry, Griggs et al. 1963) A lot of similarities exist between mammalian circulatory properties, and earlier experimental data is often derived from canine measurements.(Li 1996) Figure 1.12 (lower panel) gives an indication of values for a human aorta.(Latham, Westerhof et al. 1985)

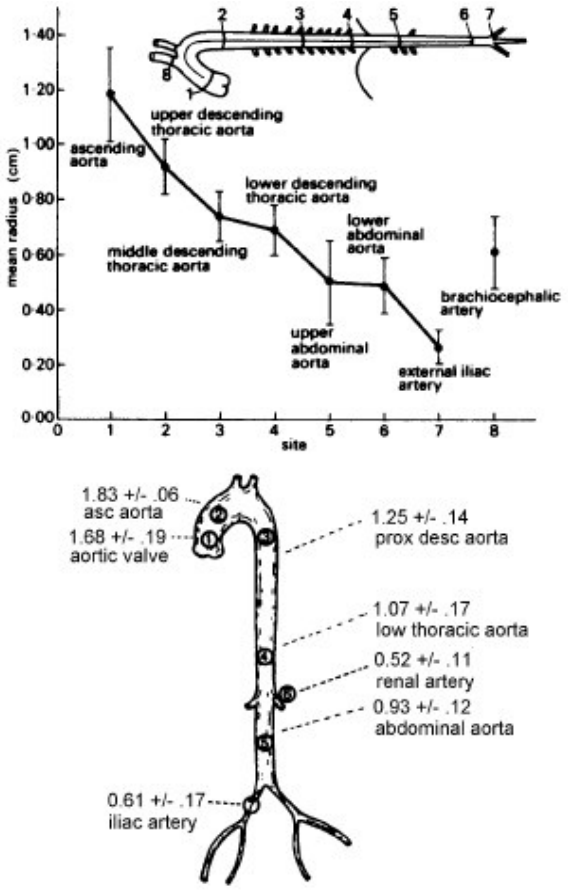

Figure 1.12 Up: Aortic tapering in dogs.(Fry, Griggs et al. 1963) Down: Radius values in a human aorta.(Latham, Westerhof et al. 1985)

A daughter branch always has a smaller diameter than the mother branch. However, although the lumen area of each daughter branch at a junction is smaller than the mother branch lumen area, the combined cross-sectional area of the daughter branches is always slightly bigger than the offspring cross-sectional area. For example, the area ratio at the aortic arch was calculated to be about 1.08 by

Li et al. (Li, Melbin et al. 1984), thus slightly bigger than 1. The consequence of this is discussed further in this chapter.

The arterial wall is not an inert and stiff hydraulic tube. It consists of non-homogeneous, organic tissue in which complex exchange and control mechanisms take place. The vessel wall consists of highly extensible elastin material, of very stiff collagen with a high tensile strength, and of smooth muscle cells that, as opposed to skeletal and cardiac muscle, mainly invaginate their cell walls rather than exerting a longitudinal shortening.(Cooke and Fay 1972) Three concentric regions can be distinguished: the tunica intima, media and adventitia (Figure 1.13). The intima layer (1) is the innermost layer and mainly takes care of exchange mechanisms through the vessel wall. This very thin layer (0.5-1 μm) is made of endothelium cells, which in general have a longitudinal direction compared to the vessel axis. The middle layer or tunica media (3) is thicker, built mainly of smooth muscle cells distributed in a more or less concentrical way, which play an important role in the mechanical properties of the vessel. For example, the arterial wall actively contracts and relaxes and can control and adapt its 'vascular tone' when influenced by vasoactive agents or by changing perfusion pressure. Intima and media layer are separated by an elastic tissue, the internal laminae (2). The tunica adventitia (5) consists primarily of connective tissue that merges with the artery surrounding tissue. In some vessels, a (somewhat thinner) elastic membrane (4) between media and adventitia is present.

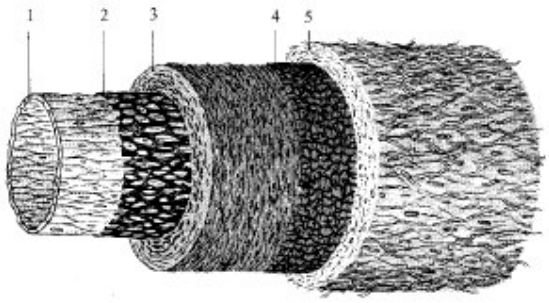

Figure 1.13 Different layers of the artery vessel wall.(Kahle, Leonhardt et al. 1992)

The relative amount of components forming the arterial wall changes from site to site along the arterial tree (Figure 1.14). The mechanical properties depend as much on the connections between elastin, collagen and muscle than on the size and orientation of the muscular layer (Kenner 1967) but in general terms, the amount of elastin diminishes when more distal from the heart, and the muscular layer increases in size, hereby also increasing the relative wall thickness. Vessels become gradually stiffer towards the periphery, hence also the terms 'elastic' (aorta and proximal portions

of its major branches) and ‘muscular’ arteries (distal portions of major branches and their descendants). This effect is sometimes referred to as ‘elastic tapering’.

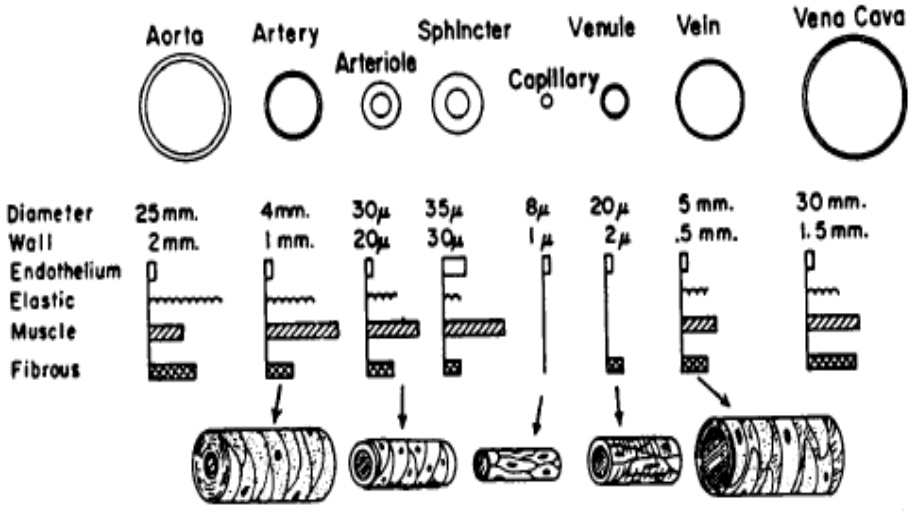

Figure 1.14 Composition of the arterial and venous wall in the systemic circulation.(Rushmer 1972)

1.8 Physiological aspects

1.8.1 Pressure and flow

The heart is a pulsatile pump, generating pressure and flow waves travelling throughout the circulatory system. A typical aortic pressure and flow waveform for one cardiac cycle is depicted in Figure 1.15.

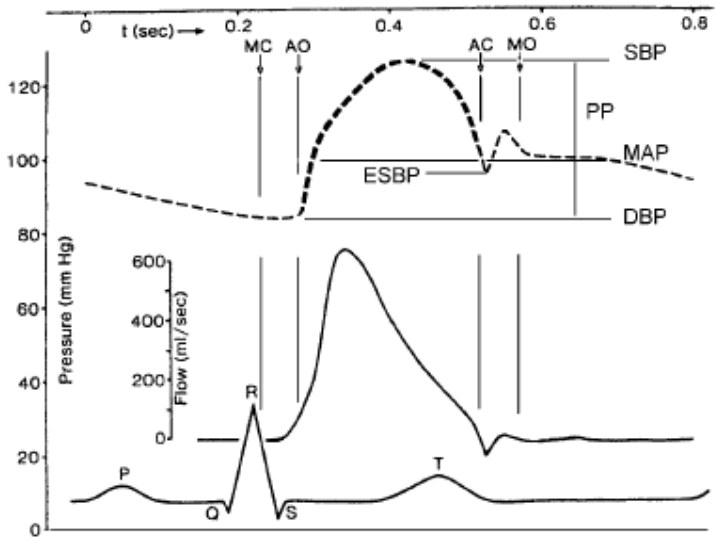

Figure 1.15 Aortic pressure and flow wave for one cardiac cycle at the aortic valve.

The timing of these arterial pressure and flow waveforms with respect to the contraction and relaxation of the heart can be read from the ECG. Important characteristics of the pressure waveform are: the peak of the pressure curve, called 'systolic blood pressure' (SBP, normal value typically around 120 mmHg), the mean arterial pressure (MAP), and the minimum of the pressure curve or 'diastolic blood pressure' (DBP, normal value typically around 80 mmHg). The difference between SBP and DBP is called pulse pressure (PP). The minimum corresponding to the closing of the aortic valve (AC), called the 'dicrotic notch', has a pressure value referred to as 'end systolic blood pressure' (ESBP).

When the pumping characteristics of the heart change (e.g. increased HR or SV during exercise), the shape of pressure and flow waves varies as well. In stationary heart conditions, the waveforms at one location can be regarded as steady-state oscillations. For example, the pressure and flow waveforms at the aortic valve depicted in Figure 1.15 will look exactly the same for every cardiac cycle provided that no metabolic changes occur. However, the waves do change shape as they travel along the arterial tree, as shown in Figure 1.16, and the reasons for this lie in the geometric and elastic characteristics of the vascular tree.

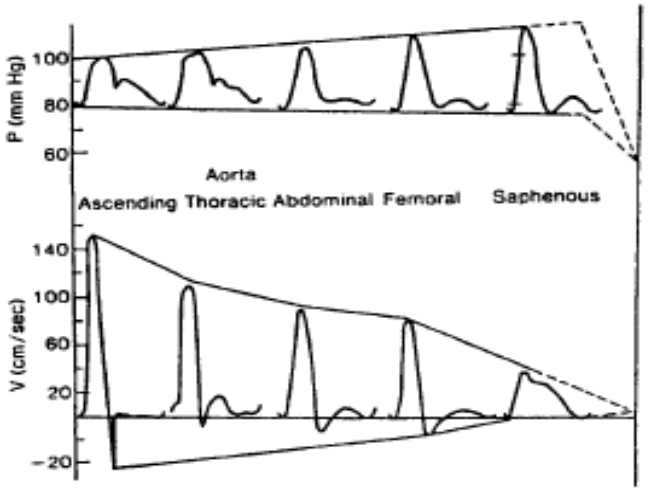

Figure 1.16 Evolution of pressure and flow wave along the arterial tree.(McDonald 1960)

1.8.2 Compliance

Figure 1.17 shows an illustration of the famous Windkessel theory by Stephen Hales (1733), who made an analogy with the buffer reservoir or compression chamber (Windkessel in German) from fire engines and the elastic recoil of vessel walls. Otto Frank (1899) transformed this analogy later on in a quantitative model.(Hales 1733; Frank 1899) Similar to how the compression chamber from the fire-engine induces dampening on the pulsatile output to provide a more continuous flow, the compliance of the arterial wall allows to store a certain blood volume during ejection that is subsequently released during the filling phase when the aortic valve is closed.

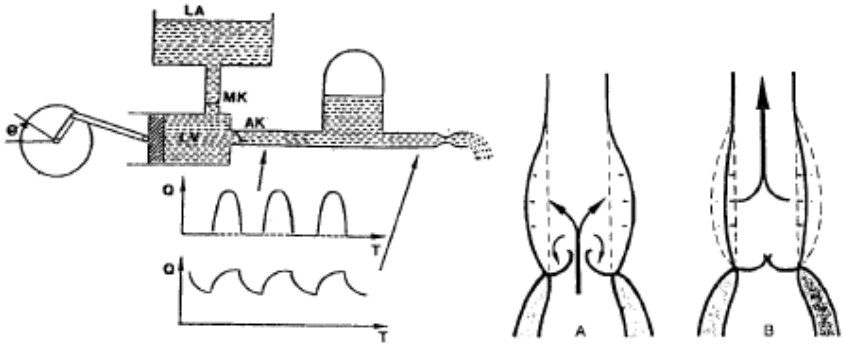

Figure 1.17 The Windkessel effect: a fire engine compression chamber (left) and ejection of blood from the ventricle into the aorta (right).(Verdonck 1993)

Since elastic properties of the vessel wall change from compliant to stiff when moving distal from the heart, the arteries lose their buffer capacity to dampen out the waves, which together with wave reflections results in steeper waveforms towards the periphery.

1.8.3 Resistance

Due to geometric tapering, arterial branches get smaller and smaller, and the resistance of an artery against perfusion increases towards the periphery. However, because of the phenomenon that the combined cross-sectional area of the daughter branches is always slightly bigger than the offspring cross-sectional area, there is in fact perfusion redistribution at every junction as shown in Figure 1.18. One can notice that as the vascular tree expands, mean pressure drops slowly until the arterioles and capillaries are reached where the largest pressure drop occurs. The mean velocity curve is slightly descending along the aorta, goes down more rapidly in the peripheral arteries and takes a steep fall at the height of the vascular beds, where the total cross-sectional area has enlarged greatly compared to central aortic site.

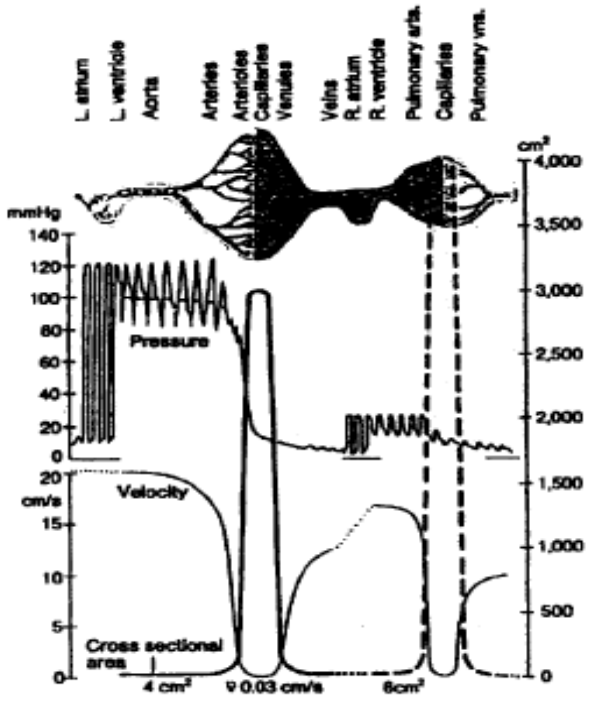

Figure 1.18 Mean pressure and velocity curves in the systemic circulation.(Schmidt and Thews 1989)

1.8.4 Wave reflections

Due to the non-uniformities in the vascular tree in terms of geometry and elasticity, reflection points are induced in this branched closed loop system and backward travelling pressure and flow waves develop. The reflection of waves is in fact the prominent factor determining their final shape. As shown in Figure 1.19, a pressure wave is actually built up by a forward wave, added with the backward travelling reflections, while the flow wave is built up by the forward wave subtracted with reflected components.(Westerhof, Sipkema et al. 1972; Li 1986; Nichols, O'Rourke et al. 1987)

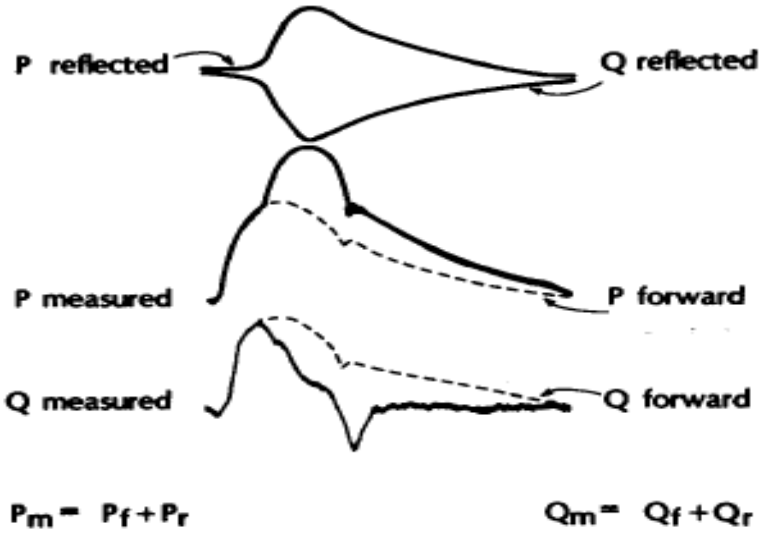

Figure 1.19 Decomposition of arterial pressure and flow in forward and reflected waves.(Nichols, O'Rourke et al. 1987)

1.8.5 Aging and pathological conditions

Under the influence of aging or pathological conditions such as 'hypertension' (high blood pressure) and 'atherosclerosis' (narrowing of the vessel lumen due to deposits of several substances, generally called 'plaque'), the waveforms change shape as well but this will not be discussed further. As an illustration, the aortic pressure and flow waveforms of an old and young subject are shown in Figure 1.20. The augmentation index (Aix), introduced in the 1980s as a simplified interpretation of the effect of wave reflections (Murgo, Westerhof et al. 1980), is defined as the ratio of ΔP and PP, with ΔP being the difference between SBP and the pressure Pi at the inflection point:

$$Aix = \pm \frac{\Delta P}{PP}$$ **Eqn. 1.2**

Type A waveforms (old subject) have an inflection point before the point of SBP, and result in a positive Aix, while for type C waveforms (young subjects) the inflection point occurs later than the point of SBP, and the Aix has a negative value.

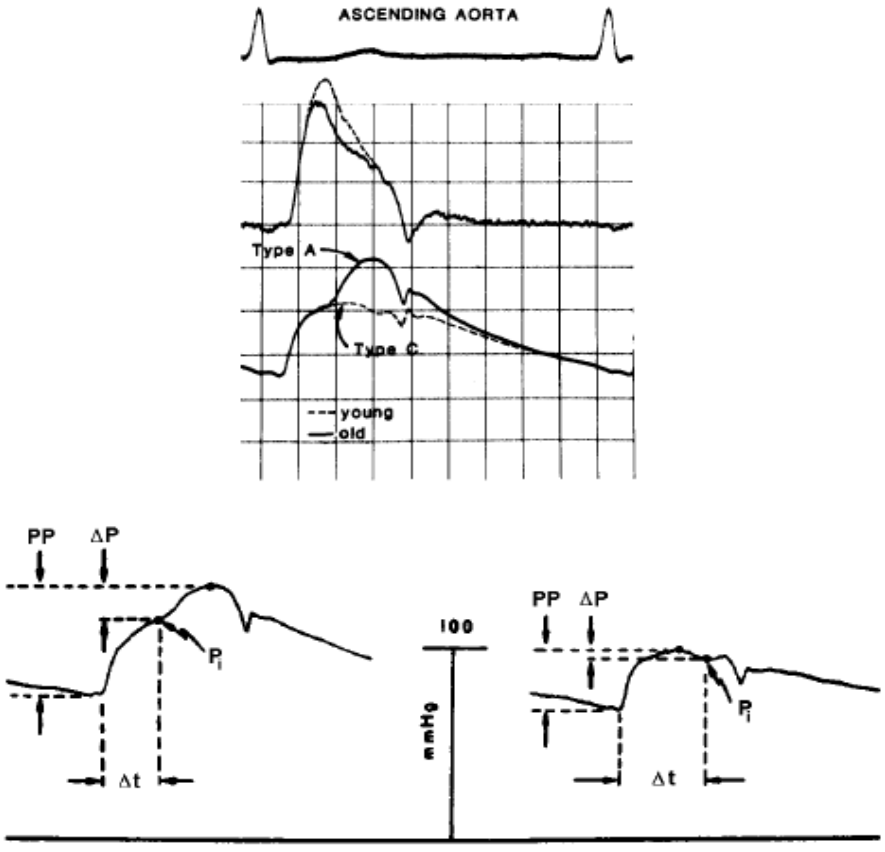

Figure 1.20 Type A and type C waveforms characterizing an older and younger person, respectively. Type A waveforms induce positive Aix indices, type C waveforms correspond to negative Aix indices.(Murgo, Westerhof et al. 1980; Nichols, O'Rourke et al. 1985)

Chapter 2

2.1 Introduction*

In the last years, Laser Doppler Vibrometry (LDV), has been applied in biomedical areas, due to its advantageous metrological characteristics. In particular, the high accuracy (about 1% of reading), high resolution (displacement resolution about 8 nm) and the non-contact nature of this technique make these instruments suitable for diagnostic purposes) and in-vivo tests [5,6,7].

In virtue of the above mentioned facilities, LDV could be an interesting alternative investigational methodology to be tested in the study of cardiac function (in terms of compression waves generated by the heart during its movement and transmitted to the chest wall), the monitoring of heart rate being a typical task in clinical environment for a great variety of patient's condition. [10]

In virtue of the above mentioned facilities, laser techniques could be an interesting alternative investigational methodology to be tested in the study of cardiac mechanics, in terms of displacement cardiology. In fact, the monitoring of heart rate is a typical task in clinical environment for a great variety of patient's condition. The possibility to obtain this information without any contact with the patient represents a future tool in many fields also outside of the clinics. In fact generally this task cannot be accomplished when patient's condition determine impairment of their health if contact with skin or any other surface has to be avoided, (e.g. severely burnt subject), or when the type of functional situation e.g. such as the case of people with (e.g. magnetic resonance imaging analysis) or people within confined environment (such as hyperbaric chamber) do not allow to put any sensor or electrodes within the examination environment. In all these situations an alternative method to the typical one must be provided to monitor heart rate activity at least from the point of view of the beat rate, with respect to heart rate obtained by normally using continuous electrocardiographic records.

The sensitivity of the proposed of the optical Vibrocardiography (VCG) (for displacement cardiography evaluation) to perform heart rate variability analysis as the ECG. HRV was already investigated and represents a quantitative marker of autonomic activity, and a powerful tool in the recognition of the relationship between the autonomic nervous system and cardiovascular mortality, including sudden cardiac death.[8]

Also the effect on the signal of the measurement position respect to the chest wall as well as the effect of the surface characteristics on the measured signal were evaluated and results show that the effect of the skin surface on the vibratory signal is an amplitude reduction with respect to the

VCG traces measured from an "optimal" surface, i.e. a 2 mm2 retro-reflective tape applied on the skin. Moreover, VCG traces measured directly from skin are affected by drop-out, but it was demonstrated that a strategy for vibrometric signal filtering including the implementation of tracking filters will allow drop-out effects avoidance .

2.2 Measurement principle

The study of displacement cardiography was performed using a single-point laser Doppler vibrometric (LDV) system. The LDV technique may accurately measure point-by-point surface velocities using interferometric techniques [1,4]. This allows to record the time history of the velocity on an acquisition point. Modern LDVs may work with a maximum frequency in the range of some tens of MHz, and with a lower limit of less than one Hertz. These features make the LDV an ideal instrument in applications where it is impossible or very difficult to use standard vibration measuring devices, such as accelerometers that, in some cases, may significantly load the structures under measure, and/or may even damage surfaces on which they are applied.

A laser Doppler vibrometer is based on the principle of the detection of the Doppler shift of coherent laser light, scattered from a small area of the vibrating specimen: surface vibrations induce a Doppler frequency shift on the impinging laser beam, and this shift is linearly related to the velocity component in the direction of the laser beam.

In this way it was established a linear connection between laser beam frequency variations and velocity and displacement values. The relationship of the Doppler frequency shift f_D and the phase change Φ introduced into the measurement beam, with the vibrational velocity v and displacement d, respectively, are expressed by:

$$f_D = 2\frac{v(t)}{\lambda} \qquad (1)$$

$$\Phi_D = 4\pi\frac{d(t)}{\lambda} \qquad (2)$$

with λ being the wavelenght of the laser light. Therefore, vibrational velocity and displacement can be obtained from Eq. (1) and Eq. (2), respectively. As the Doppler shifts are usually very small when compared to the laser fundamental frequency (1 part out of 108, typically), the only way to appreciate such small quantities is to use interferometry, so that high frequency oscillations are reduced to much lower values that can be dealt with by standard electronics. In the present study we used a single-point, direct beam laser Doppler vibrometer (Polytec GmbH, Germany) incorporating a Mach-Zender interferometer, which allows the measurement of both the vibrational velocity and displacement. Figure 1 shows the diagrammatic sketch of the optics of a laser vibrometer, in which a coherent laser beam at frequency f_0 is splitted into two equal beams (passing through a beam splitter).

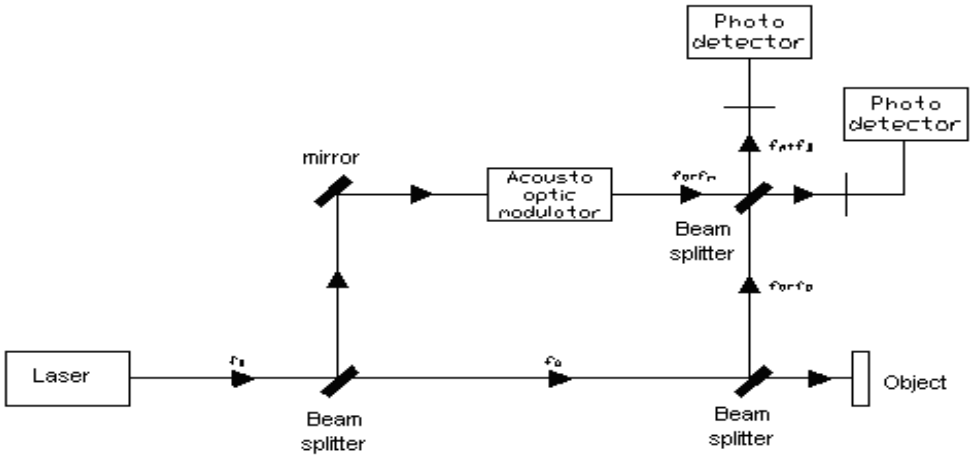

Figure 2.1 : Sketch of the optics of a typical laser vibrometer

One of the beams, i.e. the measuring beam, is focused on the vibrating object, the other one stays in the laser head and it is used as reference beam. After being reflected from the surface of the (moving) object, the measuring beam re-enters the laser head and is recombined with the reference beam. Surface displacement varies the optical path difference between the two laser beams and this results into a phase lag varying with vibration velocity: due to the Doppler effect, it is frequency shifted as $f_0 \pm f_D$ before to interfere with the reference beam. Demodulating the Doppler signal it is possible to extract the amplitude of v (see Eq. (1)) The information on the direction of the surface displacement can be extracted by means of electro-mechanical-optical shifting of the frequency of the reference beam (center frequency f_m) by means of an acousto optic modulator, the Bragg cell: in this way, from the original laser beam two beams at frequency difference f_m are obtained. Due to the low pass filter of the interferometry, which cut off the very high frequency f_0, a signal with shifted heterodyne frequency $f_m \pm f_D$ can be finally revealed at the photo detectors.

2.3 Generical experimental set up

The LDV system performs measurements of velocity, i.e. the ones carried out in the first investigation stage , with a resolution up to 0.5 μm/s. The laser head was placed at about 1.5 m from the subject chest wall. In order to simplify the measurement procedure and in order to optimise the quality of the signal (increase of the S/N ratio of the vibratory signal) a small (about 2 mm^2, weight < 1 g) adhesive retro-reflective tape was placed on the chest wall.

Short-term recordings (5 minutes) were carried out on ten healthy human subjects (five males aged from 24 to 30 years; five females aged from 23 to 30 years) at rest, lying supine on a bed. Figure 2.2 shows both the experimental set up, and the laser head positioning and the measurement point on the chest wall for VCG signal recording.

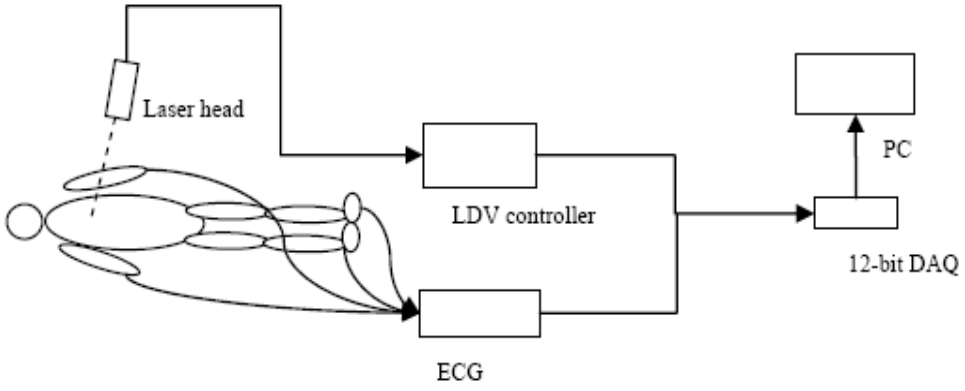

Figure 2.2 : schematic of the experimental set-up

The LDV system has a maximum velocity range of 10 m/s, a 0 to 350 kHz bandwidth, a resolution of about 1 µm/s and an accuracy in the order of 1%-2% of RMS reading. No filtering was set for the chest vibratory signals recording.

Laser power is less than 1 mW, so that no special safety measures are required, but nevertheless also with such low power levels working distances of some tens of meters are possible. Electrocardiographic traces and the velocity of vibration of the chest wall, i.e., the VCG were simultaneously recorded. The ECG is connected as in the classical configuration for the recording of the three fundamental leads. An analog-to-digital 12-bit acquisition board, together with a custom-made software program developed in a LabVIEW® environment (National Instruments, Usa), have been used to analyse and store the signals. The analog inputs were sampled at 1 kHz. A PC (Pentium IV) was used both for setting of the A/D acquisition board and for providing the storage and processing of the experimental data.

2.4 Data Analysis

From the recordings on subjects undergoing measurements, it was investigated the physiologic relationship of the ECG to the vibratory signal VCG in terms of heart rate variations by some of the

method proposed by the guidelines on standards of heart rate variability (Task Force of the European Society of Cardiology, 1996 [11]). HRV indexes were calculated for both linear and non linear quantitative description (i. e., mean value of time series, total spectral power, spectral power ratio between frequency bands, spectral entropy, fast variability index).

The measurement method is based on the assumption that the peak of the vibratory signal, measured from the chest wall, takes place in consequence of the cardiac muscle contraction triggered by the electrical signal measurable by the use of the electrocardiograph. We used heartbeat fiducial timing point provided by ECG recordings, i.e., the time of occurrence of the major local extremum of a QRS-complex (the time of the R-wave maximum): these fiducial points were obtained automatically [12]. As fiducial point in the VCG signal it was selected the first local maximum value (labelled V peak) in the vibratory trace that follows the R-wave maximum in the ECG trace (the rationale is that VCG signal is responsive to changes in myocardial contraction induced by electrical activation). This was done by using a proper own MATLAB (The MathWorks, USA) code for peak detection. [13]

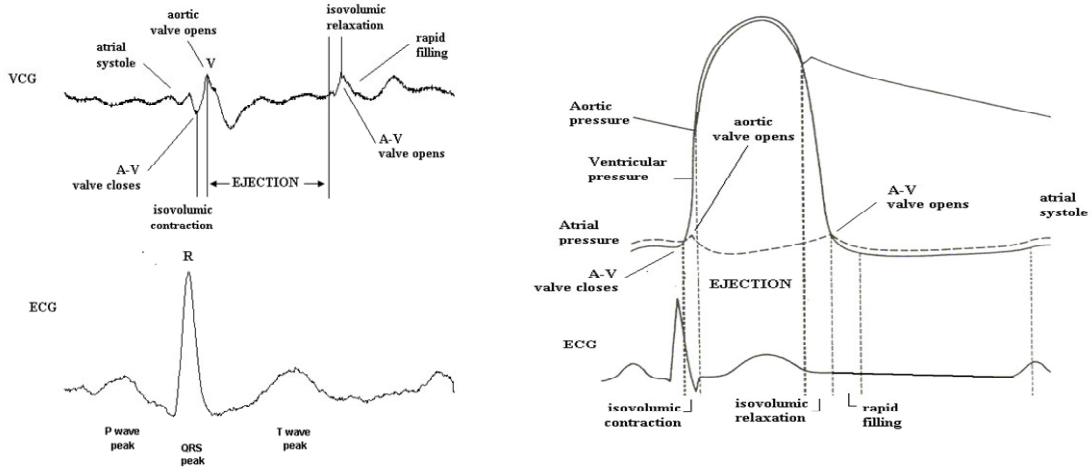

Figure 2.3 Typical human, one beat, vibrocardiogram (VCG), together with the simultaneously recorded ECG II-lead output. A simplified sketch of typical ECG, arterial, ventricular and atrial pressure waveforms is also shown.

A typical VCG beat is shown in Figure 2.3 together with the II-lead output of the ECG for the same subject. A simplified sketch of typical ECG, arterial, ventricular and atrial pressure waveforms is also shown. In order to obtain a better understanding of the VCG waveform recorded during each cardiac cycle, it was compared a VCG recorded heart beat with the atrial pressure waveform. The rationale for this choice is that we pointed the laser beam to measure parasternal chest wall movements, i.e., a position where the recorded compression waves can be primarily abscribed to the atrial activity, in a normal patients. The analysis of figure 2.3 confirms this hypothesis, clearly showing that the measured VCG closely resembles the tipical atrial pressure waveform (the comparison has to be done using the ECG trace to trigger cardiac events). The consistent similarity

in wave morphology exhibited by VCG and atrial pressure allowed to identify diastolic and systolic VCG points and events: atrio-ventricular (A-V) valve closure; isovolumic contraction phase; opening of the aortic valve (V); ejection phase; isovolumic relaxation phase; atrio-ventricular valve opening; rapid ventricular filling; atrial systole. Figure 2.3 shows that cardiac events on VCG recording are delayed, with respect to ECG, confirming the assumption that VCG signal is responsive to changes in myocardial contraction induced by electrical activation.

Starting from the above basic assumption, after the laying of the laser beam, ECG (obtained from the II-lead output) and VCG contemporary recorded were retrieved afterwards to measure the consecutive RR peak and vibrocardiographic (VV) intervals, and tachograms were built on them.

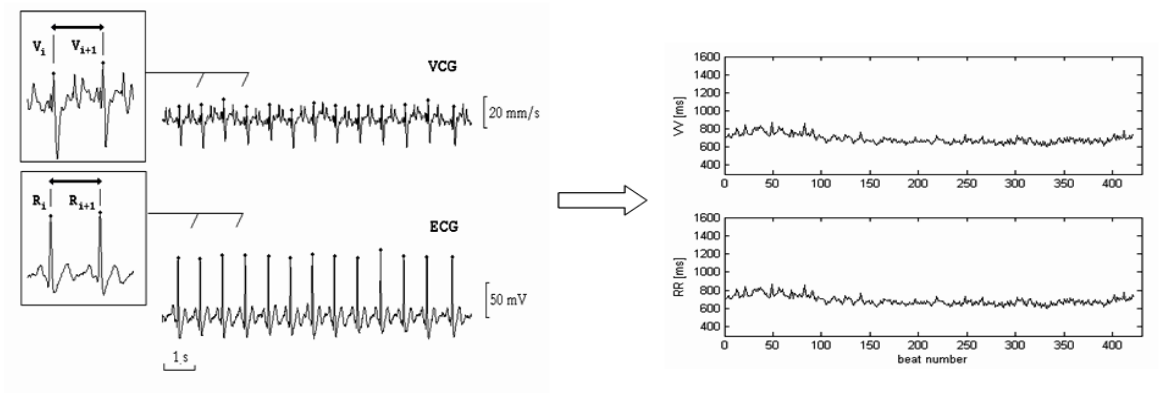

Figure 2.4 : example of tachogram construction

As an example of the time series extracted from synchronous ECG and VCG recordings, figure 2.4 shows the RR and VV tachograms relative to one subject: notably, there is high coincidence in the trend exhibited by the two time series

Before this, ECG signals were filtered with two median filters to remove the baseline wander: as also recently proposed by de Chazal et al. [13], each signal was firstly processed with a median filter of 200-ms width to remove QRS complexes and P-waves, the resulting signal was then processed with a median filter of 600 ms width to remove T-waves. The signal outcoming the second filter operation contained the baseline of the ECG signal, which was then subtracted from the original signal to produce the baseline corrected ECG signal.

Spectral analysis

A non parametric method with the Fast Fourier Transform algorithm was applied for the calculation of the power spectral density (PSD). VCG an ECG tachograms were resampled at 2 Hz [14], and

linearly interpolated. Then, both RR and VV time series were normalized (by subtracting their mean value and then dividing for the latter), and a Hanning window was applied in the time domain to reduce leakage. After the square of the fast Fourier transform was computed, the power spectrum was obtained after multiplying each frequency component by 2.66, to correct for Hanning window .Three main power spectral components are distinguished in a spectrum calculated from short term recordings: very low frequency (VLF, ≤ 0.04 Hz), low frequency (LF, 0.04 to 0.15 Hz), and high frequency (HF 0.15 to 0.40 Hz) components. From the PSD of both RR and VV tachograms total spectral power and LF/HF spectral powers ratio were calculated and compared. Moreover, we calculated also spectral entropy a descriptor of heart rate variability phenomenon that can be used as a measure of system complexity .To do this, PSD from ECG and VCG recordings extracted tachograms were normalised with respect to the total spectral power, then Shannon channel entropy was calculated on them, to have an estimate of spectral entropy of the process, as:

$$E = \sum_{i=1}^{N} p(f_i)\log\left(\frac{1}{p(f_i)}\right) \qquad (3)$$

where $p(f_i)$ is the normalised PSD value at frequency f_i, and N the number of spectral components. As stated by Acharya et al [15]. the entropy can be heuristically interpreted as a measure of uncertainty about the event at frequency f.

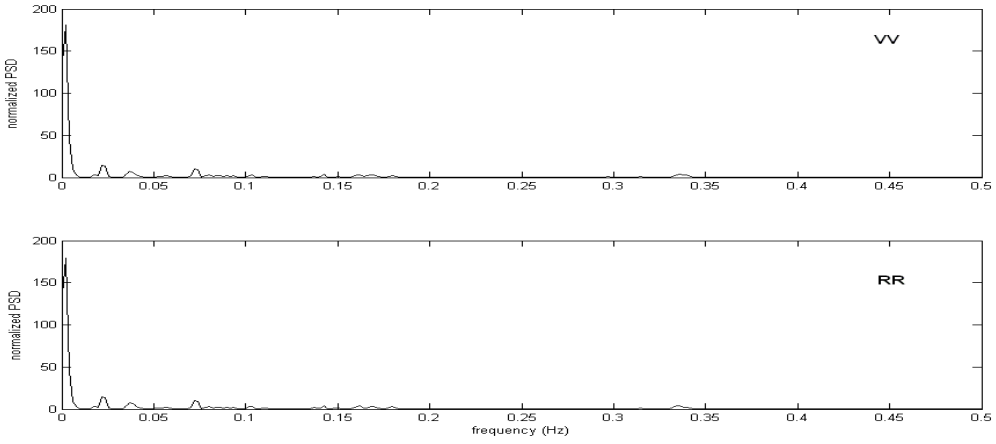

Figure 2.5 : Example (relative to one of the monitored subjects) of power spectral density (PSD) from RR and VV tachograms. The PSD is normalized to the total spectral power

As an example of PSD extracted from synchronous ECG and VCG recordings, figure 2.5 shows the RR and VV power spectrum density relative to one subject: notably, there is high coincidence in the trend exhibited by the two powers

Poincaré plot analysis

Owing to the insensitivity of traditional analysis techniques to abrupt, aperiodic changes in heart rate dynamics, dynamic methods (e. g., beat-to-beat analysis techniques) have been developed to uncover stochastic or nonlinear features in heart rate behaviour. It was shown that the normal heart rate is not regular, but varies from beat to beat in an irregular manner

Among many tools for the studies of nonlinear dynamics of heart rate, the Poincaré map of RR intervals in the ECG signal deserves special attention: in recent years, it has been massively applied to many clinical studies of HRV.[16]

The Poincaré plot is a technique taken from nonlinear dynamics, and portrays the nature of interval fluctuations in a time series. A Poincaré plot consists in a scatter-graph built up plotting samples X_{i+1} versus X_i, displaying the relationship between a point and its consecutive point in a time series. By inspecting the geometric distribution of the map points, information can be obtained about dynamic stability of periodic systems, and presence of deterministic chaos can be put in evidence. The plot provides summary information as well as detailed beat-to-beat information on the behavior of the heart. Poincaré mapping technique, shown to be useful for the analysis of dynamic systems displaying periodic/quasi-periodic behaviour, relies on synchronized events, i.e., discrete time observations of the activity of the system under investigation. Poincaré plot analysis, being a quantitative-visual technique, is a powerful tool in the investigation of HRV, with the shape of the plot categorizable into functional classes that indicate the degree of the heart failure in a subject. It must be born in mind, in the analysis of ECG related Poincaré maps, that they are expected to assume a non-structured single cluster of points configuration, in normal subjects. In fact, nonlinear dynamics considers the Poincare plot of an ECG as the two dimensional reconstructed RR interval phase-spaces, which is a projection of the reconstructed attractor describing the dynamics of the cardiac system. The RR intervals (consecutive intervals, in general) Poincaré plot typically appears as an elongated cloud of points oriented along the line-of-identity. The shape of the Poincaré plot is a measure of chaotic content in the investigated data. For short time recordings, the dispersion of points perpendicular to the line-of-identity reflects the fast beat-to-beat variability in the data .

On the Poincaré plots of RR and VV intervals fast beat-to-beat variability was quantified by computation of the standard deviation (SD_1) of the distances of the points perpendicular to the line-of-identity ,expressed as:

$$D = \frac{1}{N}\sum_{i=1}^{N}\frac{\left|y_i - (mx_i + q)\right|}{\left(1+m^2\right)^{\frac{1}{2}}} \qquad (4)$$

where (x_i, y_i) are the coordinates of a point in a Poincarè map, and $m=1$ and $q=0$ are parameters describing the line-of-identity (angular coefficient and x axis intercept, respectively). In fact, the dispersion of points perpendicular to the line-of-identity reflects the level of short term variability .

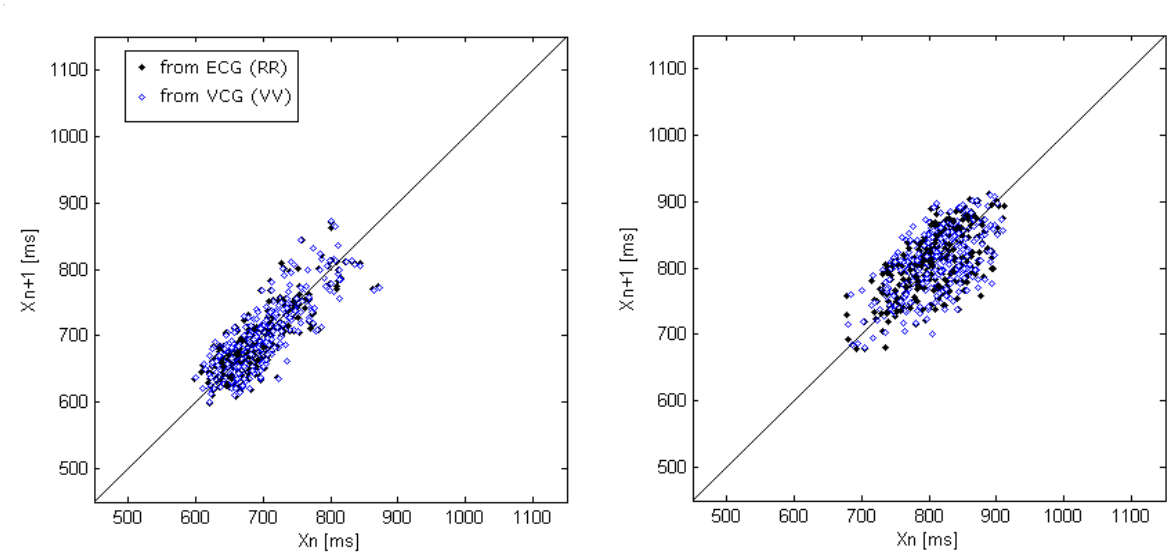

Figure 2.6 shows the Poincaré plots (X_{n+1} *vs* X_n) both for RR and VV time series, relative to two monitored subjects, a female (subject 7) and a male (subject 1).

Being Poincaré plot analysis a quantitative-visual technique, it is evident from a visual inspection of figure 2.6 that Poincaré maps from VCG and ECG assume the same, overlapped shape, i.e., an elongated cloud of points oriented along the line-of-identity.

Statistical analysis

The agreement between ECG and VCG methods measures was evaluated from two aspects: (i) agreement when these techniques are used for cardiac rate monitoring, assessing intra-individual variations on RR and VV time series; (ii) agreement when on the RR and VV time series HRV

indices are calculated. To examine the former agreement, 10 beats-to-10 beats VCG rate (VV) and heart rate (RR) for 5 min segments were compared within each subject, and the agreement between corresponding values were evaluated with the Bland and Altman test [17]: for the cardiac rate measured with the two methods, the difference against their mean value is plotted. This approach allows to evaluate if two methods for clinical measurement are interchangeable.

To examine the latter agreement, HRV descriptors calculated on intra-individual RR and VV synchronous time series were compared in terms of percent differences (the RR time series being the reference values), i.e., if X_{VV} is the quantity computed on VV series, and X_{RR} the corresponding quantity on the RR series, the percent difference is:

$$X(\%) = 100 \cdot \frac{(X_{VV} - X_{RR})}{X_{RR}} \qquad (2)$$

The positive or negative value in the percent difference tells if the quantity computed on VV time series is greater or lower than the corresponding quantity on RR time series.

In Figure 2.7 it is possible to appreciate an example of a Bland and Altman plot for two individuals investigated. It puts in evidence that provided differences within 2 standard deviations from the mean difference interval are not be clinically important, for all individuals

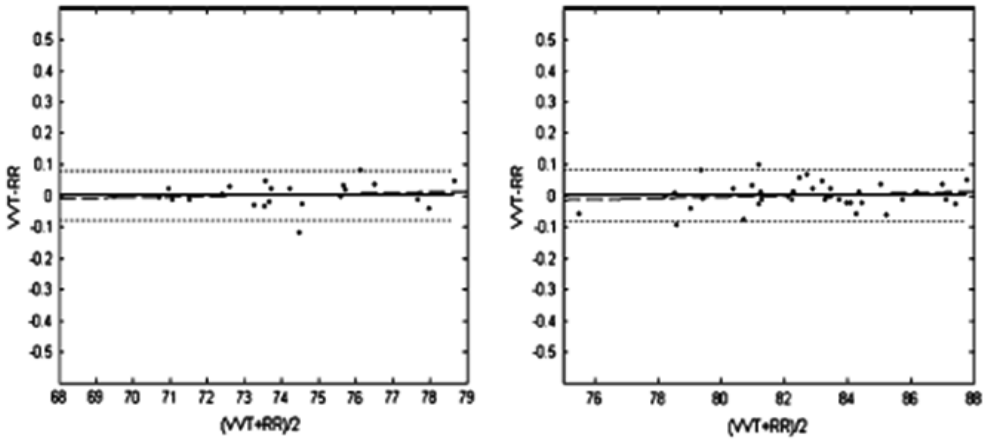

Figure 2.7 : Bland–Altman plots relative to two monitored subjects, to check differences in the assessment of the cardiac rate between ECG and VCG methods. The test was carried out on 10 beats-to-10 beats VCG rate (VV) and heart rate (RR)segment values, averaged over the entire 5 min recording length. Unit measure for both the axis is bpm. (continuous line) mean;(dotted line) ± 2SD; (dashed line) linear regression line.

Table 1 summarizes the results of the Bland and Altman test in terms of bias and of the Pearson's product moment correlation, R, which measures the strength of linear relationship between the two sets of data..

Subject number	Gender	BIAS[bpm]	R
1	M	0.0118 ± 0.118	0.087
2	M	0.003 ± 0.040	0.127
3	M	0.001 ± 0.087	-0.229
4	M	0.010 ± 0.053	0.260
5	M	-0.005 ± 0.084	-0.206
mean value* (M)		0.006	/
6	F	-0.033 ± 0.162	-0.159
7	F	0.000 ±0.044	0.234
8	F	-0.000 ± 0.046	0.019
9	F	0.001 ± 0.041	0.138
10	F	0.041 ± 0.149	-0.114
mean value* (F)		0.015	/

Table 2.1 – Results of the Bland - Altman test depicted in figure 7 in terms of bias and of the Pearson's product moment correlation, R, which measures the strength of linear relationship between the two sets of data. We remind that for each individual we applied the Bland - Altman method on the 10 beats-to-10 beats VCG rate (VV) and heart rate (RR) segment values. We can observe absence of a consistent bias, no proportional error in cardiac rate assessed by VCG, with respect to ECG, and no dependence of the difference between the two methods by the beat duration

Table 1 confirms the absence of a consistent bias (0.015 bpm mean bias for females, 0.006 bpm mean bias for males), no proportional error in cardiac rate assessed by VCG, with respect to ECG (linear relationship between means and differences assessed by very low R values both for females and males), and no dependence of the difference between the two methods by the beat duration. Results from table 1 and figure 2.7 state that we could use the two measurement methods interchangeably, for cardiac rate monitoring

2.5 Measurement issues

In this part measurement concerns will be described, some example of measurement on 4 healthy subject are reported and the effect of the position of the site of measurement on the chest wall will be discussed as well as the effect of the surface characteristics on the measured signal (it will reported the signal characteristics with and without adhesive patch or other means attached to the skin), in order to give an idea of the limits of the technique, in the perspective of its clinical application, in the future.

Surface issue

In order to evaluate the quality of the signal (increase of the S/N of the vibratory signal), a small adhesive retroreflective tape (3M) of 2 mm2 was placed on the skin in correspondence to measurement point. The effect of the presence of the reflective tape, in conjunction with the tracking filter was tested. Figure 2.8 shows 30 s recording of the vibratory signal performed in absence of reflective patch (i.e., pointing the laser beam directly on the skin) and without tracking filter: it is noticeable the presence of multiple signal drop offs.

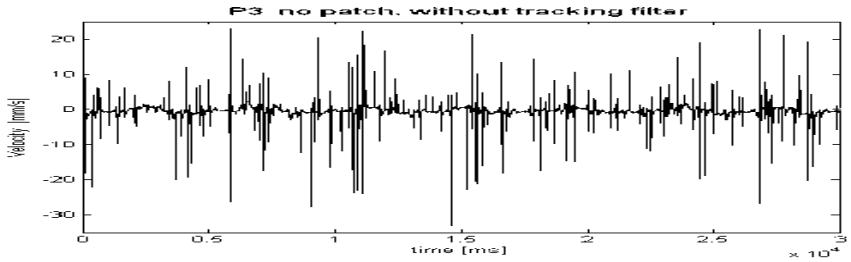

Figure 2.8 : VCG signal (30 s) measured on point 3 without retro-reflective patch and tracking filter

A remarkable reduction in the presence of drop out is obtained both by using the retro-reflective tape, and by applying the filtering strategy, as depicted in figure 2.9.

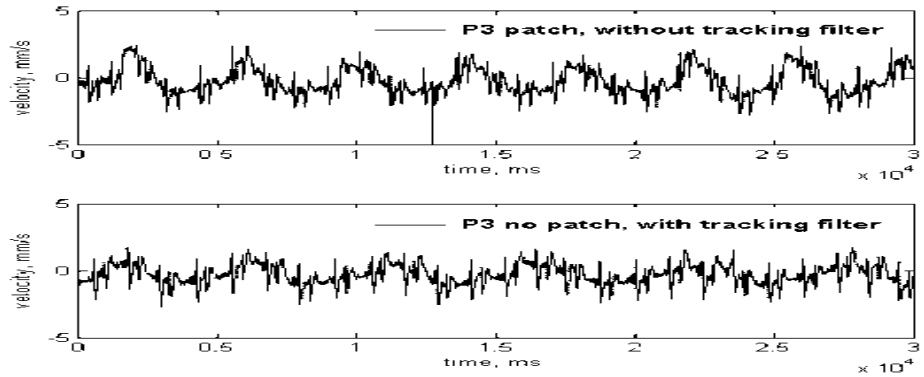

Figure 2.9 : VCG signal (30 s) measured on point 3 with and without the auxilium of the retro-reflective patch, with and without the tracking filter.

Figure 2.9 shows the feasibility to carry out the VCG analysis without retro-reflective patch. In case the VCG analysis is carried out without the use of the retro-reflective tape, it appears necessary to use the special tracking filter of the LDV controller in order to reduce the drop-out of the velocity signal .

The use of an adhesive retro-reflecting tape placed on the chest wall strongly reduce the onset of the typical drawback of the presence of a drop-out phenomenon on the vibrometric signal . In fact, the

real problem to solve when it was carried out VCG measurements was not in a significant degradation in the signal-to-noise ratio when the laser beam is pointed directly on the skin, .but in the presence of drop-out effect in the recorded velocity signal. The technique by which the vibrometer operates results in occasional velocity drop-outs, always estimating the velocity response closer to zero than reality. These drop-out areas occur more predominantly at points of maximum velocity response with small rotational components.

Alternatively, points exhibiting minimum velocity response with large rotational components are less susceptible to the noise**.** Strean et al. [18]assessed that this laser noise can be defined as "biased low", due to the fact that drop-out effects in the velocity signal produce absolute velocity data lower than similar velocity signals which do not contain drop out.

Probably the presence of drop-out in the VCG signal when the retro-reflecting tape is not used is due to small tilting movements of the chest wall (the movement of the cardiac displacement is not unidirectional) and, above all, by the fact that the specimen is not planar, i.e., in the small region pointed by the laser beam the chest wall has a finite radius of curvature, and the unavoidable small displacements of the chest surface not in the direction of the laser beam have effects similar to the ones generated by small tilting. As mentioned above, these small rotational components in the motion elicit drop-out areas predominantly at points of maximum velocity response. The presence of the small retro-reflecting tape on the chest plays the role to make the specimen more planar, thus avoiding the onset of drop-out effects. The problem of the signal drop-out in laser Doppler vibrometry is typically overcome making use of electronic tracking filters, as testified by the results shown in figures 2.8, 2.9

Measurement location

Spectral analysis and wavelet decomposition were performed on VCG traces, in order to assess, if any, possible changes in the response from four different positions on the chest (figure 2.10)

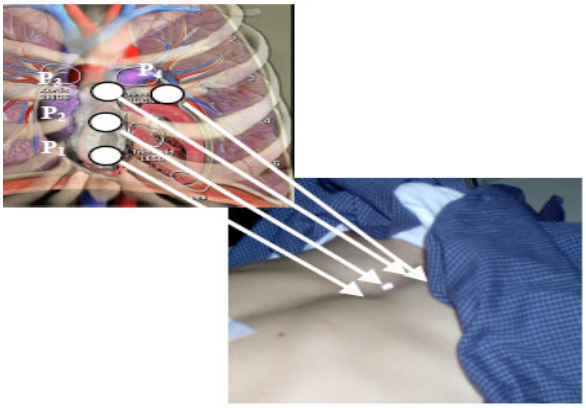

Figure 2.10 : visual description of the point evaluated

Tests were carried out on healthy young subjects (2 females, 2 males, aged 25 – 30 years) lying supine on a bed at resting. The head of the laser Doppler vibrometer was positioned vertically respect to the subject chest wall. Four different measurement points have been studied: P1 (low stern,), P2 (medium stern), P3 (high stern) and P4 (3 cm from P3, on the left).

As for spectral analysis, the power spectral density was calculated by applying the Fast Fourier Transform (FFT). The wavelet decomposition allowed a multiresolution analysis to be performed. We remind here that the continuous wavelet transform of a signal *f(t)* is defined as :

$$W_f(s,\tau) = \int_{-\infty}^{\infty} f(t) h^*_{s,\tau}(t) dt \qquad (1)$$

where *hs,τ(t)* is a set of basis functions (wavelets) and * is the complex conjugate [19]. The wavelets are generated from a single wavelet *h(t)* by scaling and translation, according to the following relationship:

$$h_{s,\tau}(t) = \frac{1}{\sqrt{s}} h\left(\frac{t-\tau}{s}\right) \qquad (2)$$

being *s* the scale factor and τ is the translation. In the present paper a discrete wavelet transform was implemented, built up with orthogonal dyadic functions, that can be expressed as:

$$h_{i,k}(t) = 2^{-\frac{i}{2}} h(2^{-i}t - k) \qquad (3)$$

VCG signals were decomposed in twelve levels by means of the mother wavelet function Daubechies 7[20], and the coefficients derived from the decomposition were implemented to obtain the signal details (referred to D1–D12). Each sub-band shows a frequency bandwidth which is the half with respect to the previous level and double with respect to the successive one, starting from the upper frequency limit of the first decomposition level which is the half of the sampling rate.

Signal details were processed and the instantaneous power for each decomposition level was computed as:

$$P_j = D_j^2 \qquad (4)$$

where *Dj* represent the reconstructed detail signal at the *j-th* level. Relative powers, i.e., the ratio of the power in each selected frequency band with respect to the total power of the VCG recorded trace, were finally calculated by integrating Eq. (4) in each sub-band 8. The VCG traces measured in the 4 different positions on the chest were compared in each sub-band, after wavelet decomposition.

Figure 2.11 shows the power spectral density of the VCG recordings on the four measurement points investigated on the chest wall: all the vibratory traces show a peak between 0.2 and 0.45 Hz, that can be clearly ascribed to the breathing activity.

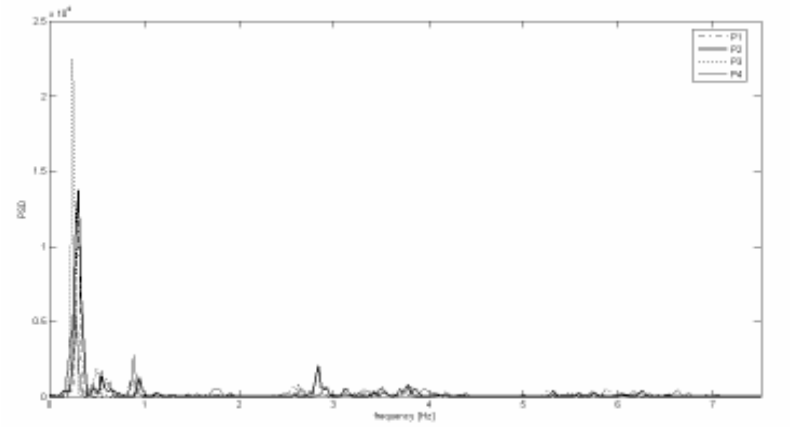

Figure 7 - PSD for point 1, 2, 3 and 4.

Figure 2.11 : power spectrum density for all the four points analyzed

Moreover, lower peaks are present in the spectrum around 1 Hz: these last can be ascribed to the cardiac frequency. Table I summarizes the results of the multiresolution wavelet decomposition of 15 s recordings in the 4 points under investigation.

Sub-Band	P1	P2	P3	P4
D1: 250-500 Hz	3.06E-12	3.55E-12	1.44E-12	4.66E-12
D2 : 125-250 Hz	2.15E-13	5.14E-11	5.50E-10	1.20E-10
D3 : 62.5-125 Hz	4.38E-13	1.37E-10	4.72E-10	4.90E-11
D4 : 31.25-62.5 Hz	7.37E-10	2.09E-10	1.91E-09	5.04E-11
D5 : 15.63-31.25 Hz	5.01E-11	9.59E-09	2.54E-09	1.17E-07
D6 : 7.81-15.63 Hz	1.55E-09	3.22E-08	1.96E-07	1.03E-06
D7 : 3.90-7.81 Hz	3.61E-06	9.99E-07	3.41E-07	2.97E-07
D8 : 1.95-3.90 Hz	7.00E-06	4.26E-06	6.66E-05	1.79E-05
D9 : 0.98-1.95 Hz	8.17E-06	1.76E-04	1.46E-05	1.12E-05
D10 : 0.49-0.98 Hz	4.28E-04	1.24E-04	1.69E-05	9.62E-06
D11 : 0.25-0.49 Hz	6.70E-04	13.11E-04	56.68E-04	12.48E-04
D12 : 0.13-0.25 Hz	1.14E-04	160.11E-04	19.86E-04	1.56E-04

Table 2.2 : Multi-resolution wavelet decomposition of 15 s recordings in the 4 points under investigation.

Relative powers in all the sub-bands were calculated: it is interesting to notice that the greatest values of relative powers are relative to the sub-band D11 (0.25-0.49 Hz) and D12 (0.13-0.25 Hz) related to the respiratory events but sub-bands D9 and D10 include the frequencies of the heart beat and in these sub-bands P1 shows the highest cumulative relative power, so it is possible to conjecture that P1 is the best measurement point .

Comments

Results show that the effect of the skin surface on the vibratory signal is an amplitude reduction with respect to the VCG traces measured from an “optimal” surface, i.e. a 2 mm2 retro-reflective tape applied on the skin. Moreover, VCG traces measured directly from skin are affected by drop-out, but we demonstrated that a strategy for vibrometric signal filtering including the implementation of tracking filters will allow drop-out effects avoidance. Spectral and multiresolution analysis put in evidence characteristics in the VCG signal that are peculiar of the measured position on the chest wall. In particular, from results wavelet decomposition, being a suitable technique for the analysis of non-stationary signals, is eligible to be a valid tool for the investigation of VCG signals.

**The content of this chapter has been published in*

- M. De Melis, M. Grigioni, U. Morbiducci, L. Scalise. Optical monitoring of heart beat . ***Modelling in medicine and Biology****, WIT press 2005 ;181-190. – Book Chapter*

- U. Morbiducci , L. Scalise , M. De Melis , M. Grigioni Optical Vibrocardiography : a novel tool for the optical monitoring of cardiac activity , ***Annals of Biomedical Engineering*** *2007 Jan;35(1) 45-58*

- L. Scalise , U. Morbiducci , M. De Melis A Laser Doppler approach to cardiac motion monitoring effects of surface and position , ***VII Conferenza AIVELA*** *2006*

Chapter 3

3.1 Introduction*

Despite recent advances in its management, the prevalence of heart failure is increasing as the population ages, and heart failure remains a major cause of disability and death. The optimal management of heart failure requires not only its accurate diagnosis, but reliable methods to determine with specificity the hemodynamic abnormalities in individual patients. These determinations will permit the most effective treatment to be selected for each patient. Similarly, it is important to be able to measure the effectiveness of such treatment and to determine whether it should modified in any way. To benefit as many patients as possible, the methods of evaluation of hemodynamic function should be safe, reliable, widely available, and cost-effective. [21]

The assessment of cardiac function is achieved by the detection and analysis of systolic and diastolic heart tones and their temporal relationships to the ECG. The primary acoustic cardiography parameters of relevance for the management of systolic heart failure is LV systolic time (LVST): the interval in milliseconds measured from S1 to S2. This interval is reduced in patients with LV dysfunction.[22]

Accordingly the most important heart sounds are the first and second sounds, or S1 and S2, which demarcate systole from diastole.

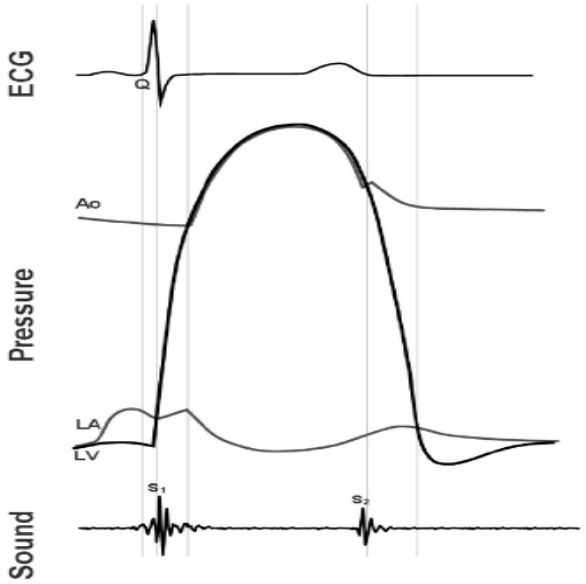

Figure 3.1 : example of normal cardiac cycle

S1 is the sound which marks the approximate beginning of systole, and is created when the increase in intraventricular pressure during contraction exceeds the pressure within the atria, causing a

sudden closing of the tricuspid and mitral, or AV valves. The ventricles continue to contract throughout systole, forcing blood through the aortic and pulmonary, or semilunar valves. At the end of systole, the ventricles begin to relax, the pressures within the heart become less than that in the aorta and pulmonary artery, and a brief back flow of blood causes the semilunar valves to snap shut, producing S2. (figure 3.1)

Although S1 and S2 are considered to be discrete sounds, it is possible to notice that each is created by the near-instantaneous closing of two separate valves. For the most part, it is enough to consider that these sounds are single and instantaneous. However, it is worth remembering the actual order of the closures, because certain conditions can split these sounds into the separate valve components. During S1, the closing of the mitral valve slightly precedes the closing of the tricuspid valve, while in S2, the aortic valve closes just before the pulmonary valve. Rather than memorize this order, if you remember that the pressure during systole in the left ventricle is much greater than in the right, you can predict that the mitral valve closes before the tricuspid in S1. Similarly, because the pressure at the start of diastole in the aorta is much higher than in the pulmonary artery, the aortic valve closes first in S2. Knowing the order of valve closure makes understanding the different reasons for splitting of heart sounds easier.

Cardiac auscultation and the timing of heart sounds have been central to bedside noninvasive diagnosis of heart failure over the past century. Cardiac auscultation began long before Theophile Laennec's fortuitous discovery of the stethoscope in 1818; descriptions of cardiac sounds date back to Hippocrates' writings, circa 400 BC.5 However, it was not until the latter half of the 19th century and the early 20th century, with the description and timing of heart sounds and murmurs and the rise of phonocardiography, that the full potential of cardiac auscultation was realized. During that important time, Carl Pierre Potain described the S3, and Willem Einthoven, Otto Frank, and Carl Wiggers played key roles in the development of modern phonocardiography, with its graphic depiction of heart sounds. Later, through the work of Aubrey Leatham and William Evans in the late 1940s (with the creation of a novel phonocardiogram with the additional capability of recording simultaneous carotid pulse tracings and ECG data) and Weissler in the 1960s (with the correlation of abnormal systolic time intervals with left ventricular [LV] dysfunction), auscultative and phonocardiographic bedside diagnosis came into its golden age .

Within the realm of auscultation and phonocardiography, analysis of abnormalities of systolic time have been among the most useful and best-studied diagnostic tool , expecially in cardiac resynchronization therapy (CRT) , . a fast and cost-effective method of atrioventricular (AV) delay optimization that also fits into the standard pacemaker follow-up workflow is desirable .

Despite the clinical acceptance of echocardiography in CRT optimization, practical aspects such as availability, time, cost, and the need for a well-trained echocardiographer limit the application of AV optimization to only a small percentage of CRT patients. This, in turn, may limit the effectiveness of CRT, since key outcome studies demonstrating the benefits of CRT routinely utilized such techniques of AV optimization. In consequence ,promising, fast, and inexpensive method for device optimization in CRT it is the study of principal cardiac mechanical events , i.e S1 and S2 .[23]

These mechanical processes produce vibrations and acoustic signals that can be recorded from the chest wall. Laser based techniques, allowing non-contact measurements and due to their advantageous metrological characteristics (in particular high resolution) might be alternative to current investigational methodologies. [1,2,8]

The aim of the present study is to go further insight in the characterization of the morphology of optical VCG traces by comparison with synchronously recorded traces accounting for well known events of the cardiac mechanics. In particular, it were chosen ECG and PCG traces, the latter being sensitive to the two major audible sounds in the healthy cardiac cycle: the first one, S1 (mitral and tricuspid valves closure) which occurs at the onset of ventricular contraction and the second one, S2 (aortic and pulmonary valves halting) which is present at the end of ventricular systole.

To compare mechanical and acoustic signals, it was used first a visual inspection to identify heart sounds on VCG trace , then it was calculated S2-S1 , i.e. filling time ; after this stage to go deeper signal processing algorithm was applied , joining:

1) wavelet based multiresolution analysis
2) amplitude envelope calculation.
3) re-calculation of the filling time for comparison

The choice for the method 1 lies in the fact that cardiac mechanics tends to be not stationary, and wavelet transform (WT) is a powerful tool for analysing such kind of signals, because of its compatibility with non-stationary random processes [19]. The good time–frequency localization is the most important advantage that wavelets have over other methods. In particular the capability to extract sub-bands details is the greatest advantage for a powerful feature extraction. Method 2 was applied in order to arrive at reliable morphological comparison, with signal that even if decomposed still have quite different dynamics. Obviously the filling time re-calculation was necessary to stress the technique , in order to have an affordable approach.[24,25]

3.2 Methods

Experimental set-up

A sketch of the set-up is depicted in Figure 3.2. A single-point, laser Doppler vibrometer (Polytec GmbH, Germany) is used to measure instantaneous velocity of the point of the surface where the laser beam is focused [4]. The LDVi laser head was positioned at a distance of about 2 m away from the chest. A Meditron Electronic Stethoscope (Welch-Allyn, U.S.A.) with a commercial ECG embedded on board is used to measure heart sounds and the II lead ECG. The measurement system was used to simultaneously record time histories of 15 s length (VCG, PCG and ECG-II_lead); ECG is used as reference for the identification of events of the whole cardiac cycle. A notebook Intel P4 is used (PC), equipped with a 12-bit A/D (DAQ) data acquisition board (PCMCIA, National Instruments, U.S.A.), with a sampling frequency of 8 kHz. Ten healthy subjects (aged from 21-27 years; mean age: 24±0.8 years) were investigated, both male and female in a seated position.

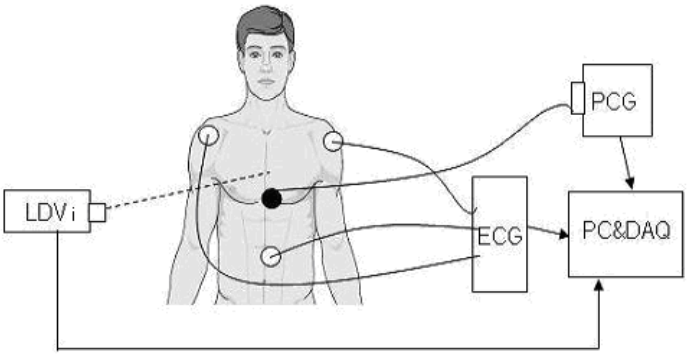

Figure 3.2 ：Scheme of the experimental set-up

Signal Processing

In order to extract temporal and morphological features, representing the underlying physiological processes, a wavelet decomposition was performed on both the vibrometric and acoustic traces. This allowed a multiresolution analysis to be performed. The wavelet transform (WT), which is a time-scale representation based on multiresolution signal decomposition, was selected for the method reported here since it is able to localize the frequency changes of a non-stationary signal and is free of any assumptions regarding the statistical characteristics of the signal [19].

Wavelet transform (WT) is usually devoted to the analysis of nonstationary signals. It is a time-scale representation based on multiresolution signal decomposition which allows one to follow the temporal evolution of the spectrum of the frequencies contained in the signal, and is free of any assumptions regarding the statistical characteristics of the signal.

Multiresolution analysis has been formulated by Mallat **[26]**, and a large body of research exists on using wavelets for signal analysis .

The continuous WT is an integral transform, a linear operation that decomposes the signal under study into a family of functions. The decomposition of a generic signal f(t) by wavelet transform requires a function adequately regular and localized, called ‘‘mother wavelet’’, from which a family of functions (the so-called ‘‘wavelet frame.’’) is built:

$$W_f(s,\tau) = \int_{-\infty}^{\infty} f(t) h^*_{s,\tau}(t) dt \quad ; \quad \textbf{eq.1}$$

where $h_{s,\tau}(t)$ is the set of basis functions (wavelets) defining the wavelet frame (* is the complex conjugate), which are generated from the single wavelet *h(t)* by scaling and translation, according to the following relationship:

$$h_{s,\tau}(t) = \frac{1}{\sqrt{s}} h\left(\frac{t-\tau}{s}\right) \quad ; \quad \textbf{eq.2}$$

where *s* is a real number different from zero (the scale factor), τ is a real number (the translation factor), and t is the abscissa on which the signal is analyzed (the time, in our study).

The transformation formalized by equation 1 and 2 allows a local analysis of *f(t)* by the wavelet *h* and evidences the presence of all members of the wavelet frame, which are all scaled representatives of the mother function. As clearly stated by Pichot and colleagues **[27]**, quantitatively the value of $W_f(s, \tau)$ is representative of the importance of the concordance of $h_{s,\tau}(t)$ to *f* near τ ,at the *s* level, i.e., the value of the wavelet transform $W_f(s, \tau)$ depends on the value of *f* near τ, with a weight proportional to *s*.

The analysis consists in sliding a window of different weights, containing the wavelet function, all along the signal *f(t)*. The weight characterizes a member of the wavelet frame with a particular dilatation factor τ. The output of the calculation of $W_f(s, \tau)$ is a list of coefficients representing the evolution of the correlation between the signal *f* and the chosen wavelet at different levels of analysis (or different ranges of frequencies) all along the signal itself) **:** hence, the sliding window containing the wavelet function automatically narrows for detecting high frequency phenomena, and widens for investigating low frequency behaviour.

In the application presented here a discrete WT is implemented (Labview, National Instruments, Austin, TX), built up with orthogonal dyadic functions that can be expressed as:

$$h_{i,k}(t) = 2^{\frac{i}{2}} h(2^{-i} t - k\tau_0); \quad \textbf{eq.3}$$

where *i* and *k* are integers. Eq. (3) is derived from Eq. (2):

- by choosing the dilatation parameter $s=2^{-i}$;

- by restricting the translation parameter τ to the discrete set of sampling points $\tau_{i,k}(t) = \frac{k}{2^i}\tau_0$, where τ_0 is a fixed constant called the sampling rate.

The mother wavelet Daubechies 7 [28], recently applied on VCG recordings [9] to evaluate the right measurement position , was used as mother wavelet for the analysis of the vibratory traces; while the Coiflet 2 was applied to the PCG traces, as proposed by Durand [25].

The algorithm used by the authors consists in decomposing and reconstructing a signal applying a series of filters in cascade. This procedure was developed by Mallat [26] and is a well known signal processing tool called the two-channel sub-band coder. The signal is like to be passed through high-pass and low-pass filters; so the original signal A_i emerges as two signals: a signal approximation A_{i+1} and a signal detail D_{i+1}. The decomposition process can be iterated, with successive approximations being decomposed in turn, so that one signal is broken down into many lower-resolution components. This structure, generally called the "wavelet decomposition tree", is reproduced in figure 3.3.

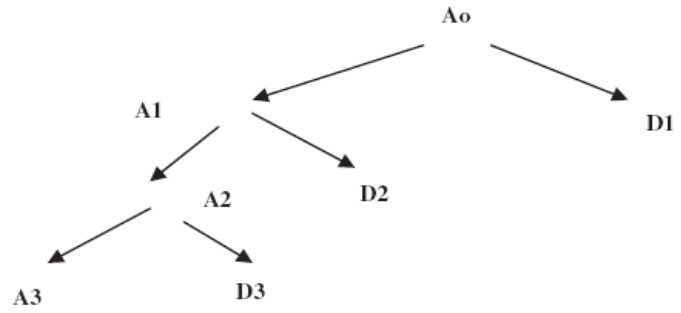

Figure 3.3 : Example of a wavelet decomposition tree , i.e. two channel sub-band coder

This procedure results in a series of details D_i, which are low scale, high frequency elements of the signal, and approximations A_i, which are high scale, low frequency elements of the signal.

According to Debbal et al. [29], who investigated heart sounds trough the use of Mallat algorithm [26], level D7 of decomposition represents the two principal components of the sound S1 and those of the sound S2. Following this indication, we focused our attention on this level of detail both on VCG and PCG traces.

After the WT decomposition of both VCG and PCG traces, amplitude envelope calculation was applied on D7 of PCG and VCG, aiming to locate the temporal events [24]. This was done computing the amplitude of the analytic signals:

$$Y_k(t) = y_k(t) + j\, H_k(t)$$

where $y_k(t)$ is the decomposed recorded signal (k=1 or 2; for PCG, VCG respectively), and $H_k(t)$ is its Hilbert transform .

3.3 Results

A typical one beat optical VCG signal measured on the chest wall is shown in Fig. 3.4 together with the PCG trace and the II-lead output of the ECG synchronously recorded.

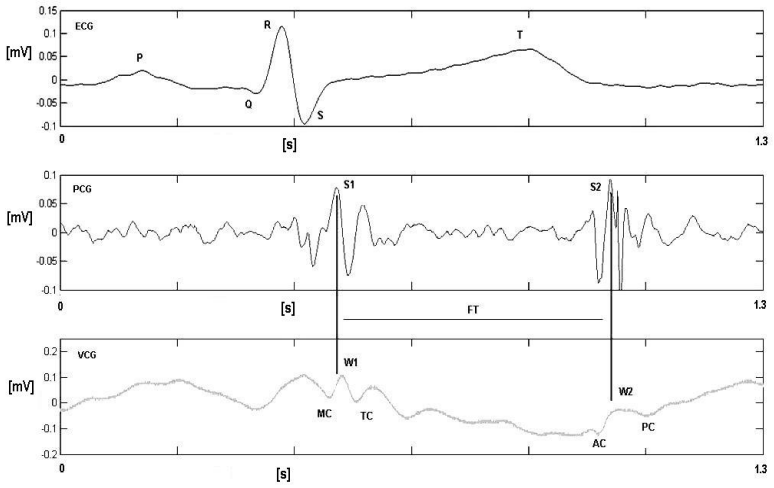

Figure 3.4 : Example of one beat recordings from VCG and PCG along with II lead ECG. On VCG trace are reported mitral and tricuspid closure (MC and TC) followed by aortic and pulmonary closure (AC and PC)

Fiducial points are identified on the traces related to different cardiac phenomena. Based on visual inspection, for VCG trace an interpretation is proposed: the S1 and S2 peaks on PCG find direct

correspondence in local maxima W1 and W2, respectively, on the VCG trace. As a consequence, the fundamental filling time interval after ventricular systole (i.e., filling time FT, time interval between S1 and S2 in PCG) is comparable with the time interval between events labeled W1 and W2 on VCG trace.

This morphological characteristics of VCG can be found on most of the beats recorded. Thereby, W1 and W2 can be considered fiducial points on the VCG trace, the underlying physiological processes being heart valves closure .

After this a mean FT was carried for all the traces . (Table 3.1) ; minimal differences were found between VCG and PCG .

Subjects	S2-S1 (pcg)	SD	W2-W1 (vcg)	SD
1	**340.71**	1.14	**335.43**	1.22
2	**309.07**	1.58	**312.47**	2.45
3	**347.43**	1.91	**355.50**	1.87
4	**291.47**	1.96	**282.47**	1.36
5	**334.54**	1.33	**342.38**	2.14
6	**283.00**	1.37	**288.06**	1.14
7	**263.33**	1.54	**268.35**	1.18
8	**298.21**	0.80	**294.57**	2.14

Table 3.1 : comparison between PCG and VCG in evaluating filling time after visual idenfication of the principal cardiac events

Figure 3.5 displays the results of the multiresolution wavelet decomposition on vibroacoustic recordings. In particular, it is depicted a 2.5s time window of the D7 decomposition on both the PCG and VCG signals. Notably, the comparison between the two details emphasizes the temporal and morphological correspondence between the complex S1 and W1, and the complex S2 and W2, for each one of the 3 cardiac cycles reported in the time window. This is like to say that it is possible to identify on VCG traces events representative of mitral (MC) and tricuspid (TC) valve closure (considered in the complex W1), and of aortic (AC) and pulmonary (PC) valve halting (considered in the complex W2), respectively.

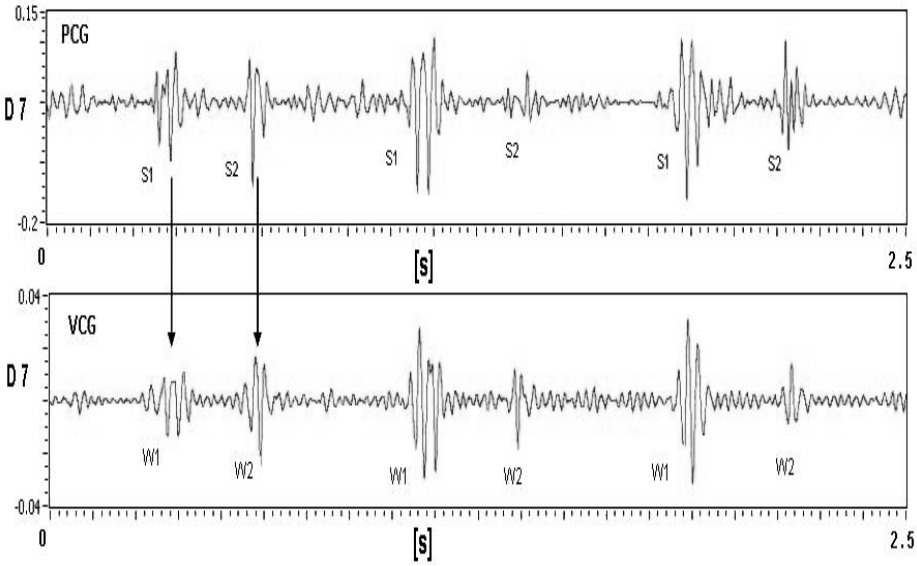

Figure 3.5: Example of wavelet decomposition (detail D7) on PCG (top) and VCG (bottom)

An example representative of the results obtained computing Hilbert transform for envelope calculation on PCG and VCG details D7, is depicted in figure 3.6.

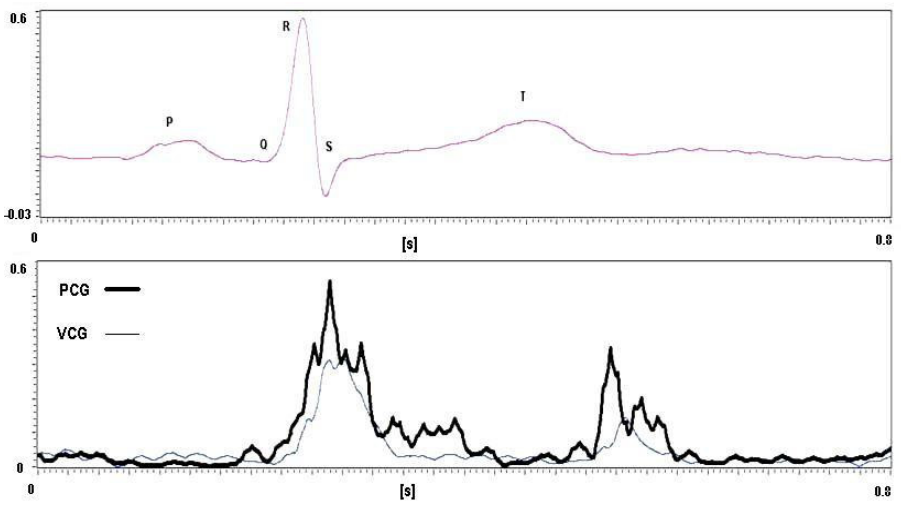

Even if the enveloped signals show different energy content, it can be clearly noticed:

- the fairly good superimposition of S1 and W1 complexes in VCG and PCG D7 envelope traces after the QRS complex (see ECG trace for reference);
- the same good superimposition of S2 and W2 related complexes at the end of T deflection on ECG.

The final step was the re-calculation of the filling time to evaluate the usefulness of thi signal processing algorithm : (table 3.2)

Subjects	S2-S1 pcg)	SD	S2-S1 pcg) - WT	SD	W2-W1 (vcg) WT	SD	W2-W1 (vcg) WT	SD
1	340.71	1.14	339.89	1.25	335.43	1.22	336.75	1.19
2	309.07	1.58	309.59	1.74	312.47	2.45	311.27	1.47
3	347.43	1.91	348.34	1.11	355.50	1.87	355.12	0.88
4	291.47	1.96	292.78	0.97	282.47	1.36	283.59	1.56
5	334.54	1.33	334.92	1.45	342.38	2.14	343.08	1.11
6	283.00	1.37	282.76	1.93	288.06	1.14	289.16	1.88
7	263.33	1.54	264.16	1.53	268.35	1.18	268.47	0.78
8	298.21	0.80	297.82	1.67	294.57	2.14	295.97	1.84

Table 3.2 filling time intervals calculated both by visual inspection and after wavelet transform

Comments

It was showed that information fusion from both electric signals and sound signals, allowed to locate events of the cardiac cycle on VCG signals. Mean filling time carried out after visual inspection for each subjects show minimal differences between phonocardiography and optical vibrocardiography as a first assessment of the usefulness of the laser non contact technique .[30]

In a following step , an signal processing algorithm by means of wavelet transform , it was demonstrated that it is analytically possible to identify the same events on VCG and PCG .

As a final stage the filling time interval was carried out after the signal processing step and the results show that this algorithm gives a better evaluation of this fundamental parameter .

To reach this goal, it was successfully tested the feasibility of using signal processing algorithms. The common morphological features identified remark that on optical vibrocardiography traces it is possible to check for mechanical events related to the pumping function of the heart like cardiac tones, occurring at valves halting. Those are really critical parameters because closure problems could carry modification in the acoustic signals, in particular the presence of other events, i.e. S3 or S4 [31]. The presence of such events therefore are revealed also by Vibrocardiography.

Results suggest that VCG traces could allow to also evaluate the filling time, a critical parameter for the cardiac functionality (it plays a fundamental role in evaluating a correct cardiac resynchronization therapy [21]).

This study, even if preliminary, has put in evidence the potency of optical Vibrocardiography in retrieving and monitoring critical parameters at the base of the cardiac activity in similarity to digital Phonocardiography. This could be an added value, if we consider that optical VCG has been recently demonstrated to be equivalent to ECG in monitoring both the cardiac rate and the heart rate variability.

Events from heart mechanics produce vibrations and sounds which are strictly related. There are different components both in vibrations on the chest and in phonocardiography: for heart sounds masking events could be stomach murmurs or respiratory events and for chest wall vibrations could be still breathing or also skin artifacts. Even if such phenomena it is considered interesting to be investigated, in the present analysis t those components were filtered out because not in the aim of the work.

Next step in the ongoing research will be the confirmation of the herein presented results on a sufficiently large number of healthy and pathologic subjects. Also in the field of signal processing, the implementation of algorithms for automatic feature extraction will be considered (segmentation, mathematical morphology, etc. [32]).

Future goals will be the confirmation of the hypothesis that the sole optical VCG signal could furnish part of the informative content that is now obtained by distinct physiological measurements, i.e., breathing, arterial pressure, cardiac sounds and electrical activity of the heart. In fact it could be thought that several functional information could be achieved from the optical signal we carried out from the vibrometer, and relevant patient's condition related to the pathology could be obtained.

The content of this chapter has been published in

- M. De Melis , U. Morbiducci, L. Scalise Identification of Cardiac Events by Optical vibrocardiography : comparison with Phonocardiography ***IEEE*** *Proceedings of EMBC 2007 –Lyon*

- L Scalise, U Morbiducci, M De Melis, M Grigioni, G Corbucci, P Bocconcelli, A Pierantozzi. Mechanical approach for programming optimal pacing in pacemakers with laser Doppler vibrometry technique: preliminary clinical results. ***ESAO 2005****, XXXIIth Annual Congress European Society for Artificial Organs, October 5-8, 2005 Bologna,. Abstract published in* ***Artif Organs****, 2005.*

Chapter 4

4.1 Introduction

Initial theories of haemodynamics had been lacking the proper measurement instruments to validate the results. The research community had to await the creations of Marey (1860), Mahomed (1872) and others to get a non-invasive quantification of pressure pulsations with so-called 'sphygmograph' devices. Although very creative, they provided merely an estimation of mean pressure added with some pulse 'variations'. An accurate measuring device only came about with the work by Otto Frank (1865-1944) in 1903 on manometry.(Marey 1860; Mahomed 1872; Frank 1903).

Since the First World War, the domination of researchers from the USA cannot be denied. Pioneers in the field of cardiovascular physiology include people like Katz (1955), Wiggers (1950, 1952) and Hamilton (1962). In England there were Bramwell and Hill (1922) and on the mainland Wetterer in Germany who introduced the electromagnetic flowmeter (1937), independently from Kolin in the USA (1936). Gregg and colleagues started recording accurate flow waves in the coronaries (1940).(Kolin 1936; Gregg 1940)

In between wars there was little advance in cardiovascular medicine. After 1944, the sphygmomanometer focused too much attention on the systolic and diastolic values, introducing many myths on what is in fact nothing more than the maximum and minimum of the pressure wave. Technological advancement kept going, introducing micromanometers and diagnostic catheters around the 1970s.[33,34] .

Invasive Pressure Measurement

A lot has changed since Stephen Hales (1677-1761) made the first direct measurement of blood pressure by inserting a glass tube in a horse neck artery. But arterial cannulation with continuous pressure transduction and waveform display remains the accepted 'gold standard' for blood pressure monitoring today. Several peripheral arteries are available for percutaneous cannulation, but radial artery pressure monitoring is most common in anaesthesia and critical care.

The arterial cannulation using an integrated needle-guidewire-catheter assembly is commonly used (Figure 4.1). The wrist is positioned and the artery identified by palpation (A). The needle is then introduced through the skin and advanced towards the artery, generally at 30° to 45° (B). A flash of arterial blood into the collection reservoir identifies the artery as the needle tip enters the vessel. The guide wire is advanced through the needle into the vessel lumen (C). The catheter is advanced over the guide wire (D). After the catheter is fully advanced into the vessel lumen, the guide-wire is

removed and a narrow bore, low compliance pressure tubing is fastened to the catheter (E). The apparatus is securely fixed to the wrist and connected to the pressure transducer. Large clinical investigations confirm a low incidence of long-term complications following radial artery cannulation.[35,36]

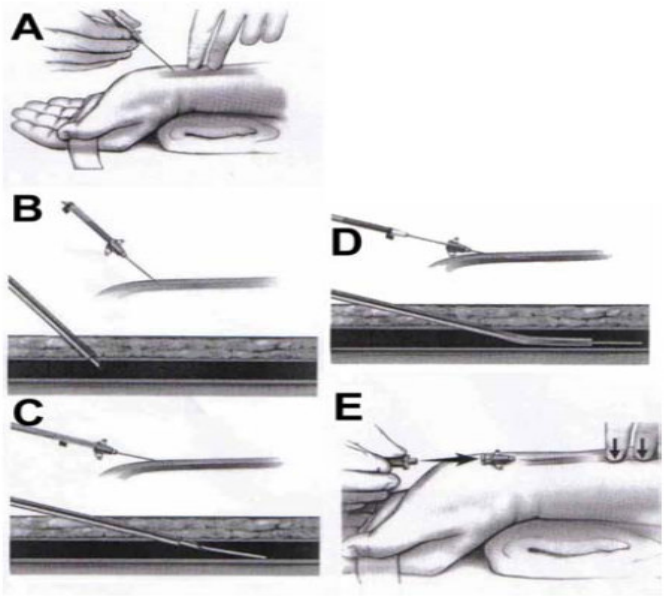

Figure 4.1 : Subsequent steps of a radial arterial cannulation**.**

Apart from routine radial pressure monitoring, invasive pressure measurements are also performed during interventions, for example while treating stenosed coronaries. The cannulation procedure is analogue as described above but most often performed from the femoral artery. Nowadays, there are two kinds of pressure measuring guidewires. Hollow fluid-filled guidewires connected to an external transducer; and guidewires with a high fidelity micromanometer at the tip. The PressureWire (Radi Medical Systems, Uppsala, Sweden) and WaveWire (Endosonics, Rancho Cordova, CA) are commercial examples of the latter. The Informer Wire (Scimed, Minneapolis, MN) on the other hand is a fluid filled catheter. Since fluid-filled lines need to be flushed, they take up more measuring time. (Figure 4.2)

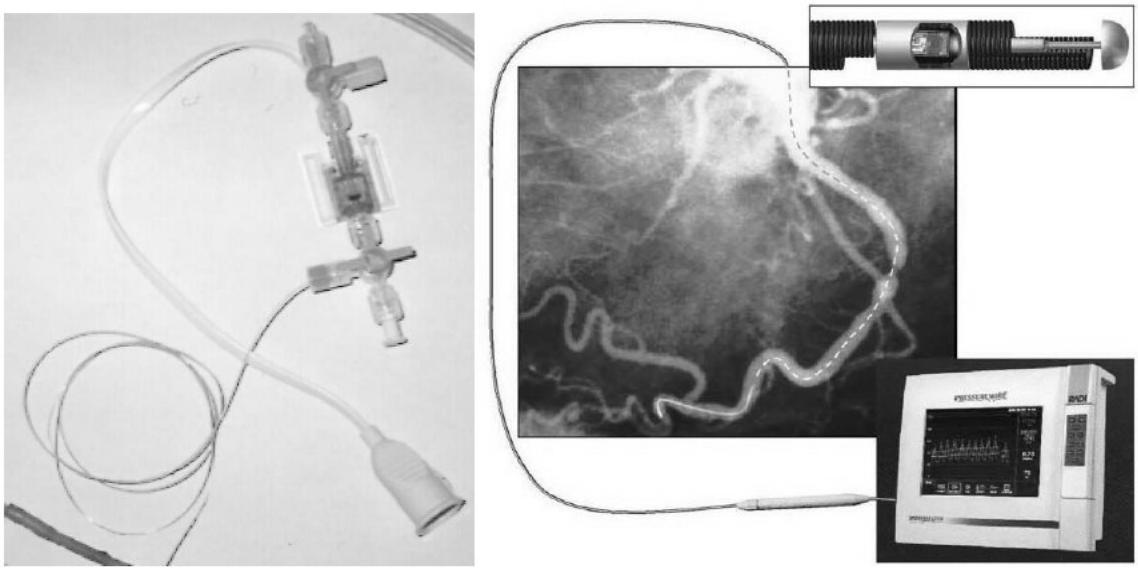

Figure 4.2 : Left: Fluid-filled catheter with external transducer (Datex-Ohmeda, Helsinki, Finland). Right: Micromanometer at cathetertip (PressureWire, Radi Medical Systems, Uppsala, Sweden)

Non invasive pressure measurements

Riva-Rocci[1] invented a device to measure cuff pressure in 1896, composed of a mercury manometer and an arm-encircling elastic cuff, inflatable with a rubber bulb. He described the measurement of systolic arterial blood pressure by determining the pressure at which the palpated radial arterial pulse disappeared as the cuff was inflated.(Riva-Rocci 1896)

Undoubtedly, the most widely used manual discrete method for blood pressure determination is the auscultation of sounds originally described by Korotkoff in 1905.Using a Riva-Rocci sphygmomanometer and cuff, Korotkoff applied a stethoscope to the artery directly below the cuff to auscultate the sounds generated as the cuff was slowly deflated . These sounds are a complex series of audible frequencies produced by turbulent flow, instability of the arterial wall, and shock wave formation created as external occluding pressure on a major artery is reduced.

The pressure at which the first Korotkoff sound is auscultated is generally accepted as the systolic pressure (‘phase I’). The sound character progressively changes (‘phases II’ and ‘III’), becomes muffled (‘phase IV’), and finally absent (‘phase V’). Diastolic pressure is recorded at phase IV or V. However, phase V may never occur in certain pathophysiologic states, such as aortic regurgitation.[37].(figure 4.3)

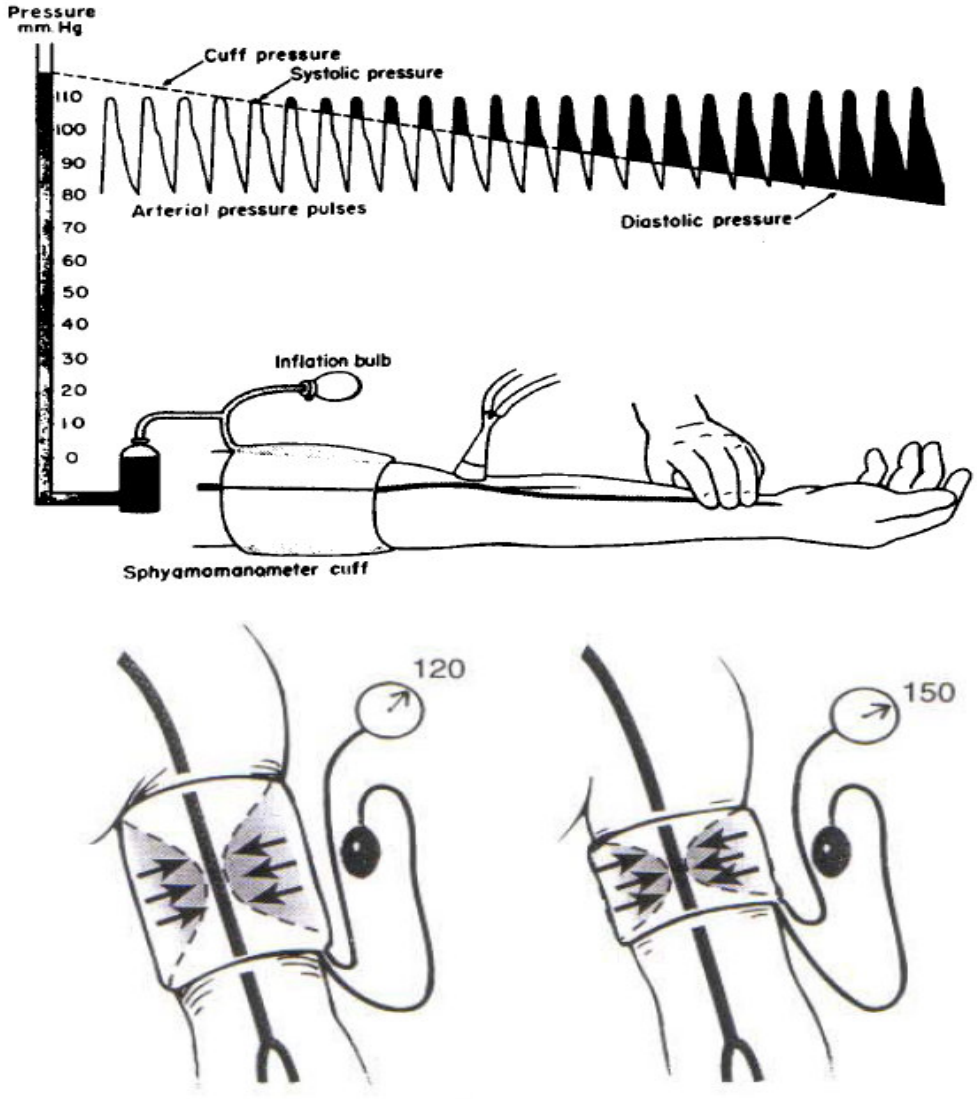

Figure 4.3 : Up: Korotkoff auscultation method.(Li 2000) Bottom: Inappropriate cuff size (right) yields erroneous blood pressure values (overestimation with too small cuff)

Common sources of error during discrete manual blood pressure measurements include selection of an inappropriate cuff size or excessively rapid cuff deflation (Figure 4.3). Limitations of manual discrete blood pressure measurement have been overcome by automated non-invasive blood pressure devices (NIBP), which are now used widely in medical care. By applying a single algorithm or method of data interpretation, NIBP devices provide consistent, reliable values for systolic, diastolic, and mean arterial pressure (MAP). Most automated NIBP devices are based on the technique termed 'oscillometry', first described by von Recklinghausen in 1931. With this method, oscillations in cuff pressure resulting from arterial pulsations during cuff deflation are sensed by the monitor and used to determine arterial blood pressure values. Peak amplitude of

arterial pulsations corresponds closely to true MAP.[38] Values for systolic and diastolic pressure are derived using proprietary formulae that examine the rate of change of the pressure pulsations (Figure 4.4). Systolic pressure is generally chosen as the pressure at which pulsations are increasing and are at 25 to 50 percent of maximum. Diastolic pressure is more difficult to determine but is commonly placed at the point where the pulse amplitude had declined by 80 percent. [39]

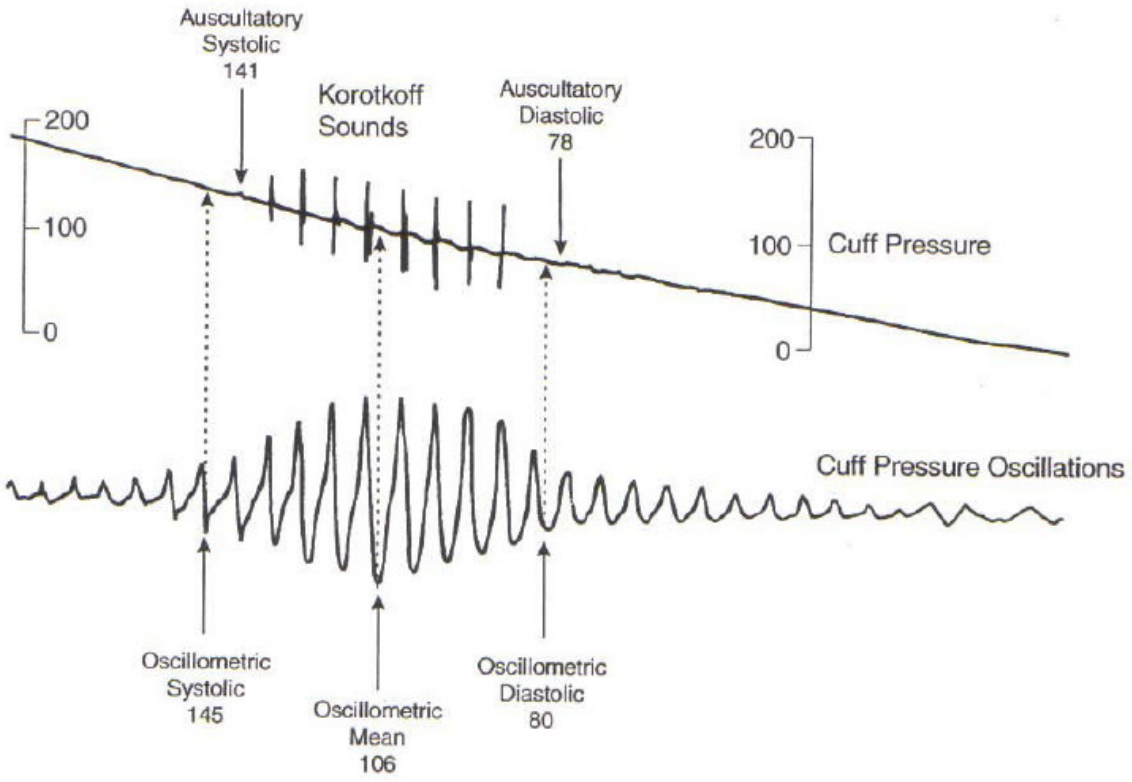

Figure 4.4 : Comparison of blood pressure measurements using Korotkoff sounds and oscillometry. Oscillometric systolic blood pressure is recorded at the point where cuff pressure oscillations begin to increase, mean pressure corresponds to the point of maximal oscillations, and diastolic pressure is measured where the oscillations become attenuated.

Under controlled clinical conditions, numerous investigators have demonstrated that automated NIBP measurements closely approximate directly (or invasively) measured arterial pressure.[40,41] However, other studies underscore the fact that marked disagreement occurs when direct and indirect (or non-invasive) pressure measurements are compared, particularly when the direct measurement is done at the radial artery or under changing clinical conditions [41] When direct brachial artery pressures have been compared with indirect methods such as manual auscultation and automated oscillometry, the relation between the indirect and direct pressures varied between patients, within patients over time, and with changing haemodynamic conditions.[43] As noted,

some authors have emphasized the lack of exact agreement between different measurements of blood pressure. Standards for performance of automated NIBP devices have been advanced by organizations such as the American Association for the Advancement of Medical Instrumentation (AAMI) and the British Hypertension Society. AAMI standards require a monitor to record blood pressure within 5 mmHg prediction error compared with the reference method, with 8 mmHg as largest standard deviaton error for this comparison.(Association for the Advancement of Medical Instrumentation 1992) However, clinical performance of an NIBP monitor should be evaluated by other criteria as well. These include the number of outlier values, duration of discrepancies, magnitude of individual errors, and performance under variable clinical conditions.

From the point of view of continuos measurement The Penaz method (1973) is based on unloading the arterial wall to measure a calibrated waveform in a finger [44]. A cuff is being placed around the middle phalanx of a finger or the base of the thumb finger (‘arterial volume clamp’ method, Figure 4.5), and blood pressure is determined by registering the cuff pressure needed to maintain a constant arterial volume (measured by light diodes or photoplethysmography). This method is commercialized in the Portapres and Finapres device (FMS Finapres Medical Systems, Arnhem, NL).

Figure 4.5 : Measuring finger arterial waveforms with the Penaz method (Finapres device, FMS Finapres Medical Systems, Arnhem, NL).

Continuous non-invasive finger blood pressure measurement devices have undergone clinical evaluations comparing their performance with direct arterial pressure measurements, which

demonstrated small overall mean differences between finger and intra-arterial pressure measurements.[45] The potential for circulatory impairment of the distal finger caused by the constantly inflated cuff has been a cause for concern. Gravenstein et al. demonstrated mild hypoxemia in the capillary blood of the fingertip during finger blood pressure monitoring, but no adverse outcomes were noted in these study patients or in others in whom finger blood pressure measurement was performed for as long as 7 hours .[46] Despite the positive comments above and its widespread use in ambulatory applications (especially related to aeronautical experiments), the Penaz method remains a peripheral monitoring technique which at the start of this thesis had not been investigated in literature as the input for a transfer function model that derives central aortic pressure (as opposed to radial arterial tonometry which is discussed further). In the work of Bos [47] , it was already shown that brachial pressure reconstruction from finger pressure measurements can only be achieved by using a digital filter/transfer function for pulse wave distortion and additional corrections with newly derived formulae for the individual pressure gradient between brachial and digital artery pressure. But these proposed corrections still needed to be validated for young and healthy subjects and load conditions with changing blood pressure and wave amplification like standing up, head-up tilt, or vasoactive drugs.

One can also deduct that the shorter the pathway is between the peripheral site of pressure recording and the aortic valve, the less the error will be that is introduced (as more distal vessels get smaller, more tortuous and with more active muscular activity), which also is in favour of any device working more proximal to the heart. Seen the fact that at the start of this thesis radial arterial tonometry was also less widespread and fairly unknown, it was chosen to continue with the tonometric technology and investigate its potential in depth .

The last to be considered but the most important for this part of the thesis is the applanation tonometry . In brief, a superficial artery, preferably supported by an underlying bone, is compressed and partially flattened (applanated) by the tonometric transducer. The balance of forces between the transducer ‘hold down pressure’ (HDP) and the internal pressure in the vessel allows to record the arterial waveform morphology. This signal must then be calibrated by e.g. cuff oscillometry from the upper arm.[48]

The technique, principles and drawbacks of arterial tonometry will be further explained in the following chapters as hand-held Millar manual probes were chosen for the pressure measurements in this thesis. Kelly et al. reported an intraobserver variability of 4.5% and an interobserver variability of 11.6% to be achieved after 4 to 6 weeks’ use of the hand-held penprobe SPT-301 (Millar Instruments Inc., Houston, TX). The principle of automated tonometry will be briefly explained here using the Colin 7000 device as an example.

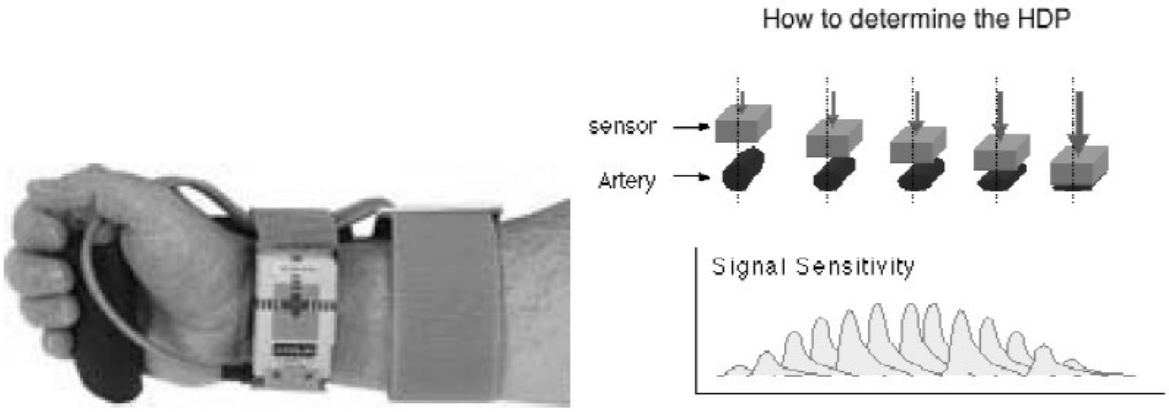

Figure 4.6 : Automated tonometric device with determination of hold down pressure (HDP).(Colin Medical Instruments Corp., San Antonio, TX).

The device consists of a sensor-array placed on the wrist over the radial artery. This sensor contains piezo-electric pressure transducers separated by 0.2 mm. A pneumatic pump presses the transducer array against the skin and tissue above the artery (HDP). To determine optimal HDP, the monitor searches through a range of pressure values until it measures a signal indicating of the form shown in Figure 4.6. When the artery is partially flattened, a graph, called a 'tomogram', is plotted to show sensor pulse amplitude versus sensor number in the array. The individual sensor elements whose pulse amplitudes are near the maximum pulse amplitude are calibrated to the systolic and diastolic values obtained in the oscillometric cuff measurement.[49] .

Apart from the common radial artery site, two alternative measuring sites have been looked at: the carotid and temporal artery. Of all superficial arteries, the carotid artery is the closest to the central aorta, with a pressure wave quite similar to the desired central pressure wave.[50] However, the fact that the artery is not supported by bone structure and the breathing pattern interferes with the registration, makes it a less appropriate site during exercise tests. In analogy with the work of the group around Yamakochi [51], the temporal artery has been investigated. It is a branch of the carotid artery, thus still close to the central aorta, and supported by the skull. With an appropriate fixation mechanism this would be a handy site during exercise, but it was found that a successful palpation of the artery in order to position the tonometer was quite difficult and more patient dependent than the radial site.

4.2 Pulse transit time

Potentially useful and convenient parameter for continuous monitoring of blood pressure could be pulse wave velocity or pulse transit time (PTT) between different regions of human body as an index of arterial stiffness so of serious hypertension condition

Pulse transit time (PTT) as a measure of the mean pulse wave velocity (PWV) is the time interval for the arterial pressure pulse to travel from the aortic valve to a peripheral site. Strictly speaking, to determine PTT, two pressure pulses have to be recorded simultaneously at two positions, proximal and distal, along the arterial tree. However, the proximal trigger pulse used to initiate the timing mechanism is often difficult to monitor, due to motion artifact and/or indistinctive pulses [53].

To overcome this difficulty, in practice, the electrocardiogram (ECG) R wave has been commonly used to initiate PTT because it is easy to detect and usually more artifact-free. The distal pulses can be recorded by an optical means, photoplethysmography, at the peripheral site, such as fingertips, earlobes, or toes . PTT has been widely used for noninvasive examination of the arterial viscoelastic properties, such as elasticity, compliance and stiffness of the vessel walls. It has also been proposed as an indicator of blood pressure . Obtaining reliable and repeatable measurement of PTT is crucial in interpreting physiological conditions clinically. It was suggested that the contact force between the measurement site and the transducer should be carefully controlled when the peripheral pressure pulse is recorded to avoid the signal deformation . The effect of sensor contact force on peripheral pressure pulse recorded by photoplethysmograph has been widely reported .The effect of sensor contact force on PTT has also been observed. Haynes noticed that as the cuff on the arm was inflated, the carotid-radial PWV gradually fell and the arterial extensibility increased . Driscoll and his colleagues investigated the influence of different applied brachial recording forces on brachio-radial PWV . Recently, the experiments carried out on healthy subjects showed that PTT, determined as the time interval from the peak of the ECG R wave to different characteristic points of photoplethysmogram (PPG), changed with varying contact force between the photoplethysmographic sensor and the fingertip [53].

Applanation tonometry , the gold standard non invasive technique, is a contact method, based on a pressure sensor that flattens the artery at the measuring spot, and detects the pressure variations within the superficial artery. Exact sensor positioning is crucial for correct measurement, and because of the necessity to deform the vessel, it is difficult to measure pressure waves at adjacent spots or it could have problems in subjects with deeper arteries.

Both problems are solved by use of laser vibrometry, because of the wave speed of the laser beam (speed of light), skin displacement measurements can be done at temporal resolution far exceeding >1kz. Being a non-contact method, a configuration with 2 or more sequentially placed sensors is no problem, provided that the devices can be made small enough to allow positioning.[1,2,8,10]

4.3 Set-up

In a first stage two single-point laser Doppler vibrometer (Polytec GmbH, Germany) was used to measure instantaneous velocity of the point of the surface where the laser beam is focused ; one it is pointed on the carotid site and the other one deployed on the femoral artery site The LDVi laser head was positioned at a distance of about 1 m away from the measurements sites. In a second step an Esaote applanation tonometer was used to retrieve pressure waveforms from carotid and femoral sites. Both in the two stages an II-lead trace from a commercial ECG was simoultaneously recorded to use it as reference The measurement system was used to simultaneously record time histories of 90 s length (VCG, Tonometer and ECG-II_lead). A notebook Intel P4 (PC) was used, equipped with a 12-bit A/D (DAQ) data acquisition board (PCMCIA, National Instruments, U.S.A.), with a sampling frequency of 1 kHz. 14 male healthy subjects (aged from 22-30 years; mean age: 26±0.9 years) were investigated, in a supine position. (figure 4.7) keeping the same environmental condition for the two measurement stages carried out a 10 minutes of temporal distance .

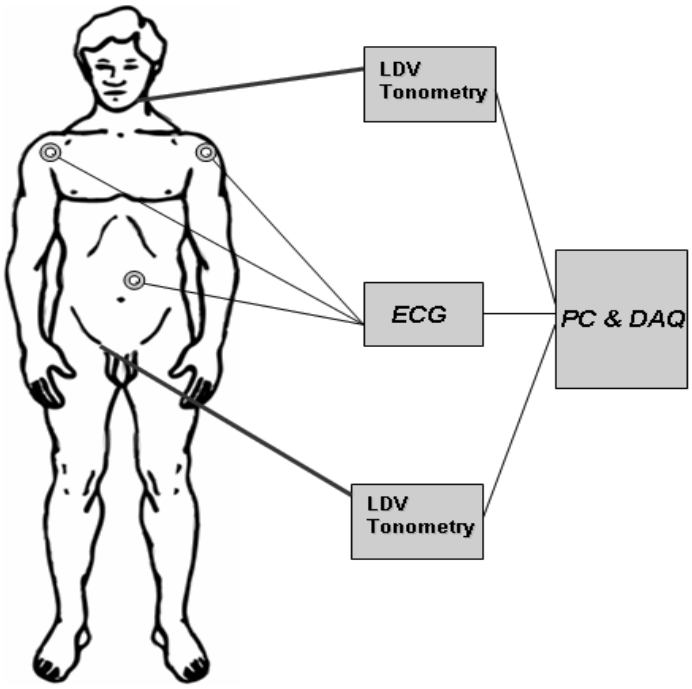

***Figure 4.7** : Pulse transit time measurement set-up*

4.4 Physiological interpretation

Being the LDV a measurement of velocity it was conjectured that , considering a simple artery model as an elastic tube , optical VCG measures a radial velocity of the artery wall ; in fact a pressure wave transmitted in a compliant tube induces volumetric changes with a velocity along the section radius. (figure 4.8)[52]

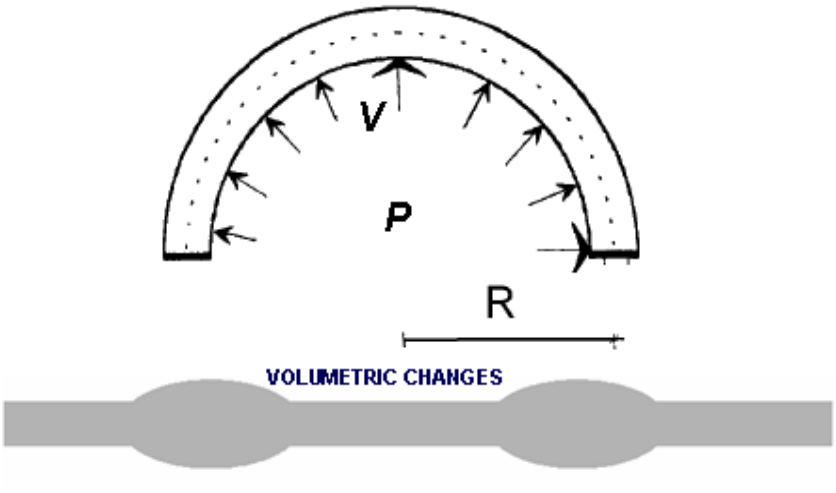

Figure 4.8 : a simple sketch of a compliant tube

Moving from this assumptions an interpretation was proposed applying the relationship between pressure and velocity in a compliant tube between radial velocity of vessel wall dilation *V* and transmural pressure *P*:

:

$$V \propto \frac{dP}{dt} \qquad \textbf{Eq. 4.1}$$

consequently :

$$P \propto \int V_w dt \qquad \textbf{Eq. 4.2}$$

so the vibrometric trace could be considered the derivative of the pressure ; following this consideration optical VCG trace was integrated in the time domain obtaining : (figure 4.9)

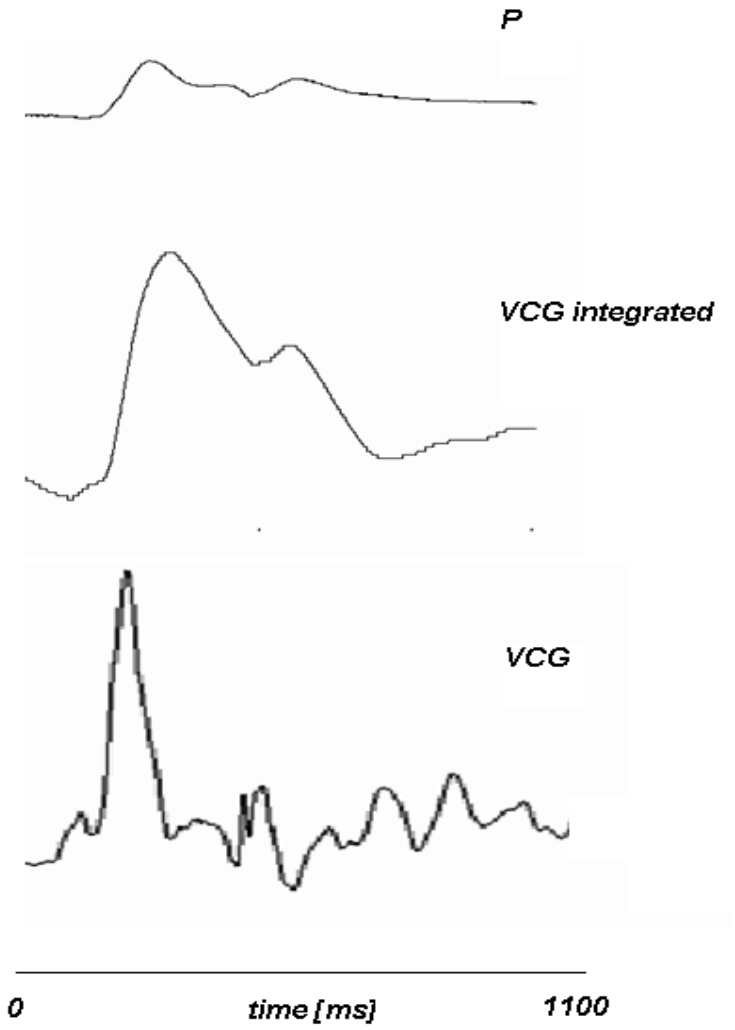

Figure 4.9 : an example of comparison between pressure , optical VCG and its integral .

4.5 Signal Processing and Analysis

An algorithm to extract PTT from pressure and VCG recordings was built up .

In a first step a Savitsky-Golay smoothing filter was used (order 10^{th}). The Savitsky-Golay filter provides a versatile smoothing filter. It uses a moving window, with an n^{th} order polynomial least-squares fitted to the points in the window. A set of polynomial coefficients is produced for each point in the window - instead of the constant for the simple moving window. The first order coefficients are multiplied by their respective points in the window and summed to calculate the smoothed point. The window is moved onto the next point and the process is repeated, always using the original data. The 'end-effects' at the start and end of the signal are managed using data mirroring.

Then a mean beat extraction strategy was followed and in particular a multiple approach was realized to evaluate the most affordable way and to consider respiratory interference :

- a first approach to the segmentation was realized with the extraction of the first 20 beats (R peak from ECG was used as gate), with a 650 ms time window , in automatic step and over those mean beat was calculated both for VCG and pressure traces .
- a second , manual, approach was followed to take in account the respiratory event on the VCG, in particular for the carotid site, extracting beats (still having R peak as gate) sited on the top of the modulation envelope (due to the respiration) by visual inspection in order to obtain 20 intervals (still 650 ms long) for mean beat calculation .

Both VCG and pressure mean beats were normalized for a reliable comparison (figure 4.10)

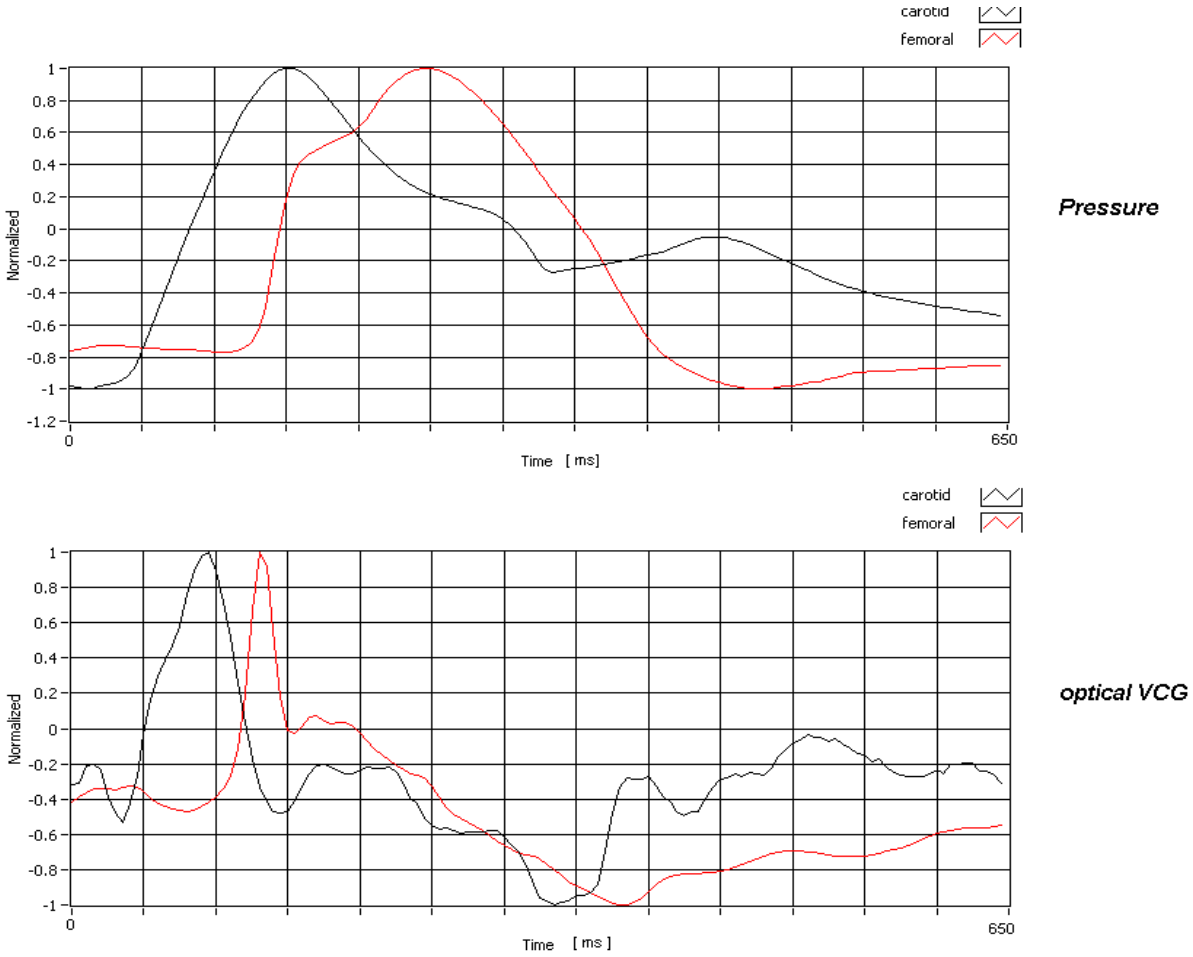

Figure 4.10 : example of the comparison between mean beats onto the carotid and the femoral site both on the pressure traces and VCG traces .

Pulse transit time is normally calculated from the foot of the pressure wave at the first point to the foot of the pressure wave as it arrives at the next point. However, difficulties are encountered in

judging accurately where the foot of the wave is. For example, is it at the point of minimal diastolic pressure, or is it at the point at which the first derivative of pressure is at a maximum. There are currently four different methods for calculating the location of foot of the wave. However, the method using the point at which the second derivative of the pressure wave is maximal (second derivative method) and the method looking at the point yielded by the intersection of a line tangent to the initial systolic upstroke of the pressure tracing and a horizontal line through the minimal point (intersecting tangent method) are the most reproducible .[54,56]

The second derivative method was choosen for pressure signal because it it easier to apply , and in particular moving from the physiological interpretation , for the VCG a first derivative method was logically used in order to find the foot of the waveform. ; after this step PTT were calculated with the two methods .(table 4.1)

subject	**Ptt_VCG** *automatic*	**Ptt_tono** *automatic*	**Differences** *automatic*	**Ptt_VCG** *manual*	**Ptt_tono** *manual*	**Differences** *manual*
S1	**75 ms**	**72 ms**	**3 ms**	**74 ms**	**72 ms**	**2 ms**
S2	**76 ms**	**71 ms**	**5 ms**	**74 ms**	**70 ms**	**4 ms**
S3	**84 ms**	**86 ms**	**2 ms**	**84 ms**	**86 ms**	**2 ms**
S4	**76 ms**	**80 ms**	**4 ms**	**77 ms**	**80 ms**	**3 ms**
S5	**63 ms**	**72 ms**	**9 ms**	**63 ms**	**74 ms**	**11 ms**
S6	**79 ms**	**81 ms**	**2 ms**	**79 ms**	**81 ms**	**2 ms**
S7	**85 ms**	**84 ms**	**1 ms**	**85 ms**	**84 ms**	**1 ms**
S8	**78 ms**	**80 ms**	**2 ms**	**78 ms**	**80 ms**	**2 ms**
S9	**64 ms**	**60 ms**	**4 ms**	**64 ms**	**62 ms**	**3 ms**
S10	**75 ms**	**80 ms**	**5 ms**	**76 ms**	**81 ms**	**5 ms**
S11	**69 ms**	**66 ms**	**3 ms**	**69 ms**	**66 ms**	**3 ms**
S12	**91 ms**	**89 ms**	**2 ms**	**91 ms**	**89 ms**	**2 ms**
S13	**61 ms**	**64 ms**	**3 ms**	**61 ms**	**64 ms**	**3 ms**
S14	**72 ms**	**77 ms**	**5 ms**	**74 ms**	**78 ms**	**4 ms**

Table 4.1 : intervals calculated with the two segmentation approaches and the derivatives method

It is possible to observe minimal differences with small preference for the second and manual method because we have in some subjects a little improvement with smaller intervals , but this approach it is really more time consuming compared to the results obtained .

A first statistical comparison was made following this last consideration on the intervals obtained with the automatic method ; a scatter plot and a linear regression were performed to evaluate a first correlation (figure 4.11)

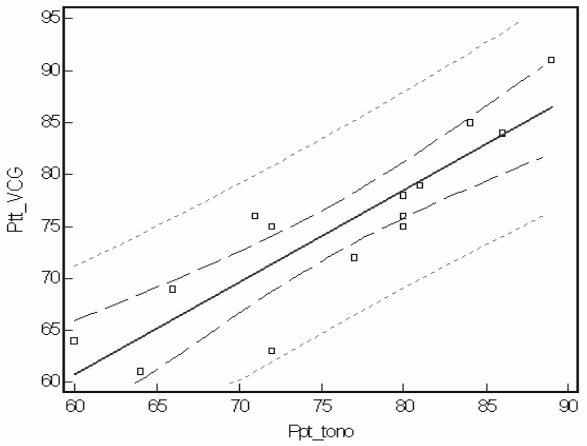

$y = 7.3436 + 0.8900\ x$

Parameter	Coefficient	Std.Error	T-value	P
Intercept	7.34361	10.19311	0.7204	0.4850
Slope	0.89001	0.13358	6.6629	<0.0001

Figure 4.11 : scatter plot and linear regression related to PTT calculated with the automatic method with VCG and tonometer

A Kruskal-Wallis statistical test [55] was performed to evaluate statistical differences on the intervals obtained with the automatic method (still considering the manual method unuseful). The Kruskal-Wallis test is a nonparametric method of testing the hypothesis that several populations have the same continuous distribution versus the alternative that measurements tend to be higher in one or more of the populations. To apply the test, we obtain independent random samples of sizes n1, n2, . . . , nm from m populations. Assume that there are N observations in all. We rank all N observations and let Ri be the sum of the ranks of the ni observations in the ith sample. The Kruskal-Wallace statistic is

$$H = [12 / (N (N + 1))] * Sum[Ri ^2 / ni , i, 1, m] - 3(N + 1). \quad \textbf{Eq. 4.3}$$

When the sample sizes are large and all m populations have the same continuous distribution, then H has an approximate chi-square distribution with m - 1 degrees of freedom. When H is large, creating a small right-tail probability (p-value), then we reject the null hypothesis that all populations have the same distribution.

In both the two cases no statistical differences were found (p=0.622) between populations , meaning that the distributions are distinct and well-defined.

A consequent step was a Bland-Altmann test [17] , that it is useful to reveal a relationship between the differences and the averages , to look for any systematic bias and to identify possible outliers. If there is a consistent bias, it can be adjusted for by subtracting the mean difference from the new method. If the differences within mean ± 1.96 SD are not *clinically* important, the two methods may be used interchangeably. (figure 4.12)

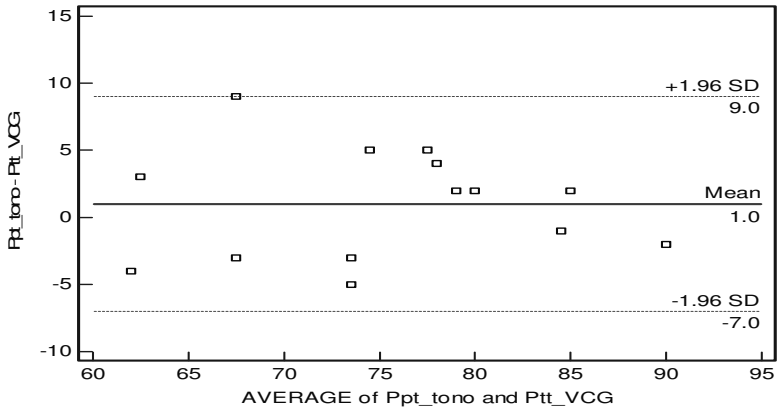

Figure 4.12 : Bland-Altmann plot of PTT calculated with VCG and Tonometer

It is evident and to be underlined that all differences are in ± 1.96 SD interval except the interval related to the subject S5 , considered an outlier and probably due to a measurement set-up malfunctioning ; but for the other subjects it is demonstrated the interchangeability of the two measurement technique.

Comments

In this chapter it was shown that that to calculate the PTT with laser vibrometry it is possible with a physiological assumption ; those results focus on the possibility to use a complete non contact technique with an higher resolution respect to applanation tonometry. Also seems to be applicable in local stiffness because in a single case study it shows potentiality , even if it needs a complete and deep measurement campaign in order to have reliable results.

Chapter 5

5.1 Introduction

Accurate biosignal acquisition and processing is critically important in a clinical environment. Due to the recent appearance of the optical VCG method, in opposition with the many detection algorithms that have been developed for the automatic processing ECG signals [12,57], aiming to detect automatically one or more of its components, no publications describe algorithms to detect features in optical VCG signals. However, there are numerous current and potential applications for optical VCG beat detection algorithms; in particular, systolic peak detection is necessary for the monitoring of the cardiac rate, and for some measures of baroreflex sensitivity.

Actually, the ability of VCG in being alternative to current methods for pulse wave velocity measurements was investigated in this thesis and described after ..In consequence both of the promising results obtained [8,10,30], and of the potency inherent to this novel method, the assessment of robust, automatic detection algorithms for these vibratory signals is strongly desirable.

Automatic beat detection algorithms are essential for many types of biomedical signal analysis and patient monitoring [57]. In fact, the manual analysis is a labor-intensive, can only be used on short signal recordings, and constitutes an error-prone task (subjective approach).

Hence, the convenience for developing automatic methods to process the biosignals, and to extract peculiar features from them is fundamental . It has been widely demonstrated that automatic analysis lead to an improvement in the recognition of patterns of cardiac diseases, thus allowing an early diagnose and, therefore, an efficient treatment [24].

Here is described an automatic detection algorithm that identifies the time-location of the systolic peak VC, which has been identified to be corresponding to the R peak in ECG trace , in optical VCG signals measured on the skin of the neck, in correspondence of the carotid artery. The algorithm is designed for subjects without significant cardiac dysrhythmias.

A detection algorithm for automatic processing of optical VCG from carotid artery is going to become of great interest, because of the fact that: it has been demonstrated its capability to be used as a surrogate of the ECG in assessing, by assuring non contact with the subjects, both cardiac rate and heart rate variability; it might be a simple, no contact approach to the clinical practice of cardiovascular screening, in particular in harsh environment, such as MR clinical practice, where ECG recordings are corrupted by artefacts and ECG cables might represent an hazard for the patients [58]. The technique may be used also to monitor subjects e.g. severely burned, for which contact with the skin needs to be minimized, or to reduce exposure risks to workers subjected to hazardous conditions [58]. Furthermore, optical VCG from carotid artery might be applied in the

future for measuring the transit time of the pulse wave in the arterial network and the arterial stiffness [53].

5.2 Optical VCG signal morphology

The morphology of the optical VCG pulse and its possible relationship to the events of the cardiac mechanics is just starting to be explored. The physiology underlying the VCG beat morphology and its components, or better what is know of it, is discussed in this section. Vital signals the meaning of which are universally established, and synchronously recorded to VCG traces, are used as reference. It was showed that information fusion from both electric signals, sound signals and pressure signals, allowed to locate events of the cardiac cycle on VCG signals.

Figure 5.1 is an example of simultaneous ECG (II-lead output) and VCG recordings, these last measured on the chest wall and on the neck, in correspondence of the carotid artery, using two LDVi systems.

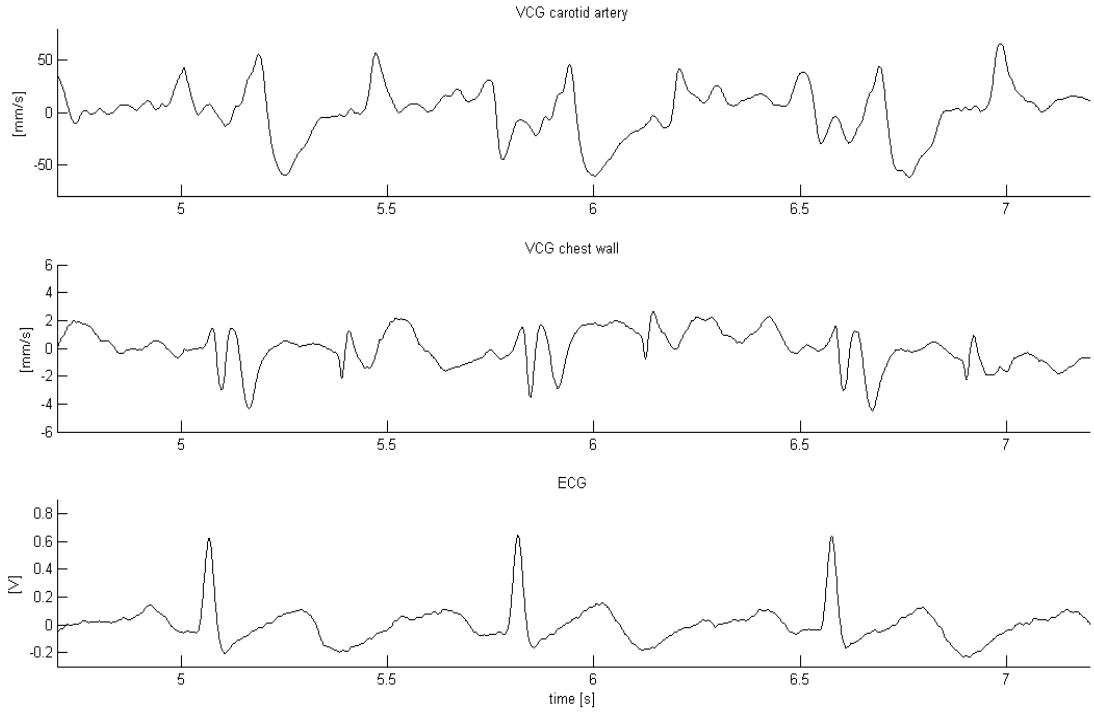

Figure 5.1

In recent studies, after visual inspection of the synchronously recorded traces was identified, on VCG, the fiducial point equivalent to the R-wave maximum on the ECG trace [8,30]. This has been

done following the procedure defined to identify fiducial points on VCG traces recorded on the chest wall and on the skin of the neck, which is based on the following assumption: the peak of the vibratory signal takes place in consequence of the pumping action of the heart, and of the heamodynamic pulse propagation in the cardiovascular network.

In particular:

- thorax movements are generated by the beating heart during its pumping function, and are transmitted to the chest wall;
- skin surface vibrations are caused by the underlying vascular wall motion of superficial arteries

This “pulsatile” movement of the vessel wall takes origin in the hemodynamic waves travelling through the arterial tree

A consequence of this basic statement is that the systolic peak component in the VCG signal must follows the R-wave maximum in the ECG trace. This allowed us to identify as the systolic peak component:

1) in the VCG beat measured on the chest wall, the peak labelled VT;
2) in consequence of the existence of a propagation delay of the haemodynamic waveform between the two sites of the cardiovascular system, the fiducial point labelled VC I in the vibrometric trace recorded on the neck in correspondence of the carotid artery.

The morphologic interpretation at point 1 is confirmed by synchronously recorded traces accounting for well known events of the cardiac mechanics. In particular, authors have recently demonstrated that a clear relationship exists between VCG and phonocardiograph (PCG) traces, the latter being sensitive to the two major audible sounds in the healthy cardiac cycle: the first one, S1 (mitral and tricuspid valves closure) which occurs at the onset of ventricular contraction and the second one, S2 (aortic and pulmonary valves halting) which is present at the end of ventricular systole. Figure 2 shows two typical optical VCG beats measured on the chest wall, together with PCG and ECG synchronously recorded traces: from visual inspection, it is evident that peaks S1 and S2 on PCG find direct correspondence in local maxima W1 and W2, respectively, on the VCG trace. Thereby, W1 and W2 can be considered fiducial points on the VCG trace, the underlying physiological processes being heart valves closure.[30]

Reminding the basic hypotheses that cardiac movements is responsive to changes in myocardial contraction induced by electrical activation, visual inspection (figure 2) confirms that, like acoustic events, also fiducial points on the vibrometric trace are delayed with respect to the electrical activity.

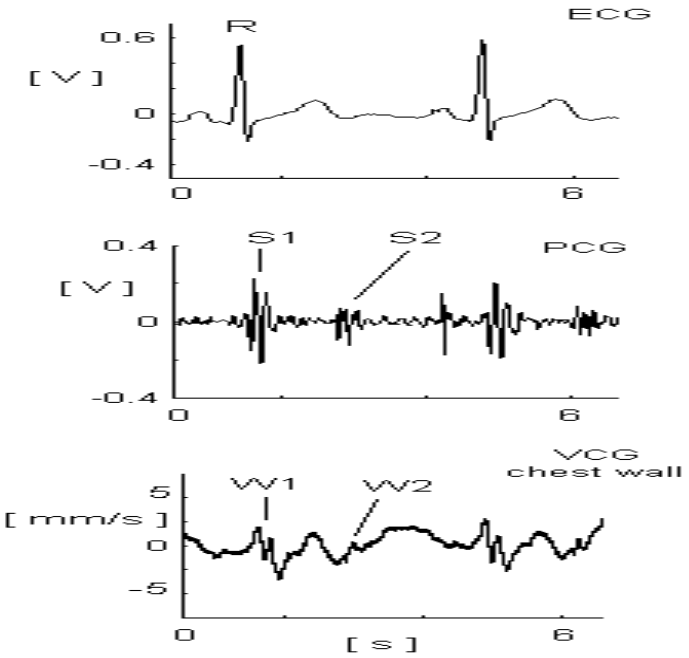

Figure. 5.2 – Example of one beat recordings from VCG and PCG along with II lead ECG. On VCG trace are reported mitral and tricuspid closure (MC and TC) followed by aortic and pulmonary closure (AC and PC).

As for point 2, figure 3 shows synchronous traces of one beat VCG recorded measuring the velocity of displacement of the skin of the neck, in correspondence of the carotid artery, and arterial pressure waveforms, this last recorded using an arterial tonometer : from a visual inspection, it is possible to appreciate the existence of a relationship between the peak of the pulse pressure and the peak VCI on the vibrometric trace. In particular optical VCG is able to catch the deformation of the carotid artery, consequence of the energy imparted to the arterial tree by the cardiac muscle contraction (the empirical relation between transmural pressure and radial velocity of vessel wall dilation has been proposed by[59].

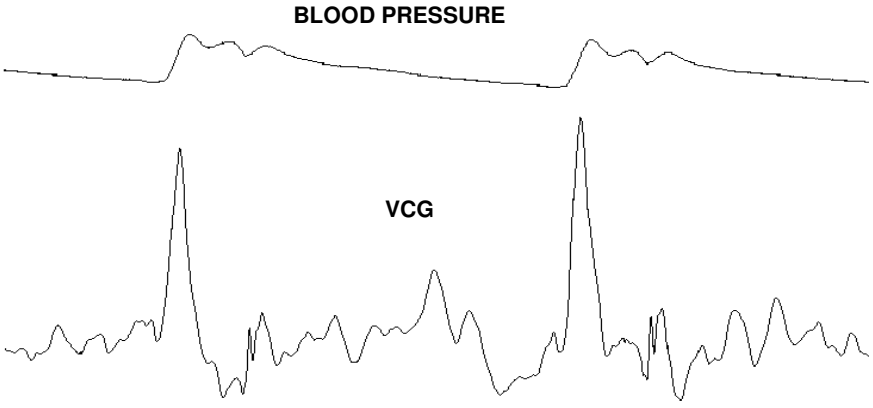

Figure 5.3 - Example of two beats recordings from optical VCG and pulse pressure measured in carotid artery by means of applanation tonometry

Recordings shown in figure 5.1, 5.3, joined with the results recently obtained by Scalise and Morbiducci [58], confirm that peak VC in the VCG beat on carotid artery is representative of the systolic peak component. Figure 5.4 shows a typical VCG beat from carotid artery together with the II-lead output of the ECG, synchronously recorded. Diastolic and systolic ECG points and events are identified. In particular, after a visual inspection of the traces, it is possible to identify by comparison with the ECG:

- the morphological complex corresponding to the atrial depolarization (P wave on ECG), labelled PI;
- the complex corresponding to the repolarization of the ventricles (T wave on ECG), labelled PII;
- the point labelled VCI in figure 5.4. This fiducial point is the local maximum value in the VCG trace, representative of the ventricular repolarization (QRS complex maximum on ECG).

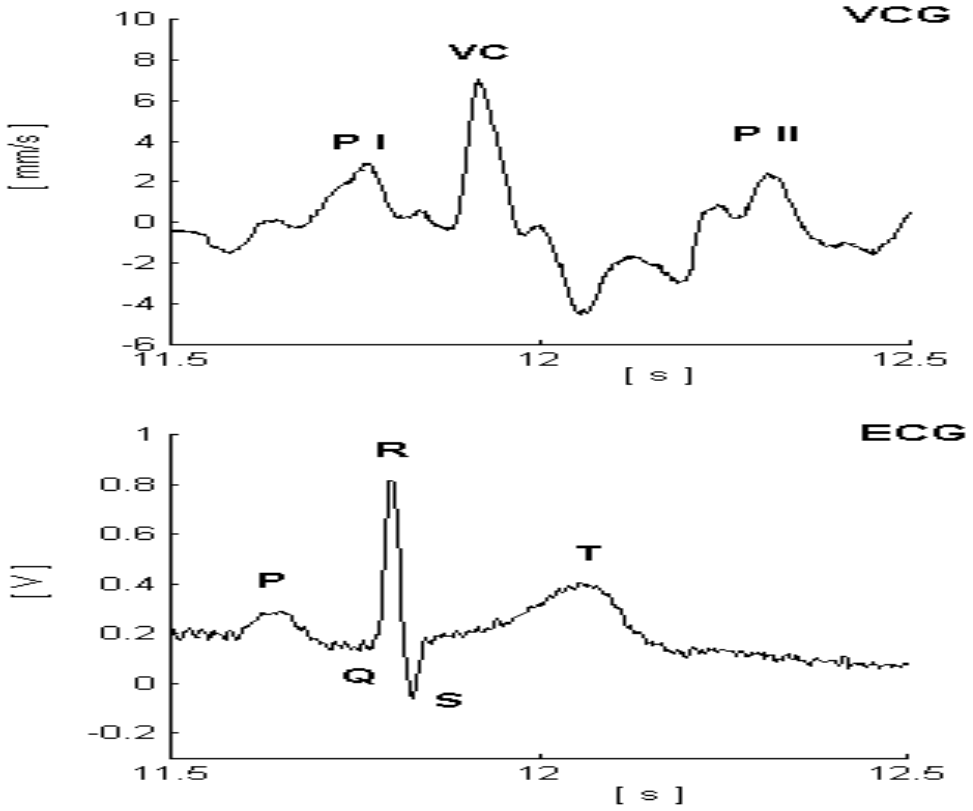

Figure 5.4 - Example of a one beat vibrocardiogram (VCG), together with the simultaneously recorded ECG II-lead output. Individual components of the cardiac cycle are labelled on the ECG trace

5.3 MATERIALS & METHODS

Validation Database

In opposition to QRS detection algorithms [MIT-BIH ECE Database. Massachusetts Inst. Technol., Cambridge. [Online]. Available: http://ecg.mit.edu], there are no standard databases available for the evaluation of optical VCG feature detection algorithms. Thus, a database was built up of N beats measuring, using laser Doppler vibrometry, the vibrations of the skin of the neck, transmitted by the propagation of hemodynamic waveforms in the carotid vessel. M healthy subjects were recorded at rest (males, aged from 21 to 40 years).

According to the scheme proposed by Aboy et al [57] .Instructions for Labeling Segments Used on the Evaluation of the BSP-Automatic Pressure Detection Algorithm. Portland State University. [Online]. Available: http://bsp.pdx.edu] for classifying traces used on the evaluation of a detection algorithm for blood pressure signals, one expert has performed manual annotations for all the recorded beats. The expert has visually classified each segment as follows:

- a segment is considered normal when noise corrupting the signal is in the order of the corrupting noise (baseline drift, power-line interference, etc.) typically present for the specific waveform;
- a segment is considered corrupted when the signal contains artifacts (device saturation, perturbation of the sensor due to sudden movement by the patient) that prevent analysis methods from being effective;
- a segment is classified as absent in the presence of a signal loss (constant) for more than 20 ms.

Once they have been classified, only normal and corrupted beats have been included in the validation database.

Experimental Set Up

The experimental set up is the one proposed in previous studies [8,10,30].

Measurements have been performed using a single-point, direct beam laser Doppler vibrometer (Polytec GmbH, Germany), characterized by a maximum velocity range of 10 m/s, a 0 to 350 kHz maximum bandwidth, a resolution of about 1 μm/s and an accuracy in the order of 1%-2% of RMS reading. The LDVi system incorporates a laser sensor working with a He-Ne laser source (632.8 nm), a Mach-Zender interferometer, and an optical modulator (Bragg cell) which allow the measurement of the instantaneous velocity (amplitude and direction) of the point of the surface

where the laser spot is focused. Exhaustive details on LDVi principle and technique can be found in [1].

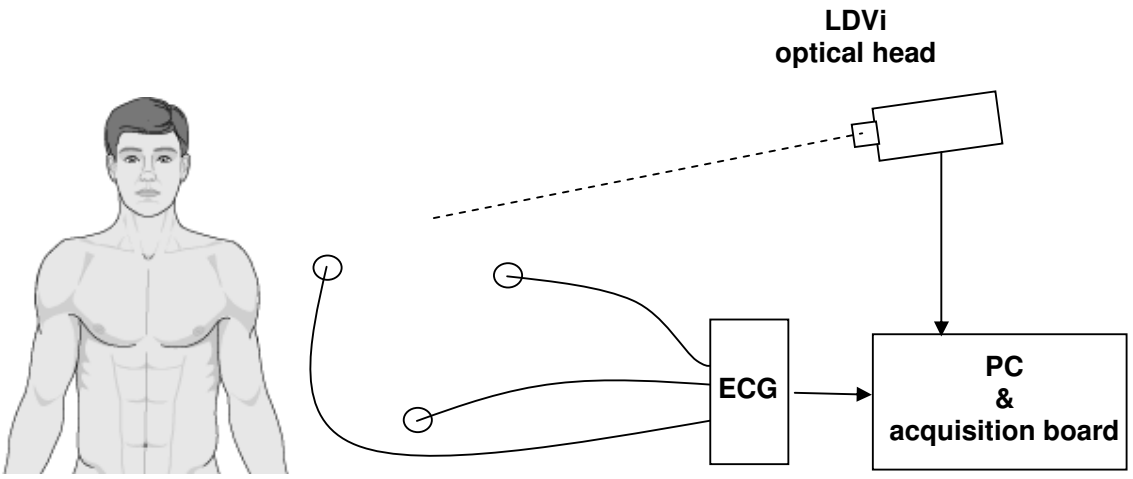

Figure 5.5 – Sketch of the experimental set-up.

Figure 5.5 depicts the experimental set-up used in this study. The optical head has been placed at about 2 m distance from the recorded subjects, pointed on the skin of the neck, in correspondence to the carotid artery. Like in previous studies a small (about 2 mm2, weight < 1 g) adhesive retro-reflective tape has been placed on the site of measurement, aiming to to optimise the quality of the vibratory signal (increase of the S/N ratio).

On each subject, optical VCG traces have been recorded synchronous to ECG (obtained from the II-lead output), at a sampling frequency of 1 kHz. A 12-bit A/D acquisition board, together with a custom-made software program developed in a LabVIEW® environment (National Instruments, Usa), have been used to store the signals.

As for safety precautions, the LDVi is a Class II B device, so that no special safety measures are required (laser power is less than 1 mW).

5.6 Algorithm Description

A - Algorithm Overview

The basic concept is to extract from the VCG signal itself a reference time series (preprocessing stage) to be used in the detection of systolic events on the raw VCG signal itself (decision stage). Figure 5.6 shows the two-stages architecture of the detection algorithm (widely employed in most ECG detection algorithms, and recently suggested in pressure detection algorithms).

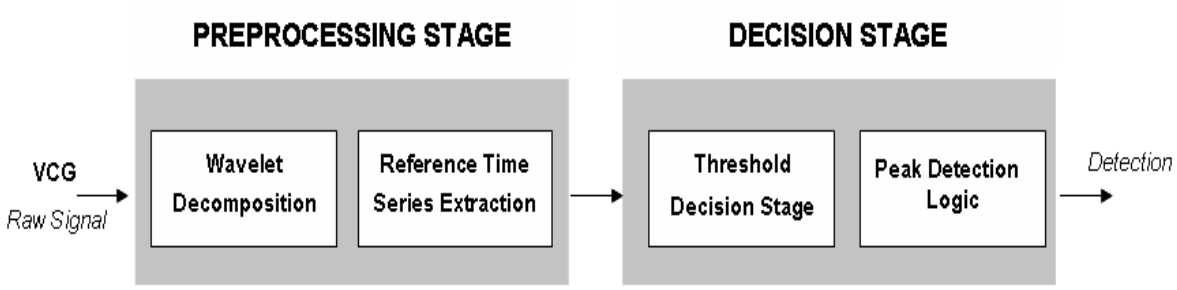

Figure 5.6 - Architecture of the detection algorithm.

The preprocessing stage extracts a reference time series from the signal, and the decision stage performs the actual component detection.A preprocessing stage extracts a reference time series from the raw VCG signal, and a decision stage, using the time series exiting from the preprocessing stage as markers for time location, decides if an incoming peak is a true component based on a user-specified logic (threshold).

B - Preprocessing stage

In this approach first it is represented the VCG signal at different scales. Then it was choose the scale that carries the most information relevant to heart signal.
The preprocessing stage relies on a combined use of wavelets and signal derivatives. Figure 5.7 shows a block diagram of the preprocessing stage of the detection algorithm, consisting of nine blocks.

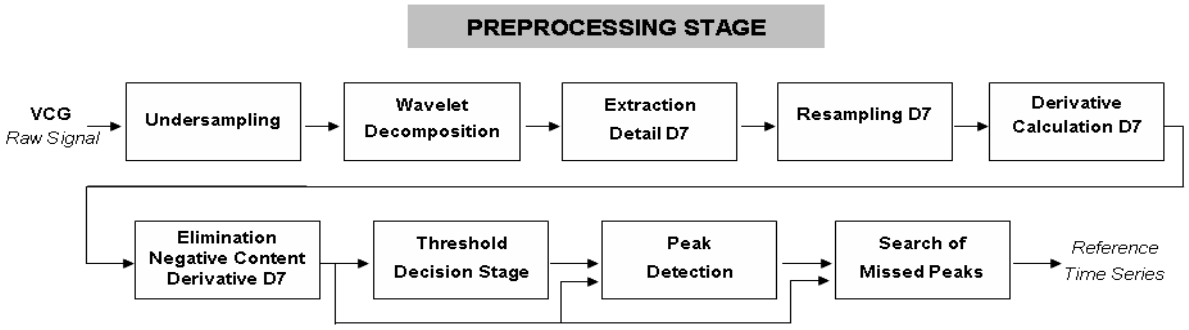

Figure 5.7 - Block diagram showing the architecture of the preprocessing stage of the algorithm proposed for peak component detection in optical VCG signals.

Once the VCG signal has been downsampled to 200 Hz the wavelet transform, i.e., a time-scale representation based on multiresolution signal decomposition, has been selected, since it is able to localize the frequency changes of a non-stationary signal and is free of any assumptions regarding the statistical characteristics of the signal. Multiresolution analysis has been formulated by Mallat [26], and a large body of research exists on using wavelets for signal analysis [19].

It is useful to remind here that the continuous wavelet transform of a signal f(t) is defined as [26]:

$$W_f(s,\tau) = \int_{-\infty}^{\infty} f(t) h^*_{s,\tau}(t) dt \qquad (2)$$

where hs,τ(t) is a set of basis functions (wavelets) and * is the complex conjugate. The wavelet transform is in fact a linear operation that decomposes the signal under study into a family of functions which are the translation and dilatation of a wavelet function named mother wavelet. The wavelets are generated from a single wavelet h(t) by scaling and translation, according to the following relationship:

$$h_{s,\tau}(t) = \frac{1}{\sqrt{s}} h\left(\frac{t-\tau}{s}\right) \qquad (3)$$

being s the scale factor and τ is the translation [26]. In the present paper a discrete wavelet transform was implemented, built up with orthogonal dyadic functions, that can be expressed as:

$$h_{i,k}(t) = 2^{-\frac{i}{2}} h(2^{-i}t - k) \qquad (4)$$

where i and k are integers.

A twelve levels decomposition has been chosen, by means of the mother wavelet function Daubechies 7 (Db7) [28], and the coefficients derived from the decomposition were implemented to obtain the signal details (referred to D1–D12).

The level of decomposition has allowed to isolate, on the vibrometric trace, the frequency sub-band of interest for the cardiac rate (corresponding to the signal detail D7). In fact, each sub-band shows a frequency bandwidth which is the half with respect to the previous level and double with respect to the successive one, starting from the upper frequency limit of the first decomposition level which is the half of the sampling rate. As we have downsampled the signal to 200 Hz, the sub-band of detail D7 is proportional to values going from 0.78 to 1.56 Hz, i.e., a range including normal heart rate.

Once generated the wavelet decomposition of the original vibrometric signal, the extraction of detail D7 is followed by the calculation of its time derivative, $\dot{D7}$, which is resampled to 1 KHz and manipulated, to obtain the non negative signal $\dot{D7}*$, as follows:

$$\dot{D7}*(t) = \begin{cases} \dot{D7}(t) & \text{if } \dot{D7}(t) > 0 \\ 0 & \text{if } \dot{D7}(t) \leq 0 \end{cases} \qquad (5)$$

The example in figure 5.8 clearly displays the strict relationship between the morphology of the signal $\dot{D7}*(t)$, and the QRS complex in the ECG trace: from a visual inspection, it is evident that in each time interval identified by two consecutive sinusoid-like convex half waves in $\dot{D7}*$ falls one VC fiducial point of the VCG recorded signal (and one QRS complex in the ECG synchronous trace).

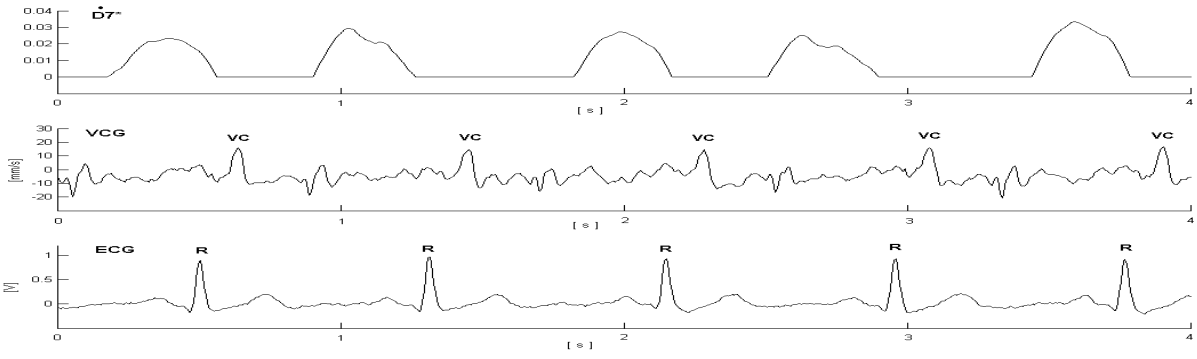

Figure 5.8

Thus, a first peak detection is performed at this stage in the algorithm, and it is used to detect all peaks in the $\dot{D}7^*$ signal, exiting from the processing stages of the raw VCG signal described above. The $\dot{D}7^*$ maxima will be employed as reference time series in the decision stage.

In consequence of the observed variability among subjects, in the dynamics of the VCG traces, the maxima detection is preceded by a stage for the tuning of parameters, on the first 20 seconds recording, needed for the setting of a threshold value. To do this, it was implemented a threshold-based peak detector algorithm inside a while loop structure.

The peak detector algorithm performs a quadratic polynomial interpolation on sequential blocks of data, the length of which W can be set by the user, together with a threshold value TH: only the interpolated data greater than TH are considered, and among them the occurrence of a maximum in the interpolating function is recognized as the occurrence of a maximum in $\dot{D}7^*$. The embedding of the peak detector inside a while loop allows the user of modifying interactively the parameters W and TH, and then evaluate immediately by visual inspection (the signal segment, and the result of the detection are plotted on the computer screen) the performance of the parameters setting in identifying maxima in the segment of signal $\dot{D}7^*$. When the identification of the maxima in the 20 s length segment of $\dot{D}7^*$ has been considered the optimum by the user, the while loop is stopped and the threshold value TH identified is given in output.

The tuning of a threshold value TH is the sole stage in the detection algorithm requiring the action of the user. However, this operation does not take more than 10 - 30 seconds to be performed.

Benchmark Parameters

Following the guidelines proposed by the Association for the Advancement of Medical Instrumentation (AAMI) [(1998) ANSI/AAMI CE57: Testing and Reporting Performance Results of Cardiac Rhythm and ST Segment Measurement Algorithms. (AAMI) Recommended Practice/American National Standard. [Online]. Available: http://www.aami.org], and in analogy with evaluation criteria of the performance of the algorithms for the QRS automatic detection on ECG traces, two benchmark parameters were used to assess the algorithms performance: sensitivity and positive predictivity. Sensitivity (Se) and positive predictivity (+P), defined as

$$S_e = \frac{TP}{TP + FN}$$

$$+P = \frac{TP}{TP + FP}$$

where TP is the number of true positives, FN the number of false negatives, and FP the number of false positives.

The sensitivity Se indicates the percentage of true beats that were correctly detected by the algorithm. The positive predictivity indicates the percentage of beat detections which can be labeled as such.

Beyond these two parameters, we calculate the detection error rate (DER) defined as:

$$DER = \frac{TP + FP}{NB}$$

where NB is the total of analyzed VCG beats.

The algorithm was validated prospectively against peak detections annotated by an expert. The performance of the algorithm was: assessed without taking into consideration whether they contained portions of significant artefact, at first; then, after an expert classified by visual inspection each segment as normal, absent, or corrupted, the algorithm performance was assessed using as the "true" peaks on the normal and corrupted segments the ones annotated by the expert.

RESULTS

The algorithm was developed using VCG signals from different subjects than those used for performance assessment.

Table I summarizes the algorithm's sensitivity, positive predictivity, and detection error rate with respect to the VC point detection, for the VCG traces. These are based on one expert's manual annotations for all N beats including segments classified as normal, corrupted, and absent. A visual inspection of ECG traces (widely used in the clinical practice) synchronously recorded have been supported the expert in the classification procedure.

Table I: Sensitivity, positive predictivity and detection error rate of the detection algorithm. These results used the expert manual annotation on 6783 beats. The recorded segments include regions of severe artefacts.

subject	beats	FP	FN	TP	Se	+P	DER
1	324	1	2	322	0.9938	0.9969	0.9969
2	291	8	8	283	0.9725	0.9725	1.0000
3	266	4	6	260	0.9774	0.9848	0.9924
4	291	6	8	283	0.9725	0.9792	0.9931
5	381	2	2	379	0.9947	0.9947	1
6	394	4	10	384	0.9746	0.9896	0.9847
7	340	6	8	332	0.9764	0.9822	0.9941
8	264	5	6	258	0.9772	0.9809	0.9962
9	295	0	0	295	1.0000	1.0000	1.0000
10	364	4	7	357	0.9807	0.9889	0.9917
11	425	1	5	420	0.9882	0.99762	0.9905
12	162	2	2	160	0.9876	0.9876	1.0000
13	234	5	5	229	0.9786	0.9786	1.0000
14	337	1	1	336	0.997	0.997	1.0000
15	220	5	8	212	0.9636	0.979	0.9863
16	277	2	4	273	0.9855	0.9927	0.9927
17	240	2	5	235	0.9791	0.9915	0.9875
18	420	8	10	410	0.9761	0.9808	0.9952
19	772	6	14	758	0.9818	0.9921	0.9896
20	185	4	6	179	0.9675	0.9781	0.9891
21	301	5	6	295	0.9801	0.9833	0.9966
tot	6783	81	123	6660	/	/	/
mean values	323	4	6	317	0.9812	0.9870	0.9941

Table5.1

The algorithm's average sensitivity on the 6783 beats is 98.12 %, with an average positive predictivity of 98.70 % and a detection error rate of 99.41 %.

Like in Aboy et al. [57], it was compared the performance of the algorithm in terms of sensitivity, positive predictivity and detection error rate, with:

- detection by visual inspection of two different experts (UM & AS), on beats classified as normal or corrupted;

- automatic detection of the QRS complex from ECG synchronously recorded traces applying the algorithm proposed by Pan and Tompkins (ref), widely used in ECG practice (on ECG signal processing, details can be found in [8]).

Table II reports the algorithm's sensitivity, positive predictivity and detection error rate on VCG signals, respectively, on 2000 randomly selected beats. The inter-expert agreement is also reported with AS used as the "true" peaks. Results in table II show that the proposed detection algorithm can

be considered as accurate as the experts are with one-another (all benchmark parameters exceed the 99 % value).

Table II - Sensitivity, positive predictivity and detection error rate of the detection algorithm validated againt two experts manual annotations of 2000 beats randomly selected in VCG traces. The table summarizes the performance of the algorithm (DA) against the two experts (UM, AS), and the results of the consistency check of the experts between themselves.

	FN	FP	Se	+P	DER
AD-AS	18	11	0.9910	0.9943	0.9967
AD-UM	14	12	0.9935	0.9942	0.9993
UM-AS	4	1	0.9980	0.9995	0.9985

Table 5.2

Table III shows the performance of the proposed algorithm against the automatic detection of the systolic event on ECG traces recorded synchronously with VCG: the R peaks on ECG recordings, used the as the “true” peaks, have been identified applying the widely used algorithm proposed by Pan and Tompkins [12].

Table III - Sensitivity, positive predictivity and detection error rate of the detection algorithm. These results used the as the “true” peaks the R peaks on ECG synchronously recorded traces, automatically detected applying the algorithm proposed by Pan and Tompkins on 6783 beats. The recorded segments include regions of severe artefacts.

subject	beats	FP	FN	TP	Se	+P	DER
1	324	0	0	324	1.0000	1.0000	1.0000
2	291	4	5	286	0.9828	0.9862	0.9965
3	266	0	0	266	1.0000	1.0000	1.0000
4	291	1	6	285	0.9793	0.9965	0.9828
5	381	0	0	381	1.0000	1.0000	1.0000
6	394	0	1	393	0.9974	1.0000	0.9974
7	340	1	1	339	0.9970	0.9970	1.0000
8	264	0	0	264	1.0000	1.0000	1.0000
9	295	0	0	295	1.0000	1.0000	1.0000
10	364	0	0	364	1.0000	1.0000	1.0000
11	425	0	0	425	1.0000	1.0000	1.0000

12	162	4	3	159	0.9814	0.9754	1.0060
13	234	0	2	232	0.9914	1.0000	0.9914
14	337	0	0	337	1.0000	1.0000	1.0000
15	220	0	0	220	1.0000	1.0000	1.0000
16	277	0	0	277	1.0000	1.0000	1.0000
17	240	0	0	240	1.0000	1.0000	1.0000
18	420	0	0	420	1.0000	1.0000	1.0000
19	772	0	0	772	1.0000	1.0000	1.0000
20	185	0	0	185	1.0000	1.0000	1.0000
21	301	0	0	301	1.0000	1.0000	1.0000
tot	6783	10	18	6765	/	/	/
mean values	323	0	1	322	0.9966	0.9979	0.9988

Table 5.3

Results in table III assess that the performance of the proposed automatic algorithm in identifying systolic events on VCG traces is equivalent to the one of the most widely used automatic algorithms [12] for QRS complex detection, on ECG synchronously recorded traces.

The potency of the proposed automatic algorithm is evident in the illustrative example of figure 5.9, showing a 2 s VCG segment and the peaks (VC) identified by the detection algorithm (synchronous ECG recording is also showed, as reference signal). The component VC usually has the highest amplitude (see figures 5.3, 5.4), however the three peaks common to VCG signals (Peak I, II and III), which are more variable and very close to peak VC, might have the same amplitude as VC, or greater. In general when this circumstance takes place, it makes the automatic detection of a peak very close to peaks of the same amplitude, very difficult : figure 5.9 displays that the detection algorithm is able to correctly identify the peak of interest also in the presence of pulse morphologies where a clearly distinguishable peak is absent.

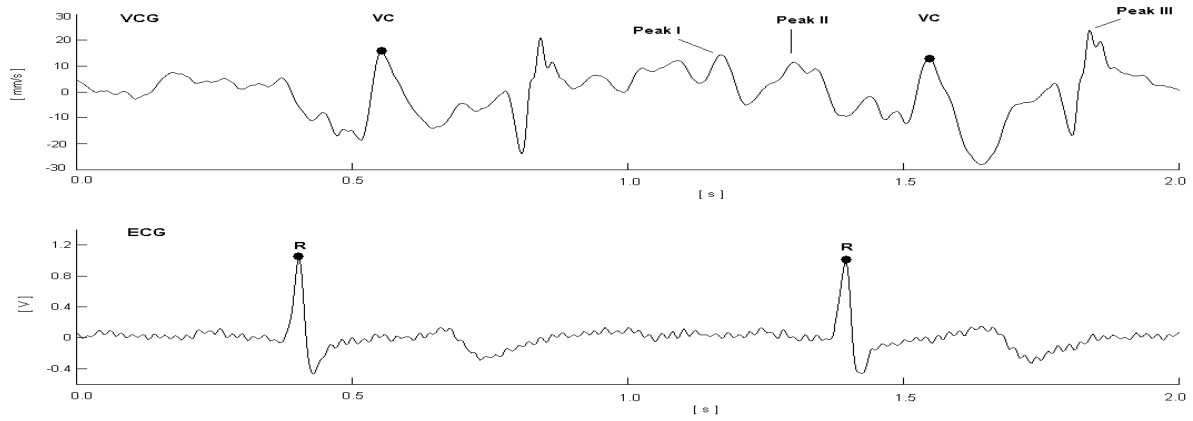

Figure 5.9

Figure 5.9 displays an example when the automatic algorithm detects a peak different than the experts in a VCG signal (synchronous ECG recording is also showed, as reference signal). Note that the VCG segment shown in figure !! is corrupted by an artefact, generated by an accentuated, voluntary movement of the subject. In opposition to the experts, the algorithm identifies a peak that can be classified as a false positive, and at the same time the correct peak is missed (false negative): thus, there is no over detection, but this specific situation reduces the algorithm's reported sensitivity, positive predictivity, and detection error rate.

However, in general, regions where artifacts due sudden movement occur have a slight effect on normal beats that are close (figure 5.10) confirms this, displaying that peaks immediately following the artifact are correctly identified): this occurs because these artifacts cannot affect the interbeat intervals extrapolated from the derivative of detail D7 (obtained after the wavelet decomposition), used to locate the event of interest in time.

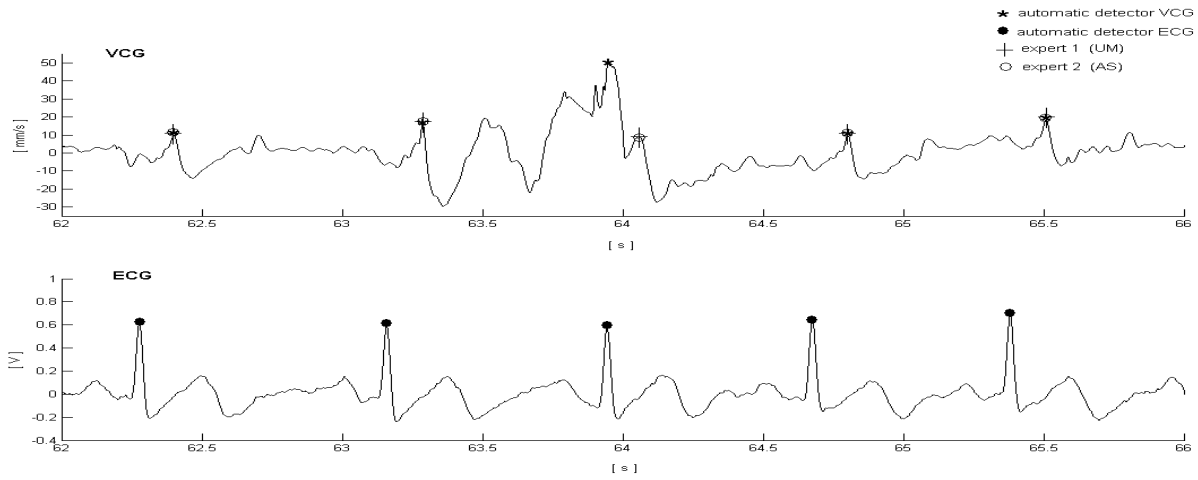

Figure 5.10

Comments

Since automatic detection algorithms are necessary for most types of systems/devices that monitor cardiac activity, we retain that the herein presented algorithm might be useful to researchers interested in biosignals with features similar to optical VCG (like seismocardiography and apexcardiography), avoiding them of either manually annotate short segments or implement their own semi-automatic, not rigorously validated, algorithms that lack the performance, generality, and robustness of modern detection algorithms for ECG signals .

There are numerous current and potential applications for pressure beat detection algorithms :

- Many pulse oximeters perform beat detection as part of the signal processing necessary to estimate oxygen saturation, but these algorithms are proprietary and cannot be used in other applications.
- Systolic peak detection is necessary for some measures of baroreflex sensitivity .
- Identification of the pressure components is necessary for some methods that assess the interaction between respiration and beat-by-beat ventricular parameters and the modulation effects of respiration on left ventricular size and stroke volume
- Detection is a necessary task when analyzing arterial compliance and the pressure pulse contour
- Beat-to-beat morphology analysis of ICP also requires robust automatic detection...

Conclusions

In this work, it has been proposed the deepening of a novel optical approach (vibrocardiography, VCG) able to evaluate some important mechanical parameters from the cardiovascular system; these parameters are: the left ventricular filling time (LVST) and the pulse transit time (PTT). The main advantage of the proposed approach is that it realises a fully non-contact measurement method to observe the compression waves that, generated by the heart during its periodic movement excited by depolarization waves, are transmitted toward the chest wall.

In the past, the vibrometric signal obtained by VCG was already demonstrated to be valid for the evaluation of the mechanical functionality of the heart, i.e. heart rate (HR) and heart variability (HRV), being possible to identify on the VCG generated signal specific reference points associated to the events of the cardiac cycle [8].
The sensitivity of the optical Vibrocardiography (VCG) to perform heart rate variability (HRV) analysis as the ECG. was already investigated and represents a quantitative marker of autonomic activity, and a powerful tool in the recognition of the relationship between the autonomic nervous system and cardiovascular mortality, including sudden cardiac death. In previous works, no significant differences (mean difference between techniques: 3.1%, [8]) were obtained from the VCG analysis of HRV in terms of gender. Males and females showed similar very low percent differences in the values of HRV descriptors calculated by means of VCG and ECG, even if higher differences where found for females, with respect to males. This can be ascribed only in part to the different chest wall movements, being them probably due to the different anatomic features of the chest in the region where the laser beam was pointed for measurements .

The VCG method was firstly studied as from the point of view of measurement issues and a general signal characterization showed that the effect of the skin surface on the

vibratory signal is, in general, a signal-to-noise reduction with respect to the VCG vibratory signals measured, in similar conditions, from an “optimal” surface, i.e. a 2 mm^2 square retro-reflective tape applied on the skin [9]. Moreover, VCG traces measured directly from skin are possibly affected by signal “drop-out” (velocity spikes due to sudden demodulator faults), in such occurrence it was proposed a strategy based on VCG signal filtering based on the use of tracking filters allowing drop-out effects avoidance. Specific spectral and multiresolution analysis puts in evidence characteristics in the VCG signal that are peculiar of the measured position on the chest wall, resulting in an optimal chest position corresponding to the low stern. Moreover from such results it came out that wavelet decomposition, a suitable technique for the analysis of non-stationary signals, is eligible to be a valid tool for the investigation of VCG signals .

Moving from this point an automatic detection algorithm based on wavelet transform was realized, it is able to identify the time-location of the systolic peak VC, which has been identified to be corresponding to the R peak in ECG trace , in optical VCG signals measured on the skin of the neck, in correspondence of the carotid artery [10,58]. Hence, the convenience for developing automatic methods to process the biosignals, and to extract peculiar features from them is fundamental; larger data set can be used in the testing and, moreover, it has been widely demonstrated that automatic analysis lead to an improvement in the recognition of patterns of cardiac diseases, thus allowing an early diagnose and, therefore, an efficient treatment.
Since automatic detection algorithms are necessary for most types of systems/devices that monitor cardiac activity, the herein presented algorithm might be useful to researchers interested in biosignals with features similar to optical VCG (like seismocardiography and apexcardiography), avoiding them of either manually annotate short segments or implement their own semi-automatic algorithms that lack the performance, generality, and robustness of modern detection algorithms for physiological signals. Identification of the VCG components is necessary for some

methods that assess the interaction between respiration and beat-by-beat ventricular parameters and the modulation effects of respiration on left ventricular size and stroke volume; finally detection is a necessary task when analyzing arterial compliance and the pressure pulse contour.

Results show that the performance of the proposed automatic algorithm in identifying systolic events on VCG traces is equivalent to the one of the most widely used automatic algorithms [12] for QRS complex detection, on ECG synchronously recorded traces.

The potency of the proposed automatic algorithm is evident in the illustrative example of figure c1, showing a 2s VCG segment and the peaks (VC) identified by the detection algorithm (synchronous ECG recording is also showed, as reference signal).

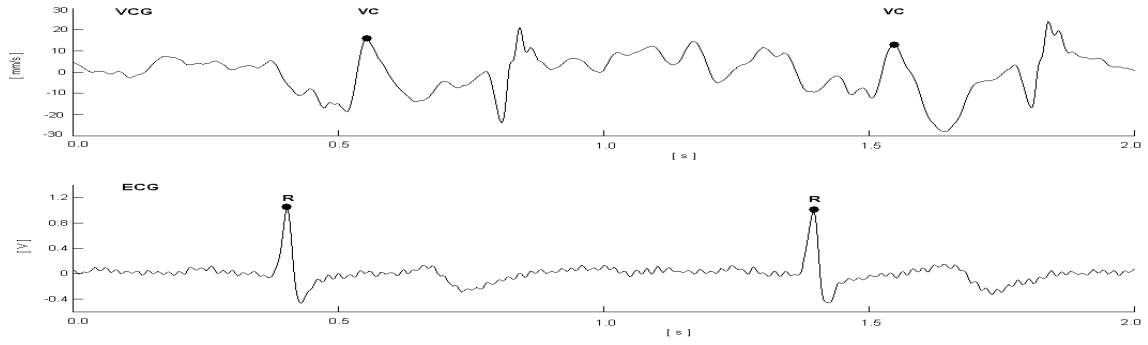

Figure c1 : example of VC peak automatic detection with an R-peak ECG detection.

One of the most important technique for the assessment of cardiac function is achieved by the detection and analysis of systolic and diastolic heart tones and their temporal relationships to the ECG. The primary acoustic cardiography parameters of relevance for the management of systolic heart failure is LV systolic time (LVST): the interval in milliseconds usually measured by standard phonocardiogram (PCG)

the first and second heart sounds (S1 and S2); this interval is typically reduced in patients with LV dysfunction respect to healthy subjects.

Moving from this base, one of the aims of this thesis was to go further insight in the characterization of the morphology of optical VCG traces by comparison with synchronously recorded traces accounting for well known events of the cardiac mechanics . In particular ECG and PCG traces were chosen, the latter being sensitive to the two major audible heart sounds in the healthy cardiac cycle: the first one, S1 (mitral and tricuspid valves closure) which occurs at the onset of ventricular contraction and the second one, S2 (aortic and pulmonary valves halting) which is present at the end of ventricular systole.

It was showed that information fusion from both electric signals and sound signals, allowed to locate events of the cardiac cycle on VCG signals. Mean filling time carried out after visual inspection for each subjects show minimal differences between phonocardiography and optical vibrocardiography as a first assessment of the usefulness of the laser non contact technique [30].

In a following step , a signal processing algorithm by means of wavelet transform was proposed ; with this it was demonstrated that it is analytically possible to identify the same events on VCG and PCG .As a final stage the filling time interval was carried out after the signal processing step and the results show that by this algorithm it is possible an optimal evaluation of LVST, which plays a fundamental role in evaluating a correct cardiac resynchronization therapy [21]). (table c1)

Subjects	S2-S1 pcg)	SD	S2-S1 pcg) - WT	SD	W2-W1(vcg) WT	SD	W2-W1 (vcg) WT	SD
1	340.71	1.14	339.89	1.25	335.43	1.22	336.75	1.19
2	309.07	1.58	309.59	1.74	312.47	2.45	311.27	1.47
3	347.43	1.91	348.34	1.11	355.50	1.87	355.12	0.88
4	291.47	1.96	292.78	0.97	282.47	1.36	283.59	1.56
5	334.54	1.33	334.92	1.45	342.38	2.14	343.08	1.11
6	283.00	1.37	282.76	1.93	288.06	1.14	289.16	1.88
7	263.33	1.54	264.16	1.53	268.35	1.18	268.47	0.78
8	298.21	0.80	297.82	1.67	294.57	2.14	295.97	1.84

Table c1 : filling time intervals calculated both by visual inspection and after wavelet transform

This study, even if preliminary, has put in evidence the potency of optical Vibrocardiography in retrieving and monitoring critical parameters at the base of the cardiac activity in similarity to phonocardiography. This could be an added value, if we consider that optical VCG , as said before , has been recently demonstrated to be equivalent to ECG in monitoring both the cardiac rate and the heart rate variability and been a fully non-contact measurement method. [8,10]

The last stage of this thesis moved from direct heart characterization to the periphery (arterial system), in fact it was aimed the use of optical VCG in retrieving the pulse transit time (PTT), a fundamental parameter in characterizing the vascular bed functionality and so in evaluating pathological conditions like hypertension [53].
PTT is the time interval for the arterial pressure pulse to travel from the aortic valve to a peripheral site and can be used to measure the mean pulse wave velocity (PWV) once known (or estimated) the distance between two measurement points
Applanation tonometry, the gold standard non invasive technique, is a contact method, based on the use of a pressure sensor that flattens the artery at the measuring spot and detects the pressure variations within the superficial artery. Correct sensor positioning is crucial for correct measurement (needing a specific skill), and because of the necessity to deform the vessel and because of the dimension of the pressure sensing heads, it is difficult to measure pressure waves at adjacent spots; measurement problems are possible in subjects with deeper arteries.
Both problems are solved by use of VCG, because of the wave speed of the laser beam (speed of light), local skin velocity displacement measurements can be done with very high sensitivity, at temporal resolution far exceeding >1 kHz. Being a fully non-contact method, a configuration with 2 or more adiacent sensors is no problem.
It was possible to observe minimal differences between VCG and tonometry in retrieving the PTT parameter in several analysis steps; the Bland-Altmann test [17]

between carried out on PTT measured with VCG and standard applanation tonometry confirms the great similarity (mean difference, 1 ms) of the two techniques (figure c2).

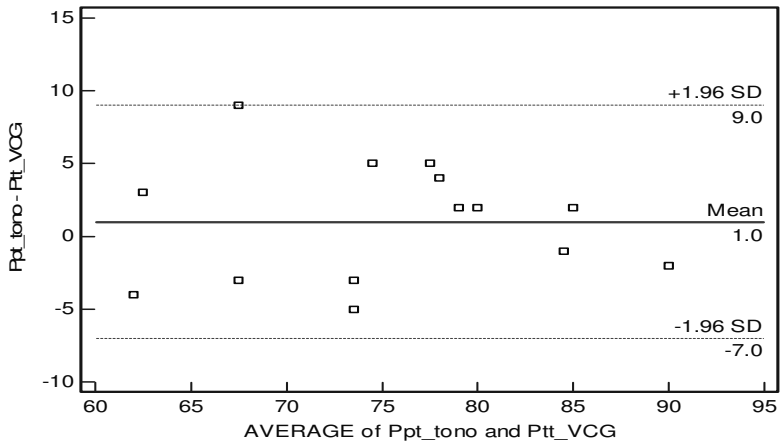

Figure c 2 : Bland-Altmann test over PTT calculated both with VCG and applanation tonometry

Future goals will be the confirmation , trough a large study , of those preliminary results that the sole optical VCG signal could furnish part of the informative content that is now obtained by distinct physiological measurements, i.e., breathing, arterial pressure, cardiac sounds and electrical activity of the heart. that normally furnish the relevant patient's condition related to the pathology.

Acknoledgements

The author wish to tank Prof. Enrico Primo Tomasini and PhD. Lorenzo Scalise for the endless support to the research activity.

Incommensurable was the help and really precious were the teachings receveid by the author from PhD Umberto Morbiducci ….definitively a master than a tutor .

Obviously the author wish to thank Prof. Patrick Segers and Prof. Pascal Verdonck and the whole staff of IBITECH (Ghent Universiteit – Flanders – Belgium) for the fundamental support in the research field and for having considered me like one of the group .

REFERENCES

[1] Tomasini, E.P., G.M. Revel, and P. Castellini. Laser based measurement, Encyclopaedia of Vibration, Academic Press, London, 699-710, 2001.

[2] Tomasini E.P., Pinotti M., Paone N., Carotid artery pulse wave measured by a laser vibrometer. Proc SPIE of the 3rd Int Conf on Vibration Measurements by Laser Techniques: Advances and Applications, Ancona, 1998; 3411: 611-616.

[3] P.Castellini, L.Scalise, Teeth mobility measurement by laser Doppler vibrometer**,** Review of Scientific Instruments, 70, 6, 2850-2855, 1999

[4] Castellini, G.M.Revel, P., Scalise, Vibration measurements for diagnosis of structural defects on human teeth, Measurement, 27, 29-42, 2000, Elsevier Science Ltd., Oxford, UK (ISSN 2632-2241).

[5] G.M. Revel, A. Scalise and L. Scalise, Measurement of stress-strain and vibrational proprieties of tendons, Measurement Science and Technology, 14, 1427 – 1436, 2003, ed. IOP Publishing Ltd

[6] Lorenzo Scalise, Paolo Castellini, Umberto Morbiducci, Costantino Del Gaudio, Mauro Grigioni, Enrico Primo Tomasini. Laser vibrometry for the study of prosthetic mechanical heart valves. Rapporti ISTISAN 05/46, 1-8 (2005)

[7] Matteo Valentino, Venerando Rapisarda, Lorenzo Scalise, Nicola Paone, Lory Santarelli, Concettina Fenga and Gian Luca Rossi, A new method for the experimental assessment of finger haemodynamic effects induced by a hydraulic breaker in operative conditions, Journal of Occupational Health 46: 253–259, 2004

[8] U. Morbiducci , L. Scalise , M. De Melis , M. Grigioni Optical Vibrocardiography : a novel tool for the optical monitoring of cardiac activity , Annals of Biomedical Engineering 2007 Jan;35(1) 45-58.

[9] L. Scalise , U. Morbiducci , M. De Melis A Laser Doppler approach to cardiac motion monitoring effects of surface and position , VII Conferenza AIVELA 2006

[10] M. De Melis, M. Grigioni, U. Morbiducci, L. Scalise. Optical monitoring of heart beat . Modelling in medicine and Biology, WIT press 2005 ;181-190. – Book Chapter

[11] Task Force of the European Society of Cardiology and the North American Society of Pacing and Electrophysiology. Heart rate variability: standards of measurement, physiological interpretation, and clinical use. *European Heart Journal* 17:354-381, 1996.

[12] Pan, J., W.J. Tompkins. Real Time QRS Detector algorithm. *IEEE Transactions on Biomedical Engineering* 32(3):230-23, 1985.

[13] de Chazal, P., M. O'Dwyer, and R.B. Reilly. Automatic Classification of Heartbeats Using ECG Morphology and Heartbeat Interval Features. *IEEE Trancactions on Biomedical Engineering* 51(7):1196-1206, 2004.

[14] DeBoer, R.W., J.M. Karemaker, and J. Strackee. Comparing spectra of a series of point events particularly for heart rate variability data. *IEEE Trans Biomed Eng*. 31(4):384-7, 1984.

[15] Acharya, R., A. Kumar, P.S. Bhat, C.M.Lim, S.S. Iyengar, N. Kannathal, and S.M. Krishnan. Classification of cardiac abnormalities using heart rate signals. *Med Biol Eng Comput.* 42(3):288-93, 2004

[16] Goldberger, A.L. Is the normal heartbeat chaotic or homeostatic? *News Physiol Sci*. 6:87-91, 1991.

[17] Bland, J.M., and D.G. Altman. Statistical methods for assessing agreement between two methods of clinical measurement. *Lancet* 307-310, 1986.

[18] Strean RF, Mitchell LD, Barker AJ. Global noise characteristics of a laser Doppler vibrometer: part II experiments using beam dynamics. Proceedings on Second International Conference on Vibration Measurements by Laser Techniques: Advances and Applications, 1996, Ancona, Italy; SPIE Vol. 2868:97-105

[19] Chui KC. An introduction to Wavelets. Volume I in Wavelet analysis and its applications, Academic Press, New York, 1992

[20] Grigioni M, Carotti A, Del Gaudio C, Morbiducci U, Albanese S, D'Avenio G. Multiresolution analysis of the aortic blood pressure variability as investigational tool in experimental fetal cardiac surgery. Annals of Biomedical Engineering, 2006

[21] Abraham WT et al., for the MIRACLE Study Group. Multicenter InSync Randomized Clinical Evaluation. Cardiac resynchronization in chronic heart failure.*N Engl J Med.* 2002;346:1845–1853

[22] Markus Roos, MD; Stefan Toggweiler, MD; Michel Zuber, MD; Peiman Jamshidi, MD; Paul Erne, MD Acoustic Cardiographic Parameters and Their Relationship to Invasive Hemodynamic Measurements in Patients With Left Ventricular Systolic Dysfunction *(CHF. 2006;12(4 suppl 1):19–24)*

[23] Ayesha Hasan, MD; William T. Abraham, MD; Lori Quinn-Tate, RN, MN; Lei Brown, RDCS, RVT; Ali Amkieh, MD Optimization of Cardiac Resynchronization Devices Using Acoustic Cardiography: A Comparison to Echocardiography *(CHF. 2006;12(4 suppl 1):25–31)*

[24] G Amit, N Gavriely, J Lessick, N Intrator Automatic extraction of physiological features from vibro-acustic heart signals: correlation with Echo Doppler Computers in Cardiology 2005

[25] Durand LG, Pibarot P. Digital signal processing of thephonocardiogram: review of the most recent advancements. Crit Rev Biomed Eng 1995;

[26] S. Mallat, A theory for multiresolution signals decomposition: the wavelet representation, IEEE Trans. Pattern Anal. Mach. Intell. 11 (1989) 674–693.

[27] Vincent Pichot, Jean-Michel Gaspoz, Serge Molliex, Anestis Antoniadis, Thierry Busso, Frederic Roche, Frederic Costes, Luc quintin, jean-rene´ lacour, and jean-claude barthelemy . Wavelet transform to quantify heart rate variability and to assess its instantaneous changes *J Appl Physiol* 86:1081-1091, 1999.

[28] Daubechies I. Orthonormal bases of compactly supported wavelets. Commun Pure Appl Math, 1988;41:909–996

[29] S.M. Debbal, F. Bereksi-Reguig, Analysis of the second heart sound using continuous wavelet transform, J. Med. Eng. Technol. 28 (4) (2004)151–156.

[30] M. De Melis , U. Morbiducci, L. Scalise Identification of Cardiac Events by Optical vibrocardiography : comparison with Phonocardiography IEEE Proceedings of EMBC 2007 -Lyon

[31] Tavel ME. Clinical Phonocardiography & External Pulse Recording. 3rd ed. Chicago: Year Book Medical Publishers Inc.; 1978.

[32] H. Liang, S. Lukkarinen, I. Hartimo, Heart sound segmentation algorithm based on heart sound envelogram, Computers in Cardiology 24 (1997).

[33] Mills, C. J. and Shillingford, J. P. (1967). “A catheter tip electromagnetic velocity probe and its evaluation.” Cardiovasc Res 1: 263-73.

[34] Murgo, J. P. and Millar, H. (1972). “A new cardiac catheter for high fidelity differential pressure recordings.” Proc Ann Conf Engng Med Biol 14: 303-304.

[35] Mandel, M. and Dauchot, P. (1977). “Radial artery cannulation in 1000 patients: precautions and complications.” J Hand Surg 2 2(6): 482-5.

[36] Slogoff, S., Keats, A. and Arlund, C. (1983). “On the safety of radial artery cannulation.” Anesthesiology 59(1): 42-7.

[37] Goldstein, S. and Killip, T. (1962). “Comparison of direct and indirect arterial pressures in aortic regurgitation.” N Engl J Med 267: 1121-1124.

[38] Posey, J. A., Geddes, L. A., Williams, H. and Moore, A. G. (1969). “The meaning of the point of maximum oscillations in cuff pressure in the indirect measurement of blood pressure. 1.” Cardiovasc Res Cent Bull 8(1): 15-25.

[39] Gorback, M. S. (1988). Considerations in the interpretation of systemic pressure monitoring. Complications in critical care medicine. P. D. Lumb and C. W. Bryan-Brown. Chicago, Year Book Medical Publishers: 296.

[40] Davis, R. F. (1985). "Clinical comparison of automated auscultatory and oscillometric and catheter-trasnducer measurements of arterial pressure." J Clin Monit 1(2): 114-9.

[41] Ramsey, M. 3rd. (1991). "Blood pressure monitoring: automated oscillometric devices." J Clin Monit 7(1): 56-67.

[42] Nystrom, E., Reid, K. H., Bennett, R., Couture, L. and Edmonds, H. L. J. (1985). "A comparison of two automated indirect arterial blood pressure meters: with recordings from a radial arterial catheter in anesthetized surgical patients." Anesthesiology 62(4): 526-30.

[43] Gravlee, G., Bauer , S., O'Rourke, M. and Avolio, A. (1989). "A comparison of brachial, femoral and aortic intraarterial pressures before and after cardiopulmonary bypass." Anaesth. Intensive Care 17: 305-311.

[44] Penaz, J. (1973). Photoelectric measurement of blood pressure, volume and flow in the finger. Digest of the 10th International Conference on Medical Engineering, Dresden, Germany.

[45] Smith, N., Wesseling, K. and de Wit, B. (1985). "Evaluation of two protoype devices producing noninvasive, pulsatile, calibrated blood pressure measurement from a finger." J Clin Monit 1(1): 17-29.

[46] Gravenstein, J. S., Paulus, D. A., Feldman, J. and McLaughlin, G. (1985). "Tissue hypoxia distal to a Penaz finger blood pressure cuff." J Clin Monit 1(2): 120-5.

[47] Bos, W. J. W. (1995). Measurement of finger and brachial artery pressure. PhD Thesis. Amsterdam, Universiteit van Amsterdam.

[48] Matthys, K. and Verdonck, P. (2002). "Development and modelling of arterial applanation tonometry: a review." Technology and Health Care 10(1): 65-76.

[49] Sato, T., Nishinaga, M., Kawamoto, A., Ozawa, T. and Takatsuji, H. (1993). "Accuracy of a continuous blood pressure monitor based on arterial tonometry." Hypertension 21: 866-874.

[50] Karamanoglu, M. and Fenely, M. P. (1996). "Derivation of the ascending aorta-carotid pressure transfer function with an arterial model." Am J Physiol 271: H2399-H2404.

[51] Tanaka, S. and Yamakoshi, K. (1996). "Ambulatory instrument for monitoring indirect beat-to-beat blood pressure in superficial temporal artery using volume-compensation method." Med Biol Eng Comput 34: 441-447.

[52] Fung Y.C. Biomechanics – Circulation , Springer 1997

[53] Justine Ina Davies and Allan D. Struthers Pulse wave analysis and pulse wave velocity: a critical reviewof their strengths and weaknesses Hypertension 2002

[54] Segers P, Rietzschel ER, De Buyzere ML, Vermeersch SJ, De Bacquer D, Van Bortel LM, De Backer G, Gillebert TC, Verdonck PR; Asklepios investigators. Noninvasive (input) impedance, pulse wave velocity, and wave reflection in healthy middle-aged men and women. Hypertension. 2007;49(6):1248-55

[55] Kruskal H., W. Allen Wallis Use of Ranks in One-Criterion Variance Analysis William *Journal of the American Statistical Association*, Vol. 47, No. 260 (Dec., 1952), pp. 583-621 doi:10.2307/2280779

[56] Millasseau Sandrine C., Andrew D. Stewart, Sundip J. Patel, Simon R. Redwood and Philip J. Chowienczyk Evaluation of Carotid-Femoral Pulse Wave Velocity: Influence of Timing Algorithm and Heart Rate *Hypertension* 2005;45;222-226

[57] Aboy M , McNames J, Thong T, Tsunami D, Ellenby MS, and Goldstein B. An Automatic Beat Detection Algorithm for Pressure Signals. IEEE Transactions on Biomedical Engineering 2005;52(10):1662:1670

[58] Scalise L, Morbiducci U. Non-contact cardiac monitoring from carotid artery using optical vibrocardiography. Med Eng Phys. 2007 Jul 9

[59]O'Rourke MF, R Kelly, and A Avolio, The Arterial Pulse, Lea & Febiger, Philadelphia, PA (1992)